



**EXPLORING COMBINED VERSUS SINGLE MODE OF INHIBITION
OF *MYCOBACTERIUM TUBERCULOSIS* RNA POLYMERASE AS A
THERAPEUTIC INTERVENTION TO OVERCOME DRUG
RESISTANCE CHALLENGES: ATOMISTIC PERSPECTIVES**

CLEMENT AGONI

217036027

A thesis submitted to the College of Health Sciences, University of KwaZulu-Natal, Westville, in
fulfilment of the requirements of the degree of

Masters

in

Medical Sciences (Pharmaceutical Chemistry)

Supervisor

Prof. Mahmoud Soliman

2017

**EXPLORING COMBINED VERSES SINGLE MODE OF INHIBITION
OF *MYCOBACTERIUM TUBERCULOSIS* RNA POLYMERASE AS A
THERAPEUTIC INTERVENTION TO OVERCOME DRUG
RESISTANCE CHALLENGES: ATOMISTIC PERSPECTIVES**

by

Clement Agoni

217036027

2017

A thesis submitted to the College of Health Sciences, University of KwaZulu-Natal, Westville, in
fulfilment of the requirements of the degree of

Masters

in

Medical Sciences (Pharmaceutical Chemistry)

2017

This is the thesis in which the chapters are written as a set of discrete submitted manuscripts, with an overall introduction and final summary.

This is to certify that the contents of this thesis are the original research work of Clement Agoni.

As the candidate's supervisor, I have approved this thesis for submission.

Supervisor: Signed: *Mahmoud E. Soliman* Name: Prof. Mahmoud E. Soliman Date: 27/11/2017

PREFACE

This thesis details the ensuing major chapters in this thesis with this chapter included.

Chapter 1:

This chapter introduces the background of the study, its rationale, relevance and the aims and objectives. This chapter also includes the summarized outline of this thesis.

Chapter 2:

This chapter unveils a detailed literature appraisal of TB as an epidemic, the co-infection of TB and HIV, various experimental techniques for diagnosis TB, TB treatment, highlights of drug resistance in TB, Rifampin resistance, insights into current therapeutic approaches for and Rifampin resistance and the *Mtb* RNAP as an anti-TB target for the rational and *in silico* design of potential inhibitors of TB.

Chapter 3:

Chapter 3 describes Computer-Aided Drug Design as applied in the studies reported in this thesis. It also provides theoretical insights into the various molecular modelling tools and techniques that were employed to investigate the various conformational changes, structural conformations and the impact of the induced single active mutation on co-bound and singly bound *Mtb* RNAP.

Chapter 4: (Submitted work- this chapter is presented in the required format of the journal and is the final revised submitted version)

This chapter presents results from the study titled “Co-inhibition as a strategic therapeutic approach to overcome Rifampin resistance in TB therapy: Atomistic insights”. Article was submitted the journal of Future Medicinal Chemistry.

Chapter 5: (Submitted work- this chapter is presented in the required format of the journal and is the final revised submitted version)

This chapter presents results from the study titled “Synergistic Interplay of The Co-administration of Rifampin And Newly Developed Anti-TB Drug: Could It Be a Promising New Line of TB Therapy?”. Article was submitted to the journal of Receptor and Signal Transduction.

Chapter 6: Proposes future work, recommendations, and concluding remarks.

DECLARATION 1 – PLAGIARISM

I, **Mr. Clement Agoni**, declare as follows:

1. That the work described in this thesis has not been submitted to UKZN or other tertiary institution for the purposes of obtaining an academic qualification, whether by myself or any other party.
2. This thesis does not contain other persons' data, pictures, graphs or other information, unless specifically acknowledged as being sourced from other persons.
3. This thesis does not contain other persons' writing, unless specifically acknowledged as being sourced from other researchers. Where other written sources have been quoted, then:
 - a. Their words have been re-written, but the general information attributed to them has been referenced.
 - b. Where their exact words have been used, then their writing has been placed in italics and inside quotation marks, and referenced.
4. This thesis does not contain text, graphics or tables copied from the Internet, unless specifically acknowledged, and the source being detailed in the thesis and in the references section. A detail contribution to publications that form part and/or include research presented in this thesis is stated (include submitted manuscripts).

Signed: *Mahmoud E. Soliman*

Date: 27/11/2017

DECLARATION 2 – LIST OF SUBMITTED ARTICLES

1. Co-inhibition as a Strategic Therapeutic Approach to Overcome Rifampin Resistance in TB Therapy: Atomistic Insights

Contribution:

Clement Agoni: Author- Main contributor, contributed by literature reviews, data analysis, interpretation of the result as well as compilation and writing of manuscripts

Dr. Pritika Ramaharack: contributed to the manuscript writing and providing technical support

Prof. Mahmoud E. Soliman: Supervisor

2. Synergistic Interplay of The Co-administration of Rifampin And Newly Developed Anti-TB Drug: Could It Be a Promising New Line of TB Therapy?

Contribution:

Clement Agoni: Main contributor, contributed by literature reviews, data analysis, interpretation of the result as well as compilation and writing of manuscripts

Dr. Pritika Ramaharack: Contributed to the manuscript editing and providing technical support

Prof. Mahmoud E. Soliman: Supervisor

RESEARCH OUTPUT

1. **Clement Agoni**, Ramharack P . and Soliman M E (2017) Co-inhibition as a Strategic Therapeutic Approach to Overcome Rifampin Resistance in TB Therapy: Atomistic Insights, *Future Medicinal Chemistry*, Manuscript ID: FMC-2017-00197 (**submitted for publication**)

APPENDIX A: Supplementary Documents

2. **Clement Agoni**, Ramharack P. and Soliman M E (2017) Synergistic Interplay of The Co-administration of Rifampin And Newly Developed Anti-TB Drug: Could It Be a Promising New Line of TB Therapy?, *Receptor and Signal Transduction*, Manuscript ID: LRSTS-2017-0113 (**submitted for publication**)

APPENDIX B: Supplementary Documents

Other research outputs

1. Bji I., Olotu FA, **Clement Agoni**, Adeniji E., Khan S., El Rashedy A., Cherqaoui D. and Soliman M E (2017) Covalent inhibition in drug discovery: filling the void in literature (review), *Current topics in medicinal chemistry* (**Submitted for publication**)
2. Bji I., Olotu FA, **Clement Agoni**, Adeniji E., Khan S., El Rashedy A., Cherqaoui D. and Soliman M E (2017) An updated on the discovery and development of heat-shock protein inhibitors as anti-cancer therapy (review), *Expert Opinion on Drug Discovery* (**Submitted for publication**)

Conferences

1. CHPC National Conference, 3-7, 2017, Velmore Hotel Estate, Pretoria
Role: Poster presentation on “Co-inhibition as a Strategic Therapeutic Approach to Overcome Rifampin Resistance in TB Therapy: Atomistic Insights”

Signed:



Date: 27/11/2017

DEDICATION

This work is dedicated to the Almighty God the giver of life, thanking him for his unfailing grace, faithfulness, favour and unequalled love towards me.

This is also dedicated to my parents and the entire Agoni family for their love and support throughout my studies. They deserve more than one dedication for being such a supportive family towards my journey of life to “live to leave a legacy-L³”.

ACKNOWLEDGEMENTS

I wish to express my sincere gratitude and a gigantic thanks to my supervisor **Prof. Mahmoud E. Soliman** for being so supportive, listening, giving the best advice, guidance, patience and moral support during the course of my degree. He taught me so much, not only in the field pharmaceutical chemistry but in the journey of life with his periodic motivational speeches.

My thanks also goes out to, Dr. Pritika Ramharack. Your guidance and technical support made me confident of myself as a young computational chemist. It was a privilege working with you.

A big thank you to the UKZN Molecular Bio-computation and drug design research group (2017/2018 group) for sharing their research knowledge with me.

You all are highly appreciated. It's been wonderful working with you all.

To the friends I made along this journey that have positively contributed to my progress at one stage or another, I am eternally grateful.

My profound gratitude goes to CHPC for their resources and technical support.

My appreciation also goes to UKZN College of Health Sciences for the financial support throughout the course of my study.

TABLE OF CONTENTS

PREFACE	i
DECLARATION 1 – PLAGIARISM.....	iii
DECLARATION 2 – LIST OF SUBMITTED ARTICLES	iv
RESEARCH OUTPUT	v
TABLE OF FIGURES.....	x
LIST OF TABLES	xii
LIST OF ABBREVIATIONS.....	xiii
LIST OF AMINO ACIDS	xiv
ABSTRACT	xv
CHAPTER 1.....	1
1 Introduction	1
1.1 Background and rational of study	1
1.2 Aims and objectives of this study.....	2
1.3 Novelty and significance of study	3
CHAPTER 2.....	6
2 Background on the etiological agent of tuberculosis	6
2.1 Introduction	6
2.2 TB incidence	6
2.3 TB and HIV	7
2.4 Mode of Transmission.....	8
2.5 Diagnosis of Tuberculosis & Drug Susceptibility Testing.....	9
2.6 Tuberculosis treatment	10
2.7 Drug resistance in TB.....	11
2.8 Explored anti-TB Resistance remedies	13
2.9 Mycobacterium Tuberculosis RNA Polymerase as an anti-TB target	14
CHAPTER 3.....	25
3 Introduction to computational chemistry and molecular modelling.....	25
3.1 Introduction	25
3.2 Quantum Mechanics.....	25
3.3 Molecular Mechanics	29

3.4	Quantum Mechanics/Molecular Mechanics (QM/MM).....	31
3.5	Force-Fields.....	32
3.6	Molecular Dynamics	32
3.7	Molecular Dynamics Post analysis.....	33
	Submitted Article	42
	CHAPTER 5.....	61
	Submitted Article	61
	CHAPTER 6.....	88
	Conclusion and Future Perspectives	88
	6.1 Conclusions.....	88
	6.2 Future Scope and beyond	89
	APPENDIX	91
	APPENDIX A	91
	APPENDIX B	91

TABLE OF FIGURES

Figure 2.1: Estimated TB incidence rates from the 2017 Global TB reports	7
Figure 2.2: Estimated HIV prevalence in new and relapse TB cases from the 2017 Global TB report.....	8
Figure 2.3: Crystal structure of <i>Mtb</i> RNAP showing the various subunits (A), single binding with Rifampin alone (B) and co-binding with both Rifampin and DAAPI (C)	15
Figure 3.1: A graphical representation of a two-dimensional potential energy surface	29
Figure 3.2: Diagrammatical depiction of bonded and non-bonded interactions acting in molecular motion	30
Figure 3.3: Characterization of the QM/MM components	31
Figure 4.1: X-ray crystal structure of <i>Mtb</i> RNAP showing binding active sites (A) and bound (B) of RIF and DAAPI	46
Figure 4.2: Schematic depiction of <i>Mtb</i> RNAP complex stability increase upon binding of Rifampin and DAAPI	50
Figure 4.3: Binding free energy of Rifampin (RIF) in the absence and presence of DAAPI	51
Figure 4.4: Comparative compactness of Rifampin binding site residues of <i>Mtb</i> RNAP in the presence and absence of DAAPI	53
Figure 4.5. Total residue binding free energies, van der Waals (vdW), electrostatic (Elec) energy components for residues with binding energies > -1 kcal/mol and corresponding ligand interactions for Rifampin (RIF) (A) DAAPI (B)	55
Figure 5.1. 3D structure of <i>Mtb</i> RNAP depicting RIF's active site mutation (SER429→LEU429)..	66
Figure 5.2: 2D structure of DAAPI and Rifampin	67
Figure 5.3: Residue Interaction Network around mutation site (S429L) of <i>Mtb</i> RNAP upon single binding with Rifampin alone (A and B) and co-binding with Rifampin and DAAPI (C and D)	72
Figure 5.4: Number of inter-molecular hydrogen bond (H-bond) interactions observed during the molecular dynamic simulation in singly bound (A) and co-bound (B) systems in both mutated and the wild systems	76

Figure 5.5: The Root Mean Square Fluctuations (RMSF) of mutant S429L (black) with respect to wild type *Mtb* RNAP (red) for 50 ns trajectory using C α atoms upon single binding and co-binding.....78

LIST OF TABLES

Table 2.1: Current TB treatment regimens according to World Health Organization	11
Table 2.2: List Anti-TB agents and their corresponding enzyme targets	12
Table 2.3: Recently resolved X-ray of <i>Mtb</i> RNAP structures	16
Table 4.1: Binding free energy of DAAPI and RIF bound alone and when co-bound to <i>Mtb</i> RNAP.....	51
Table 5.1: MM/GBSA-based binding free energy profile of Rifampin in all simulated system	74

LIST OF ABBREVIATIONS

AAPs	N α -aroyl-N-aryl-phenylalaninamides
CADD	Computer Aided Drug Design
EMB	Ethambutol
HIV/AIDS	Human Immunodeficiency Virus/Acquired Immune Deficiency Syndrome
INH	Isoniazid
LTBI	Latent TB Infection
PZA	Pyrazinamide
MD	Molecular Dynamics
MDR-TB	Multidrug-resistant Tuberculosis
MM/GBSA	Molecular Mechanics/Generalized Born Surface Area
MM/PB-SA	Molecular Mechanics Poisson Boltzman-Surface Area
MM	Molecular Mechanics
<i>Mtb</i>	Mycobacterium Tuberculosis
PCR	Polymerase Chain Reaction
QM	Quantum Mechanics
QM/MM	Quantum Mechanics/Molecular Mechanics
RIF	Rifampicin
RIN	Residue Interaction Network
RMSD	Root Mean Square Deviation
RMSF	Root Mean Square Fluctuation
RNAP	RNA Polymerase
RoG	Radius Of Gyration
RRDR	Rifampin Resistance-Determining Region
RR-TB	Rifampin Resistant TB
TB	Tuberculosis
TDR-TB	Totally Drug Resistant TB
WHO	World Health Organization
XDR-TB	Extensively Drug Resistant TB
ZN	Ziehl-Neelson

LIST OF AMINO ACIDS

Three letter code	Amino acid
ALA	Alanine
ARG	Arginine
ASN	Asparagine
CYS	Cysteine
GLN	Glutamine
GLU	Glutamic Acid
GLY	Glycine
HIS	Histidine
ILE	Isoleucine
LEU	Leucine
LYS	Lysine
MET	Methionine
PHE	Phenylalanine
PRO	Proline
SER	Serine
THR	Threonine
TRP	Tryptophan
TYR	Tyrosine
VAL	Valine

ABSTRACT

The impact of Rifampin resistance on the overall global epidemic of antimicrobial resistance has become very prominent in recent years and is eventually stifling current efforts being made to control tuberculosis drug resistance. Rifampin resistance has significantly contributed to making TB the leading cause of morbidity from an infectious disease globally. The RNA polymerase of *Mycobacterium tuberculosis* has been extensively explored as a therapeutic target for Rifampin resistance with recent studies exploring synergistic inhibition as an effective approach, by combining Rifampin and other drugs in the TB drug resistance. Apart from the paucity of data elucidating the structural mechanism of action of the synergistic interaction between Rifampin and DAAPI, previous studies did not also utilize the X-ray crystal structure of *Mtb* RNAP due its unavailability.

This thesis used advanced computational tools to unravel molecular insights into the suppression of the emergence of resistance to Rifampin by a novel $N\alpha$ -aroyl-*N*-aryl-phenylalaninamides (AAPI) prototype inhibitor, DAAPI, co-bound to *Mtb* RNAP with Rifampin. Our studies revealed co-binding induced a stable *Mtb* RNAP protein structure, increased the degree of compactness of binding site residues around Rifampin and subsequently improved the binding affinity of Rifampin.

Studies in this thesis further provide an atomistic mechanism behind Rifampin resistance when the recently resolved crystal structure of *Mycobacterium tuberculosis* RNA polymerase is subjected to a single active site mutation. We also identified and rationalized the structural interplay of this single active site mutation upon co-binding of Rifampin with the novel inhibitor, DAAPI. Our findings report that the mutation distorted the overall conformational landscape of *Mycobacterium tuberculosis* RNA polymerase, resulting in a reduction of binding affinity of Rifampin and an overall shift in the residue interaction network of *Mycobacterium tuberculosis* RNA polymerase and upon single binding. Interestingly, co-binding with DAAPI, though impacted by the mutation exhibited improved Rifampin binding interactions amidst a distorted residue interaction network.

Findings establish a structural mechanism by which the novel inhibitor DAAPI stabilizes *Mycobacterium tuberculosis* RNA polymerase upon co-binding with Rifampin, thus suppressing Rifampin resistance. We also provide vital conformational dynamics and structural mechanisms of mutant enzyme-single ligand and mutant enzyme-dual ligand interactions which could potentially

shift the current therapeutic protocol of TB infections, thus aiding in the design of novel *Mycobacterium tuberculosis* RNA polymerase inhibitors with improved therapeutic features against the mutant proteins.

CHAPTER 1

1 Introduction

1.1 Background and rational of study

The studies presented in this thesis is geared towards comprehending and giving molecular insights in the recently resolved *Mycobacterium tuberculosis* (*Mtb*) RNA Polymerase (RNAP), while unraveling the potential of co-inhibition as a solution to the Rifampin resistance in TB treatment. One of the major problems in the treatment of TB is the rapid emergence of several drug resistant strains [1,2], which leads to the ineffectiveness of several potent anti-TB drugs, such Rifampin [1,3]. Initial *in silico* exploration of the conformational properties of this enzyme and a further investigation of the mechanism of drug resistance will provide valuable information in the continuous search for an answer to Rifampin resistance and possibly anti-TB drug resistance. These insights will also be relevant in the design and development of more potent inhibitors targeting different drug resistant strains of *Mtb*.

Mycobacterium Tuberculosis RNAP has proven over the years to be a viable and efficient target for the treatment of TB as it catalyzes a very critical process of RNA transcription by inhibiting the elongation of essential nucleotides [4]. However, the unavailability of its x-ray crystal structure hampered the efforts of previous *in silico* studies, since they were mostly based on homology models from available crystal structures of related organisms. With the recently resolved *Mtb* RNAP [5], it is strategic to provide molecular insights into the dynamic and structural conformations of this protein when exposed to single binding with Rifampin or co-binding with Rifampin and a novel inhibitor.

The suppression of the emergence resistance to Rifampin by a co-administered novel N α -aroyl-N-aryl-phenylalaninamides (AAPI) prototype, DAAPI, acting at a separate binding sites on *Mtb* RNAP, as experimentally demonstrated by Lin *et al* [5], is a very crucial finding towards the search of a solution to Rifampin resistance. These novel co-administered drugs elicit their function by binding separately from the binding pocket of Rifampin. By inhibiting the activity of *Mtb* RNAP with a mechanism different from that of Rifampin, these novel inhibitors provide an additive antibacterial activity, while also suppressing the emergence of resistance to Rifampin [5]. The current treatment regimen against RR-TB is based on a cocktail of second-line anti-TB drugs as recommended by the

WHO treatment guidelines [6]. The cocktail includes; isoniazid, pyrazinamide, streptomycin, and ethambutol and is administered over a period of 9 to 12 months [6,7].

Molecular modelling techniques have emerged as close complements to experimental studies in modern drug discovery process and in the understanding of very complex biological phenomena [8]. Various computational tools such as molecular dynamics (MD) simulation and advanced post dynamic analysis have played a huge role in precise molecular level understanding of the interaction drug molecules to targets. In this thesis, MD simulations and enhanced post analysis techniques e.g. Root Mean Square Deviation (RMSD), Root Mean Square Fluctuation (RMSF), Radius of Gyration (RoG), Molecular Mechanics energies combined with the Poisson–Boltzmann or Generalized Born and Surface area continuum solvation (MM/PBSA and MM/GBSA) based binding free energy analysis, Residue Interaction Network (RIN) were employed to understand the detailed molecular impact of single active site mutation on the binding landscape of Rifampin amidst single and co-binding with DAAPI and to also unveil the molecular and structural and conformations of single and co-binding of both Rifampin and DAAPI on *Mtb* RNAP.

1.2 Aims and objectives of this study

Studies reported in this thesis has two distinct aims.

- To explore the molecular insights into the suppression of the emergence of resistance of Rifampin by a novel $N\alpha$ -aroyl-N-aryl-phenylalaninamides (AAPI) prototype inhibitor co-bound to *Mtb* RNAP with Rifampin, through the accurate probing of the molecular dynamics and conformational changes of *Mtb* RNAP. To achieve this, we;
 - Perform MD simulations on unbound *Mtb* RNAP, complex of *Mtb* RNAP with both Rifampin and DAAPI, complex of *Mtb* RNAP and Rifampin and complex of *Mtb* RNAP and complex of *Mtb* RNAP and DAAPI in four different systems (APO, RIFDAAPI, RIF and DAAPI)
 - Calculate the binding free energy of Rifampin and DAAPI when they are each singly bound and when co-bound to *Mtb* RNAP
 - Characterize the binding landscape of *Mtb* RNAP and its structural alteration when bound to Rifampin and DAAPI simultaneously
 - Perform per-residue based decomposition for the active site residues of Rifampin and DAAPI.

- To understand the molecular impact of a single active site amino acid mutation on *Mtb* RNAP on the binding of Rifampin and the novel AAPI prototype. To achieve this aim, we;
 - Generate a mutant *Mtb* RNAP by substituting serine 429 with leucine at the active site of Rifampin using Chimera
 - Perform MD simulations on the following systems; complex of mutant *Mtb* RNAP with Rifampin alone, complex of mutant *Mtb* RNAP with both Rifampin and DAAPI, complex of wild *Mtb* RNAP with Rifampin only and complex of wild *Mtb* RNAP with both Rifampin and DAAPI (mRIF, mRIFDAAPI, RIF, RIFDAAPI)
 - Investigate the general stability of the various system throughout the simulation period
 - Investigate the stability the various simulated systems during the across the simulation period
 - Perform the multiple post dynamics analyses coupled with MM/GBSA based binding free energy calculation to understand the effect of the mutation
 - Perform and explore the residue interaction network of *Mtb* RNAP amidst single active site mutation and co-binding with more Rifampin and DAAPI
 - Perform hydrogen bond analyses on simulated systems.

1.3 Novelty and significance of study

The crystallization of the protein structure of *Mtb* RNAP was recently reported by Lin *et al* [5]. There has been no evidence of *Mtb* RNAP crystal structure prior to this report. As a result, all previous *in silico* studies on *Mtb* RNAP have been based on homology models or from closely related structures like the RNAP of *Escherichia coli* [9,10]. These crystal structures usually denote a single snapshot of the many possible conformations of the enzyme hence portraying a stiff view of the position of the atoms that are normally partly agitated by crystal packing. The conformational dynamics of *Mtb* RNAP is yet to be explored per our knowledge. With crystallographic structures representing only a specific snapshot of many possible conformations, probing of several crystal structures of the enzyme would provide important insights into the dynamic motions that should occur between varying conformations. Even though crystallographic B-factors indicate the true static or dynamic mobility of residues [11], it is still difficult to infer the precise dynamic features of protein structures. The recent resolving of the *Mtb* RNAP X-ray crystal structure of *Mtb* RNAP makes it strategic to perform molecular dynamic simulations since this provides a robust tool to understand the conformational

landscape of the enzyme. In a recent report, the possibility of a novel *Mtb* RNAP-targeting inhibitor to suppress the emergence of resistance to Rifampin was experimentally predicted [5]. However, *in silico* techniques to explore the molecular insights into this possibility is yet to be explored. Using sophisticated molecular techniques, this study reports the first account of the conformational dynamics of the first crystal structure of *Mtb* RNAP unbound and upon co-binding with both Rifampin and the novel AAPI inhibitor, DAAPI. We will also provide insights into the understanding of the mechanism of Rifampin resistance by unveiling the impact of single active site mutation on the binding affinity of Rifampin and DAAPI amidst single binding or co-binding. This should provide an invaluable contribution to the design of potent inhibitors targeting *Mtb* RNAP.

Reference

1. Rothstein DM. Rifamycins, alone and in combination. *Cold Spring Harb. Perspect. Med.* 6(7) (2016).
2. Luciani F, Sisson SA, Jiang H, Francis AR, Tanaka MM. The epidemiological fitness cost of drug resistance in *Mycobacterium tuberculosis*. *Proc Natl Acad Sci U S A.* 106(34), 14711–14715 (2009). Available from: http://www.ncbi.nlm.nih.gov/entrez/query.fcgi?cmd=Retrieve&db=PubMed&dopt=Citation&list_uids=19706556 <http://www.pnas.org/content/106/34/14711.full.pdf>.
3. Udawadia ZF, Amale RA, Ajbani KK, Rodrigues C. Totally drug-resistant tuberculosis in India. *Clin. Infect. Dis.* 54, 579–581 (2012).
4. Gill SK, Garcia GA. Rifamycin inhibition of WT and Rif-resistant *Mycobacterium tuberculosis* and *Escherichia coli* RNA polymerases in vitro. *Tuberculosis.* 91(5), 361–369 (2011).
5. Lin W, Mandal S, Degen D, *et al.* Structural Basis of *Mycobacterium tuberculosis* Transcription and Transcription Inhibition. *Mol. Cell.* 66(2), 169–179.e8 (2017).
6. WHO. Treatment of tuberculosis: guidelines. Available from: www.who.int/tb/publications/2010/9789241547833/en/.
7. Prasad V, Singhal R, Umer K. First and second line drug resistance in pulmonary among treatment naïve tuberculosis patients in a district under Revised National Tuberculosis Control Programme (RNTCP) in New Delhi. *J. Epidemiol. Glob. Health.* 5(4), 365–373 (2015). Available from: <http://dx.doi.org/10.1016/j.jegh.2015.04.002>.
8. Chaudhari R, Tan Z, Huang B, Zhang S. Computational polypharmacology: a new paradigm for drug discovery. *Expert Opin. Drug Discov.* 12(3), 279–291 (2017).
9. Molodtsov V, Nawarathne IN, Scharf NT, *et al.* X-ray crystal structures of the *Escherichia coli* RNA polymerase in complex with benzoxazinorifamycins. *J. Med. Chem.* 56(11), 4758–4763 (2013).

10. Molodtsov V, Scharf NT, Stefan MA, *et al.* Structural basis for rifamycin resistance of bacterial RNA polymerase by the three most clinically important RpoB mutations found in *Mycobacterium tuberculosis*. *Mol. Microbiol.* 103(6), 1034–1045 (2017). Available from: <http://doi.wiley.com/10.1111/mmi.13606>.
11. Yuan Z, Bailey TL, Teasdale RD. Prediction of protein B-factor profiles. *Proteins Struct. Funct. Genet.* 58(4), 905–912 (2005).

CHAPTER 2

2 Background on the etiological agent of tuberculosis

2.1 Introduction

Tuberculosis (TB) is an infectious disease caused by *Mycobacterium Tuberculosis (Mtb)* [1,2]. Despite the availability of well-structured treatment options, a functional vaccine and an overall resultant cure, tuberculosis is still a major global health concern [1,2]. As discovered and reported by Robert Koch in 1882, TB is an airborne infectious disease caused by organisms of the *Mtb* complex [2–4]. Most of the reported TB cases have been caused by *Mtb* or the closely related *Mycobacterium africanum*, even though there are few reported cases in which zoonotic members of the complex such as *Mycobacterium bovis* or *Mycobacterium caprae* also cause the disease [5]. However, it is important to note that *Mtb* has no other known environmental reservoir apart from humans [6] probably accounting for being the highest causative agent of the TB disease amongst the *Mtb* complex. Clinically, TB patients have been classified as having a latent TB infection (LTBI) or and an active TB disease. In Latent tuberculosis infection, there is no evidence of clinically manifested active TB amidst persistent response of the immune system to *Mtb* antigen stimulation [7–9]. Individuals with LTBI risk development of active TB disease by a process of TB reactivation, especially in immunocompromised conditions such as Human Immunodeficiency Virus/Acquired Immune Deficiency Syndrome (HIV/AIDS), whose risk is much higher [8]. It is estimated that about one third of the world population has LTBI, of which many are oblivious for their condition. Active TB disease begins when *Mtb* overcomes an individual's immune defense system. This results in the multiplication of the bacteria and eventual progression of LTBI to the active TB disease [7].

2.2 TB incidence

TB is currently ranked above HIV/AIDS as the leading cause of morbidity from an infectious disease and still features prominently in the top ten causes of death worldwide [1]. Over the years, TB has proven to be a disease of the poor with highest prevalence being in developing countries with predominantly low-income and middle-income populations [1,10,11]. According to the 2017 global TB report, about 10.4 million new cases of TB were recorded worldwide in 2016 with 45% occurring in the World Health Organization (WHO) South-East Asia Region, 25% in WHO African Region, 17% in WHO Western Pacific Region, 7% in WHO Eastern Mediterranean Region, 3% in the European Region and an estimated 3% in the WHO Region of the Americas. In 2016, countries with the largest number of incident cases included India, China, Philippines, Indonesia and Pakistan, which

collectively accounted for 56% of total global incidence while South Africa and Nigeria each accounted for 4% each [1].

South Africa retains its position as one of the countries with the leading TB burden globally with an estimated 428,000 total TB incidence in 2016 [1]. This has been complicated by the notable high HIV prevalence in South Africa as with an increase in the reported TB and HIV co-infection cases [1].

Estimated TB incidence rates, 2016

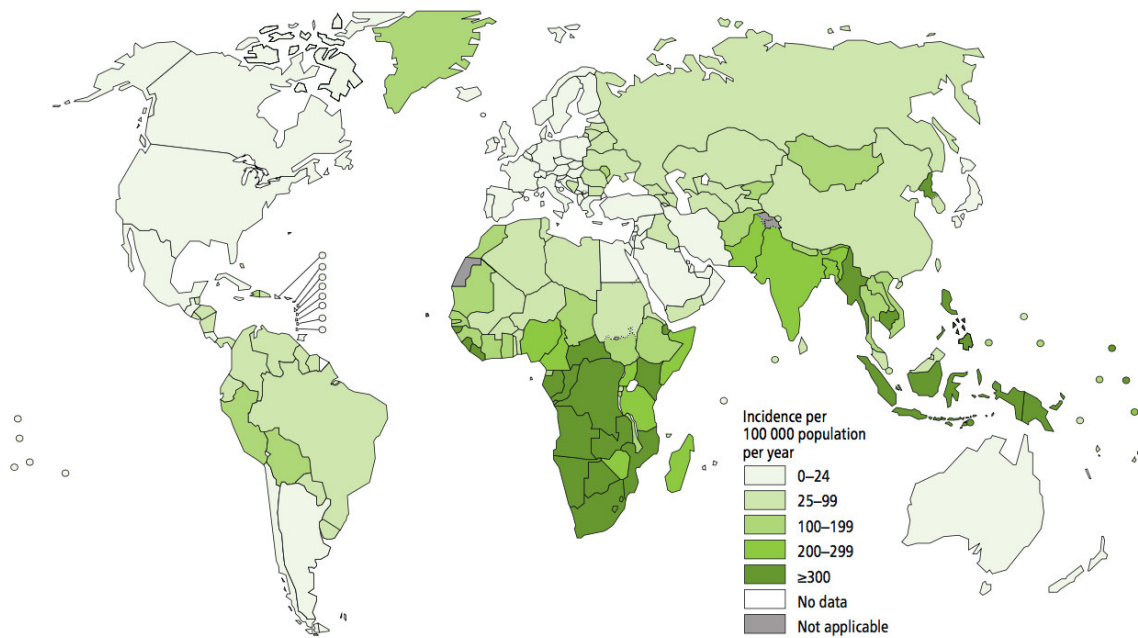


Figure 2.1 Estimated TB incidence rates from the 2017 Global TB reports [1].

2.3 TB and HIV

People living with HIV has accounted for 10% of all new TB cases, with countries in the WHO Africa Region accounting for the highest co-infection estimates globally [1]. Parts of Southern Africa recorded an over 50% of new TB and HIV cases. The WHO African Region reportedly has the highest burden of HIV-associated TB, with 81% of notified infected individuals having a previously documented HIV test report [1]. The percentage of known HIV-positive TB patients on anti-retroviral therapy exceeds 90% in India, Malawi, Kenya, Namibia, Swaziland and Mozambique [1]. Co-infection with TB and HIV collectively constitute the leading cause of morbidity from infectious diseases. There is a rapid deterioration of an individual's immune defense mechanism in the presence

of these two pathogens since they potentiate each other, thereby resulting in premature deaths [12]. Together with drug resistance, the co-infection of TB and HIV hampered global TB control efforts most especially in high burden areas such as sub-Saharan Africa [13,14]. In South Africa, it is reported that approximately 70% of persons infected with active TB disease are simultaneously infected with HIV [15]. Co-infection of TB with HIV single handedly increased the reactivation of LTBI by 20 fold [16,17].

Estimated HIV prevalence in new and relapse TB cases, 2016

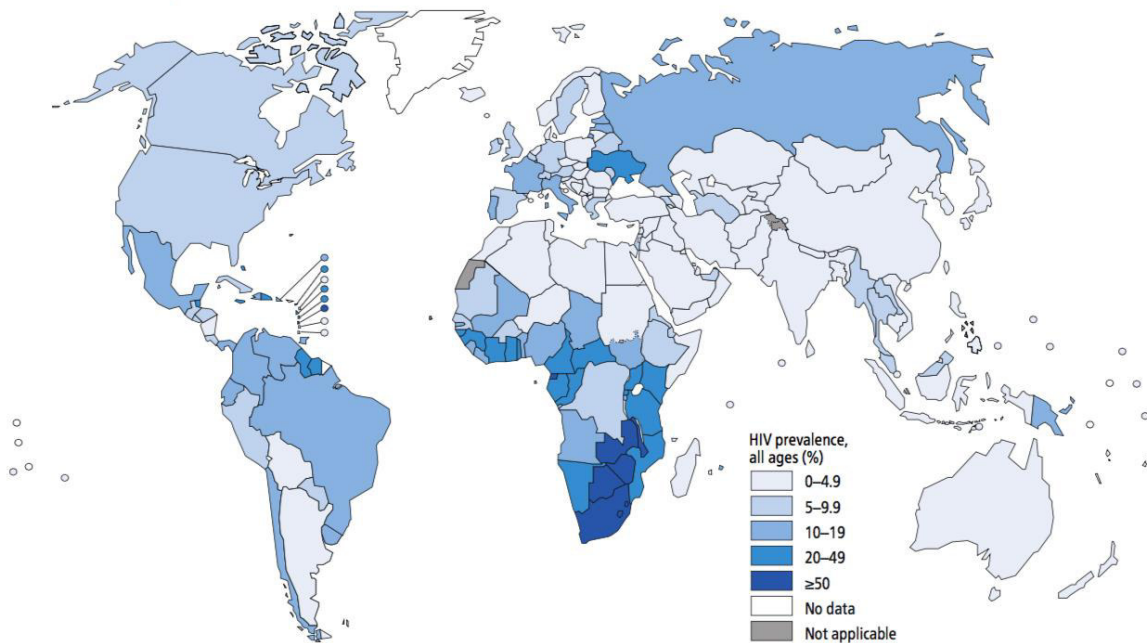


Figure 2.2 Estimated HIV prevalence in new and relapse TB cases from the 2017 Global TB report [1].

2.4 Mode of Transmission

Aerosols containing *Mtb* from an infected person serves as the main route of transmission. Upon the entry, *Mtb* targets alveoli of host lungs [12,18,19]. In response, macrophages and other immune cells are assembled by host during this early stage of the infection [20]. Even though *Mtb* can infect other body organs and tissues such as the spine, the brain and the kidney [21,22], *Mtb* commonly settles in the lungs characterized by symptoms such as such as weight loss, loss of appetite, night sweats,

coughing of sputum and/or blood, fever, fatigue and chills [1,18,23]. Depending on an individual's immune system, *Mtb* in an infected individual can be classified as latent TB (inactive) or become active and referred to as TB disease [23]. The re-emergence of TB in a previously infected individual may be triggered by factors such as smoking, immunosuppression, alcohol, genetic factors, HIV infection and indoor air pollution [18,23].

2.5 Diagnosis of Tuberculosis & Drug Susceptibility Testing

The management of TB is enhanced by early diagnosis of the infection and the performance of drug susceptibility testing [24]. Sputum smear microscopy and culture based technology remain a vital technique in the diagnosis of TB [25]. The Ziehl-Neelson (ZN) staining technique is used in the detection of *Mtb* [25,26]. The principle behind this technique is based on the differential acid fast staining property of the *Mtb* due to the mycolic acid structure of the bacterial cell [25]. Smears of sputum are prepared on glass slides. Dried smears are then stained with phenol fuschin [25]. The smear is then decolorized using acid alcohol [25]. The decolorized smear is then counterstained with either Methylene or malachite green [25]. Alternatively, Auramine-rhodamine staining can be used in place of the ZN stain [25]. After decolorization with acid alcohol, Auramine-rhodamine staining protocol counterstains with potassium permanganate. Using UV illumination, the fluorescence of stained bacteria can then be viewed [27].

Bacterial culture is a sensitive and specific approach for the diagnosis of bacterial infections such as TB [26]. The culture of bacteria requires appropriate media for the growth of the organism, which can either be solid or liquid [26]. The commonly used media for the growth of *Mtb* are; Lowenstein-Jensen (LJ); Middlebrook 7H10/11 and Middlebrook 7H9, a liquid media [28]. For growth and isolation, bacterial cultures usually require a period of 3-6 weeks [29]. Currently the reference media for the culture of *Mtb* is the liquid media. The liquid media is linked with higher recovery of the tubercle bacilli coupled with a faster detection time [30]. Diagnostic tools such as the BACTEC (Johnson Laboratories) and BACTEC-MGIT (Johnson Laboratories) employs colorimetric systems for culture based assays and have reportedly improved detection time of the tubercle bacilli of *Mtb* [29].

A recently introduced tool, the Xpert MDR/RIF (Cepheid) assay, incorporates polymerase chain reaction (PCR) and molecular beacon technology to yield a significantly higher mycobacterial

sensitivity than sputum smear microscopy [31]. Apart from rapidly diagnosing TB, this fully automated technique simultaneously detects Rifampin resistance as well, thereby allowing for early treatment of drug resistant TB while awaiting corroboration from drug susceptibility testing, the gold standard for the phenotypic determination of drug resistance [31].

2.6 Tuberculosis treatment

The battle against this killer bacteria begun many decades ago with discovery of potent antibiotics against it, the first being streptomycin in 1943 [32]. This served as a stepping-stone for many other studies leading to the discovery of the current therapeutic regimens such as rifampicin in 1963 among many others, which are available for clinical use now [33,34]. Most of these antibiotics target various structural components of the *Mtb*. They act by inhibiting the synthesis of critical structures required for the maturation of *Mtb*, with the eventual aim of eliminating *Mtb* [34]. TB-targeted drug agents are designed to either inhibit; cell wall biosynthesis, RNA synthesis or protein synthesis [35]. For instance the first-line anti-TB drugs, Isoniazide, acts by inhibiting the biosynthesis of mycolic acids, essential components of the cell wall of *Mtb* [36], while Rifampin interferes with the synthesis of a DNA-dependent RNA by inhibiting the activity of the DNA-dependent RNA polymerase enzyme [35]. Also, second-line injectables which are mainly aminoglycosides function by blocking the initiation of protein synthesis in *Mtb* [37], while fluoroquinolones inhibit the activity of the enzymes DNA gyrase and topoisomerase IV which results in the death of *Mtb* [38].

Table 2.1: Current TB treatment regimens according to World Health Organisation [39].

Group 1: First-line oral agents	Isoniazid; rifampicin; ethambutol; pyrazinamide
Group 2: Injectable agents	Kanamycin; amikacin; capreomycin; streptomycin
Group 3: Fluoroquinolones ofloxacin	Levofloxacin; moxifloxacin; gatifloxacin
Group 4: Oral bacteriostatic second-line agents	P-aminosalicylic acid; cycloserine; terizidone; ethionamide; protionamide
Group 5: Agents with unclear efficacy	Clofazimine; linezolid; amoxicillin; imipenem; clarithromycin; thioacetazone; bedaquiline; delamanid; meropenem; high dose of isoniazid;

Currently approved first line antibiotics for drug-susceptible *Mtb* include rifampin (RIF), isoniazid (INH), pyrazinamide (PZA) and ethambutol (EMB) mostly administered over a period of six months [40,41]. Provided an infected person follows through the prescribed treatment course, the current standard first line antibiotic treatment regimen is effective enough to ensure the clearance bacterial bacilli [42]. However, the long-term treatment periods associated with first and second line anti-TB agents has resulted in the emergence of *Mtb* strains that are resist to these anti-TB drugs [43,44]. In addition to the first line antibiotic treatment regimen against *Mtb*, there are four other groups [33].

2.7 Drug resistance in TB

Upon the discovery of these many potent antibiotics against the bacteria, there was a general excitement within scientific community since these proved to be very effective and provided a functional cure. However, this excitement was short lived when there were reports of resistance of *Mtb* to antibiotics [45–47]. Unfortunately, drug resistance has persisted till now and has gotten to a point where it poses a major challenge to disease control globally [48,49]. Drug resistance in TB treatment has compounded the already grave TB control challenge, with infected persons having to go through a prolonged, expensive and limited treatment course, with a risk of about 10-30% of these

cases resulting in treatment failure and death [50]. Drug resistance by *Mtb* is usually associated with spontaneous and random bacteria chromosomal mutation that renders *Mtb* unsusceptible to specific anti-TB agents [51]. Several genes have been implicated in TB resistance as illustrated in the table below with the corresponding drugs involved.

Table 2.2: List of Anti-TB agents and their corresponding enzyme targets [52].

Drug	Genes (s) implicated in resistance
Rifampin	<i>rpoB</i> : β -subunit of RNA polymerase
Isoniazide	<i>katG</i> : catalase-peroxidase <i>oxyR-ahpC</i> : alkylhydrokinase reductase <i>inhA</i> : enoyl-ACP reductase <i>kasA</i> : β -ketoacyl acyl carrier protein synthase
Ethionamide	<i>inhA</i> : enoyl-ACP reductase
Streptomycin	<i>rpsL</i> : ribosomal protein S12 involved in : 16S RNA
Fluoroquinolones	<i>gyrA</i> : DNA gyrase
Pyrazinamide	<i>pncA</i> : pyrazinamidase
Ethambutol	<i>embCAB</i> : Arabinosyl transferase

Resistance of *Mtb* to at least two of the most efficacious front treatment regimen, Rifampin and Isoniazide has been classified by WHO as Multidrug-resistant Tuberculosis (MDR-TB) [1]. The 2017 Global TB report reported an estimated 490 000 new MDR-TB cases in 2016 alone, with an estimated 100 000 confirmed cases of Rifampicin-resistant TB (RR-TB) [1]. Conferring with the numerous studies that have reported primary resistance as a major contributor to the increase of MDR-TB in South Africa [53–57], an estimated 19,000 new TB cases in 2016 were attributed to MDR-TB.

Over time, there has also been the emergence of the *Mtb*, not only resistant to Rifampin and Isoniazide but also resistant to any fluoroquinolone and at least one of the second-line injectables (amikacin, kanamycin and capreomycin) which have been classified as extensively drug resistance tuberculosis (XDR-TB) [30,58]. XDR-TB discovered in 2006 in South Africa [59], reportedly has higher

incidence rates than the total TB burden in some low incidence areas such the United States of America [60]. More recently, there has also been reports of resistance to all first and second line TB drugs described as totally drug resistant TB (TDR-TB) [61]. General treatment timelines for MDR TB ranges from 18–24 months with weak second-line TB drugs [62,63]. According to a 2009 report by the National Health Laboratory Services in South Africa, majority of reported MDR-TB and XDR-TB cases occur in KwaZulu-Natal, Western Cape and Eastern Cape Provinces [64].

2.7.1 *Rifampin Resistance*

Rifampin resistance contributes significantly to the overall TB drug resistance menace [50]. Rifampin resistant TB (RR-TB) occurs as a result of point mutations, nucleotide deletions or insertions in an 81—base pair region of the *rpoB* gene [65,66]. The *rpoB* gene codes for the β -subunit of DNA-dependent RNA polymerase [67]. Approximately 95% of all reported Rifampin resistant isolates exhibit a single mutation in this 81-base region of *rpoB* [68]. Mutations usually occur in a cluster of codons ranging from 507 to 533 of the *rpoB* gene, a region also known as the Rifampin resistance-determining region (RRDR). Mutations on codons 526 and 531 are the most common implicated codons in RR-TB [43,44]. Nonetheless, there have been reports of RR-TB resulting from mutations occurring outside the RRDR [69]. Rifampin resistance though very rare, is used as a marker MDR-TB since it usually occurs in concurrence with isoniazid [58,70].

2.8 *Explored anti-TB Resistance remedies*

Bedeveled with the challenge of the various types of drug resistance, there has been the need for the development of innovative treatment protocols to curtail the continuous rise of TB fatalities resulting from TB resistance. Combinational therapeutic methods came in as one of the options, in which several antimicrobial drugs have been combined over the years towards the treatment of TB [71,72]. In 1950, the British Medical Journal reported of the first combinational antimicrobial therapeutic regimen for TB involving para-aminosalicylic acid and streptomycin, which served as a model from which new drugs were subsequently discovered [73]. This was again re-echoed by Fox *et al* in 1999 [74]. Combining drugs for the treatment of TB has subsequently proven to be very effective method of suppressing the emergence of drug resistance in active *Mtb* infection after its first application [75]. However, it is important to recognize that, the overall efficacy depends largely on choosing the right drugs to combine as well as the receptor that will be targeted [73]. It is however unfortunate that

despite the success of combinational therapy over the years, *Mtb* drug resistance is still a global concern, mostly due to the emergence of resistant strains [55]. These strains are shown to exhibit point mutations at binding sites of known TB drugs, altering the binding affinity of these potent drug and hence their efficacy [76–78].

Treatment of RR-TB usually involves an increase in duration of therapy to about 9 to 12 months from the initial 6 months due to its associated with poorer clinical outcomes [50,79,80]. A therapeutic cocktail of second line agents are recommended for the treatment of RR-TB as stipulated in the WHO guidelines [50]. Streptomycin, isoniazid, ethambutol and pyrazinamide over a period of 9 months can be used to treat isolated cases of RR-TB [81].

2.9 *Mycobacterium Tuberculosis* RNA Polymerase as an anti-TB target

One of the major enzymes that have been targeted in the discovery of anti-TB drugs is the DNA-dependent RNA polymerase (RNAP) [72]. It is the target enzyme for the frontline line anti-TB drug Rifampin, an antibiotic which has proven over the years to be very essential in anti-TB therapeutic protocols [50,72,82–84]. RNAP has been widely reported to exist in two forms, an RNAP core and RNAP holo [85–88]. According to studies by Rodrigue *et al* in 2006 and 2007, Manganeli *et al* in 2004, the RNAP is involved in the catalysis of RNA synthesis, however, it is incapable of starting transcription from a promoter. Therefore, RNAP would require a factor called σ^A holoenzyme for promoter specific transcription initiation. Even though RNAP has been an effective target for Rifampin, *Mtb* has been reported to have developed resistance to Rifampin [77]. Rifampin resistance has gradually become a global health concern with as many as 600,000 new cases annually [50,72,84]. Therefore, to target RNAP any further for potential anti-TB inhibitors, there was the need to consider either Rifampin derivatives that were unaffected by the current Rifampin binding site or developing entirely new inhibitors that were not linked to Rifampin at all and function by binding to a separate binding site on RNAP, hence not affected by any substitutions in the Rifampin binding site [84]. This has however been challenging due to the previous unavailability of an X-ray crystal structure of *Mtb* RNAP, until they were recently reported [89].

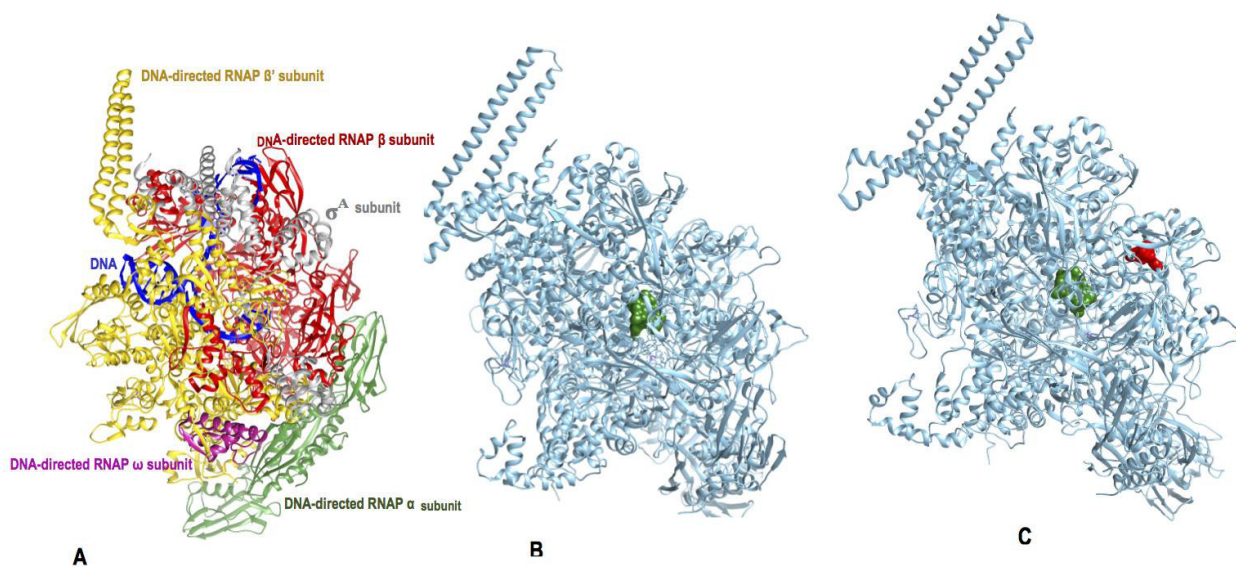


Figure 2.3: Crystal structure of *Mtb* RNAP showing the various subunits (A), single binding with Rifampin alone (B) and co-binding with both Rifampin and DAAPI (C).

Over the years several crystal structures of *Mtb* RNAP have been resolved and deposited in the Protein Data Bank. However, the continuous inundation of the scientific community with new findings on *Mtb* RNAP has prompted the resolving of new crystal structures. These structures incorporate the most recent experimentally validated fundamental characteristics and unveiled new structural features in the enzyme, which can serve as the basis for rational drug design.

Lin *et al* recently reported the first ever X-ray crystal structure of the DNA-dependent enzyme RNA polymerase enzyme of *Mtb*, in its wild type, in complex with Rifampin (a known frontline anti-TB drug), in complex with DAAP1 (a prototype class from set of novel of inhibitors called $N\alpha$ -aroyl-N-aryl-phenylalaninamides (AAPs) and in complex with both Rifampin and DAAP1 [89]. This novel prototype class (DAAP1) was reported to exhibits potent, selective, stereospecific activity against Mycobacterial RNAP [89]. This novel inhibitor also exhibit potent, selective and stereospecific activity against Mycobacteria, notably *Mtb*, *Mycobacterium smegmatis* and *Mycobacterium avium* [89].

Table 2.3: Recently resolved X-ray of *Mtb* RNAP structures.

X-ray Crystal Structure	Resolution (Å)	Ligand/Inhibitor	PDB Entry	Reference, Date of publication
<i>Mtb</i> transition initiation complex	3.9	Zn, Mg	5UHA	Lin <i>et al</i> (Jan 2017)
<i>Mtb</i> transition initiation complex with Rifampin	4.29	Zn, Mg, Rifampin	5UHB	Lin <i>et al</i> (Jan 2017)
<i>Mtb</i> transition initiation complex containing 3nt RNA in complex with Rifampin	3.8	Zn, Mg, Rifampin	5UHC	Lin <i>et al</i> (Jan 2017)
<i>Mtb</i> transition initiation complex containing 4nt RNA in complex with Rifampin	4.01	Zn, Mg, Rifampin	5UHD	Lin <i>et al</i> (Jan 2017)
<i>Mtb</i> transition initiation complex with D-AAP1	4.04	Zn, Mg, Nalpha-(benzenecarbonyl)-N-(2-methylphenyl)-D-phenylalaninamide	5UHG	Lin <i>et al</i> (Jan 2017)

<i>Mtb</i> transcription initiation complex in complex with D-IX336	4.34	Zn, Mg, N-(2-methylphenyl)-Nalpha-(selenophene-2-carbonyl)-D-phenylalaninamide	5UHF	Lin <i>et al</i> (Jan 2017)
<i>Mtb</i> tuberculosis transcription initiation complex in complex with D-AAP1 and Rifampin	3.97	Zn, Mg, N-(2-methylphenyl)-Nalpha-(selenophene-2-carbonyl)-D-phenylalaninamide, Rifampin	5UHG	Lin <i>et al</i> (Jan 2017)
<i>Mtb</i> transcription initiation complex containing 3 nt of RNA	3.75	Zn, Mg	5UH5	Lin <i>et al</i> (Jan 2017)
<i>Mtb</i> transcription initiation complex containing 2ntRNA in complex with Rifampin	3.84	Zn, Mg, Rifampin	5UH6	Lin <i>et al</i> (Jan 2017)
Beta' <i>Mtb</i> SI of Mycobacterium	2.2	No ligand/inhibitor	5UH7	Lin <i>et al</i> (Jan 2017)

tuberculosis RNA polymerase				
<i>Mtb</i> transcription initiation complex containing 4nt RNA	4.18	Zn, Mg	5UH8	Lin <i>et al</i> (Jan 2017)

Reference

1. World Health Organization (WHO). WHO | Global tuberculosis report 2017. Available from: http://www.who.int/tb/publications/global_report/en/.
2. Daniel TM. The history of tuberculosis. *Respir Med.* 100(11), 1862–70 (2006).
3. Gradmann C. Robert Koch and the white death: From tuberculosis to tuberculin. *Microbes Infect.* 8(1), 294–301 (2006).
4. Barnes DS. Historical perspectives on the etiology of tuberculosis. *Microbes Infect.* 2(4), 431–440 (2000).
5. Bos KI *et al.* Pre-Columbian mycobacterial genomes reveal seals as a source of New World human tuberculosis. *Nature.* 514, 494–497 (2014).
6. Comas I, Coscolla M, Luo T, *et al.* Out-of-Africa migration and Neolithic coexpansion of Mycobacterium tuberculosis with modern humans. *Nat. Genet.* 45(10), 1176–1182 (2013). Available from: <http://www.nature.com/doi/10.1038/ng.2744>.
7. Houben RM, Dodd PJ. The global burden of latent tuberculosis infection: a re-estimation using mathematical modelling. *PLoS Med.* 13(10) (2016).
8. Achkar JM, ER. J-A. Incipient and subclinical tuberculosis: defining early disease states in the context of host immune response. *J Infect Dis.* 204, (Suppl. 4): S1179–86 (2011).
9. Guirado E, Mbawuiké U, Keiser TL, Arcos J, Azad AK, Wang SH *et al.* Characterization of host and microbial determinants in individuals with latent tuberculosis infection using a human granuloma model. *MBio.* 6(1), 2537–2614. (2015).
10. Muniyandi M, Ramachandran R. Socioeconomic inequalities of tuberculosis in India. *Expert Opin. Pharmacother.* 9(10), 1623–1628 (2008). Available from: <http://www.tandfonline.com/doi/full/10.1517/14656566.9.10.1623>.
11. Nadjane Batista Lacerda S, Cristina de Abreu Temoteo R, Maria Ribeiro Monteiro de Figueiredo T, *et al.* Individual and social vulnerabilities upon acquiring tuberculosis: a literature systematic review. *Int. Arch. Med.* 7(1), 35 (2014). Available from: <http://www.intarchmed.com/content/7/1/35>.
12. Egwaga SM, Cobelens FG, Muwinge H, Verhage C, Kalisvaart N, Borgdorff MW. The impact of the HIV epidemic on tuberculosis transmission in Tanzania. *AIDS.* 20(6), 915–921 (2006).
13. Raviglione M, Smith I. XDR tuberculosis -implications for global public health. *N.Engl. J. Med.* 356, 656–659 (2007).
14. Chindelevitch L, Menziers N, Pretorius C, Stover J, Salomon J, Cohen T. Evaluating the potential impact of enhancing HIV treatment and tuberculosis control programmes on the burden of tuberculosis. *J R Soc Interface.* 12, 1–14 (2015).
15. National Strategic Plan for HIV, STIs and TB (2012 -2016). Available from: www.sahivsoc.org/upload/documents/National_Strategic_Plan_2012.pdf.

16. Getahun H, Gunneberg C, Granich R, Nunn P. HIV Infection – Associated Tuberculosis : The Epidemiology and the Response. *50*, 201–207 (2010).
17. Selwyn PA, Hartel D, Lewis VA, Schoenbaum EE, Vermund SH et al. A prospective study of the risk of tuberculosis among intravenous drug users with human immunodeficiency virus infection. *N Engl J Med.* 320, 545–550 (1989).
18. Sakamoto K. The Pathology of Mycobacterium tuberculosis Infection. *Vet. Pathol.* 49(3), 423–439 (2012).
19. Cook GM, Berney M, Gebhard S, et al. Physiology of Mycobacteria. *Adv. Microb. Physiol.* 55 (2009).
20. Cooper AM. Cell-Mediated Immune Responses in Tuberculosis. *Annu. Rev. Immunol.* 27(1), 393–422 (2009). Available from: <http://www.annualreviews.org/doi/10.1146/annurev.immunol.021908.132703>.
21. Be N a, Kim KS, Bishai WR, Jain SK. Pathogenesis of central nervous system tuberculosis. *Curr. Mol. Med.* 9(2), 94–99 (2009).
22. Eastwood JB, Corbishley CM, Grange JM. Tuberculosis and the kidney. *J. Am. Soc. Nephrol.* 12(6), 1307–14 (2001). Available from: <http://jasn.asnjournals.org/content/12/6/1307.short>.
23. Smith I. Mycobacterium tuberculosis pathogenesis and molecular determinants of virulence. *Clin Microbiol Rev.* 16(3), 463–496 (2003).
24. Karakousis P. Mechanisms of Action and Resistance of Antimycobacterial Agents. *Antimicrob. Drug Resist.* 8, 271–291 (2006).
25. Madhukar P, Schito M. Tuberculosis Diagnostics in 2015 : Landscape , Priorities , Needs , and Prospects. *J Infect.* 211, (Suppl 2):21–8 (2015).
26. Dorman S. New diagnostic tests for tuberculosis: bench, bedside, and beyond. *Clin. Infect. Dis.* 50, S173–S177 (2010).
27. Lipsky BA, Gates J, Tenover FC, Plorde JJ. Factors affecting the clinical value of microscopy for acid-fast bacilli. *Rev Infect Dis.* 6(2), 214–22 (1984).
28. Saito H. Laboratory media for the cultivation of tubercle bacillus. *Kekkaku.* 73(5), 329–37 (1998).
29. Naveen G, Peerapur B V. Comparison of the Lowenstein-Jensen medium, the middlebrook 7H10 medium and MB/BACT for the isolation of Mycobacterium tuberculosis (MTB) from clinical specimens. *J Clin Diagnostic Res.* 6(10), 1704–9 (2012).
30. World Health Organization (WHO). Companion handbook to the WHO guidelines for the programmatic management of drug-resistant tuberculosis. Available from: http://apps.who.int/iris/bitstream/10665/130918/1/9789241548809_eng.pdf?ua=1&ua=1.
31. WHO. Automated real-time nucleic acid amplification technology for rapid and simultaneous detection of tuberculosis and rifampicin resistance: Xpert MTB/RIF assay for the diagnosis of pulmonary and extrapulmonary TB in adults and children. Available from:

<http://apps.who.int/iris/handle/10665/112472>.

32. Bates JH. Tuberculosis chemotherapy: The need for new antituberculosis drugs is urgent. *Am. J. Respir. Crit. Care Med.* 151, 942–943 (1995).
33. WHO. Treatment of tuberculosis: guidelines. Available from: www.who.int/tb/publications/2010/9789241547833/en/.
34. Zumla A, Chakaya J, Centis R, D'Ambrosio L, Mwaba P, Bates M. Tuberculosis treatment and management—an update on treatment regimens, trials, new drugs, and adjunct therapies. *Lancet Respir Med.* 3(3), 220–34. (2015).
35. Zhang Y, Yew WW. Mechanisms of drug resistance in *Mycobacterium tuberculosis*. *Int. J. Tuberc. Lung. Dis.* 19, 1276–1289 (2015).
36. Wiseman B, Carpena X, Feliz M, *et al.* Isonicotinic acid hydrazide conversion to isonicotinyl-NAD by catalase-peroxidases. *J. Biol. Chem.* 285, 26662–26673 (2010).
37. Caminero JA, Sotgiu G, Zumla A, Migliori GB. Best drug treatment for multidrug-resistant and extensively drug-resistant tuberculosis. *Lancet Infect. Dis.* 10, 621–629 (2010).
38. Sreevatsan S, Stockbauer KE, Pan X. Ethambutol resistance in *Mycobacterium tuberculosis*: Critical role of embB mutations. *Antimicrob. Agents Chemother.* 41, 1677–1681 (1997).
39. Pontali E, Matteelli A, Migliori GB. Drug-resistant tuberculosis. *Curr. Opin. Pulm. Med.* 19, 266–272 (2013).
40. Combs DL, O'Brien RJ, Geiter LJ. USPHS Tuberculosis Short-Course Chemotherapy Trial 21: effectiveness, toxicity and acceptability: the report of the final results. *Ann Intern Med.* 112, 397–406 (1990).
41. Cui Z-J, Yang Q-Y, Zhang Hong-Yu, Qiang Z, Zhang Q-Y. Bioinformatics Identification of Drug Resistance-Associated Gene Pairs in *Mycobacterium tuberculosis*. *Int. J. Mol. Sci.* 17, 1417 (2016).
42. Hoagland DT, Liu J, Lee RB, Lee RE. New agents for the treatment of drug-resistant *Mycobacterium tuberculosis* ☆. *Adv. Drug Deliv. Rev.* 102, 55–72 (2016). Available from: <http://dx.doi.org/10.1016/j.addr.2016.04.026>.
43. Palomino J, Martin A. Drug Resistance Mechanisms in *Mycobacterium tuberculosis*. *Antibiotics.* 3(3), 317–40 (2014).
44. Da Silva PEA, Palomino JC. Molecular basis and mechanisms of drug resistance in *Mycobacterium tuberculosis*: Classical and new drugs. *J Antimicrob Chemother.* 66(7), 1417–30 (2011).
45. Luciani F, Sisson SA, Jiang H, Francis AR, Tanaka MM. The epidemiological fitness cost of drug resistance in *Mycobacterium tuberculosis*. *Proc Natl Acad Sci U S A.* 106(34), 14711–14715 (2009). Available from: http://www.ncbi.nlm.nih.gov/entrez/query.fcgi?cmd=Retrieve&db=PubMed&dopt=Citation&list_uids=19706556 <http://www.pnas.org/content/106/34/14711.full.pdf>.
46. Udwardia ZF, Amale RA, Ajbani KK, Rodrigues C. Totally drug-resistant tuberculosis in India. *Clin. Infect. Dis.* 54, 579–581 (2012).

47. Dooley SW, Jarvis WR, Martone WJ, Snider Jr D. Multidrug-resistant tuberculosis. *Ann Intern Med.* 117, 257–9 (1992).
48. Zumla A, Abubakar I, Raviglione M. Zumla A, Abubakar I, Raviglione M, et al. Drug-resistant tuberculosis – current dilemmas, unanswered questions, challenges, and priority needs. *J Infect Dis.* 205, S228–S240. (2012).
49. Zumla A, Nahid P, Cole ST. Advances in the development of new tuberculosis drugs and treatment regimens. *Nat. Rev. Drug Discov.* 12(5), 388–404 (2013). Available from: <http://www.nature.com/doi/10.1038/nrd4001>.
50. Global TB Report W. World Health Organization. Global Tuberculosis Report 2016.
51. David HL. Probability distribution of drug resistant mutants in unselected populations of *Mycobacterium tuberculosis*. *Appl Microbiol.* 20, 810–4 (1970).
52. Heifets LB, Cangelosi GA. Drug susceptibility testing of *Mycobacterium tuberculosis*: a neglected problem at the turn of the century. *Int J Tuberc Lung Dis.* 3, 564–81 (1999).
53. Gandhi N, Moll A, Sturm A, Pawinski R, Govender T, Lalloo U. Extensively drug-resistant tuberculosis as a cause of death in patients co-infected with tuberculosis and HIV in a rural area of South Africa. *Lancet.* 368, 1575–1580 (2006).
54. Royce S, Falzon D, van Weezenbeek C, et al. Multidrug resistance in new tuberculosis patients: burden and implications. *Int J Tuberc Lung Dis.* 17, 511–3 (2013).
55. Cox H, McDermid C, Azevedo V, Muller O, Coetzee D. Epidemic levels of drug resistant tuberculosis (MDR and XDR-TB) in a high HIV prevalence setting in Khayelitsha, South Africa. *PLoS One.* 5, e13901 (2010).
56. Victor T, de Haas P, Jordaan A, van der Spuy, GD, Richardson M, van Soolingen D. Molecular characteristics and global spread of *Mycobacterium tuberculosis* with a Western Cape F11 genotype. *J Clin Microbiol.* 42, 769–772 (2004).
57. Strauss O, Warren R, Jordaan A, Streicher E, Hanekom M, Falmer A. Spread of a low-fitness drug-resistant *Mycobacterium tuberculosis* strain in a setting of high human immunodeficiency virus prevalence. *J Clin Microbiol.* 46, 1514–1516 (2008).
58. Shah NS, Wright A, Bai GH, et al. Worldwide emergence of extensively drug-resistant tuberculosis. *Emerg. Infect. Dis.* 13(3), 380–387 (2007).
59. Prevention C for DC and. Emergence of *Mycobacterium tuberculosis* with extensive resistance to second-line drugs worldwide, 2000 –2004. .
60. Lim J, Gandhi N, Mthiyane T, Mlisana K, Moodley J, Jaglal P. Incidence and Geographic Distribution of Extensively Drug-Resistant Tuberculosis in KwaZulu-Natal Province, South Africa. *PLoS One.* 10, e0132076 (2015).
61. WHO. “Totally Drug-Resistant TB ”.WHO consultation on the diagnostic definition and treatment options. .
62. Mukherjee JSJ, Rich MLM, R. SAA, et al. Programmes and principles in treatment of multidrug-resistant tuberculosis. *Lancet.* 363, 474–481 (2004). Available from: <http://www.sciencedirect.com/science/article/pii/S0140673604154962>.

63. Ahuja SD, Ashkin D, Avendano M, *et al.* Multidrug Resistant Pulmonary Tuberculosis Treatment Regimens and Patient Outcomes: An Individual Patient Data Meta-analysis of 9,153 Patients. *PLoS Med.* 9(8) (2012).
64. National Health Laboratory Services. National Institute for Communicable Diseases annual report 2009. Available from: http://www.nicd.ac.za/assets/files/Annual_report_2009.pdf.
65. Blanchard J. Mechanisms of drug resistance in Mycobacterium Tuberculosis. *Annu Rev Biochem.* 65, 215–39 (1996).
66. Somoskovi A, Parsons L, Salfinger M. The molecular basis of resistance to isoniazid , rifampin , and pyrazinamide in Mycobacterium tuberculosis. *Respir Res.* 2, 164–8 (2001).
67. Telenti A, Imboden P, Marchesi F, *et al.* Detection of rifampicin-resistance mutations in Mycobacterium tuberculosis. *Lancet.* 341(8846), 647–651 (1993).
68. Nachega JB, Chaisson RE. Tuberculosis Drug Resistance: A Global Threat. *Clin Infect Dis.* 36, S24–S30 (2003).
69. Heep M, Rieger U, Beck D, Lehn N. Mutations in the beginning of the rpoB gene can induce resistance to rifamycins in both Helicobacter priori and Mycobacterium tuberculosis. . *Antimicrob Agents Chemother.* 44(4), 1075–7 (2000).
70. Aristoff PA, Garcia GA, Kirchhoff PD, Showalter HD. Rifamycins--obstacles and opportunities. *Tuberc.* 90(2), 94–118 (2010). Available from: <http://www.ncbi.nlm.nih.gov/pubmed/20236863>.
71. Ramo S, Ng C, Anderson H, *et al.* Synergistic Drug Combinations for Tuberculosis Therapy Identified by a Novel High-Throughput Screen □ †. 55(8), 3861–3869 (2011).
72. Rothstein DM. Rifamycins, alone and in combination. *Cold Spring Harb. Perspect. Med.* 6(7) (2016).
73. Amaral L, Viveiros M. Why thioridazine in combination with antibiotics cures extensively drug-resistant Mycobacterium tuberculosis infections. *Int J Antimicrob Agents.* 39(5), 376–80 (2012).
74. Fox W, Ellard GA, Mitchison DA. Studies on the treatment of tuberculosis undertaken by the British Medical Research Council Tuberculosis Units, 1946–1986, with relevant subsequent publications. *Int J Tuberc Lung Dis.* 3, S231–S279 (1999).
75. Selkon JB, Devadatta S, Kulkarni KG, *et al.* The emergence of Isoniazid-resistant cultures in patients with. *Bull. World Health Organ.* 31, 273–294 (1964).
76. Escalante P, Ramaswamy S, Sanabria H, *et al.* Genotypic characterization of drug-resistant Mycobacterium tuberculosis isolates from Peru. *Tuber Lung Dis.* 79(2), 111–8 (1998). Available from: <http://www.ncbi.nlm.nih.gov/pubmed/10645449>.
77. Lahiri N, Shah RR, Layre E, *et al.* Rifampin Resistance Mutations Are Associated with Broad Chemical Remodeling of Mycobacterium tuberculosis. *J. Biol. Chem.* 291(27), 14248–14256 (2016). Available from: <http://www.ncbi.nlm.nih.gov/pubmed/27226566> <http://www.pubmedcentral.nih.gov/articlerender.fcgi?artid=PMC4933180> <http://www.jbc.org/lookup/doi/10.1074/jbc.M116.716704>.

78. Ramaswamy S, Musser JM. Molecular genetic basis of antimicrobial agent resistance in *Mycobacterium tuberculosis*: 1998 update. *Tuber Lung Dis.* 79(1), 3–29 (1998). Available from: <http://www.ncbi.nlm.nih.gov/pubmed/10645439>.
79. Iseman MD. Treatment of multidrug- resistant tuberculosis. *N Engl J Med.* 329, 784–91 (1993).
80. Kritski AL, R de JLS, Andrade MK *et al.* Re-treatment tuberculosis cases: factors associated with drug resistance and adverse outcomes. *Chest.* 111, 1162–7 (1997).
81. Hong Kong Chest Service British Medical Research Council. Controlled trial of 6-month and 9-month regimens of daily and intermittent streptomycin plus isoniazid plus pyrazinamide for pulmonary tuberculosis in Hong Kong. *Am Rev Respir Dis.* 115, 727–35 (1977).
82. Artsimovitch I, Vassylyeva MN, Svetlov D, *et al.* Allosteric Modulation of the RNA Polymerase Catalytic Reaction Is an Essential Component of Transcription Control by Rifamycins. *Cell.* 122, 351–363 (2005).
83. Campbell EA, Korzheva N, Mustaev A, *et al.* Structural Mechanism for Rifampicin Inhibition of Bacterial RNA Polymerase. *Cell.* 104, 901–912 (2001).
84. Aristoff PA, Garcia GA, Kirchhoff PD, *et al.* Rifamycins - Obstacles and opportunities. *Tuberculosis.* 90(2), 94–118 (2010).
85. Borukhov S, Nudler E. RNA polymerase holoenzyme: Structure, function and biological implications. *Curr. Opin. Microbiol.* 6(2), 93–100 (2003).
86. Murakami KS, Darst SA. Bacterial RNA polymerases: The whole story. *Curr. Opin. Struct. Biol.* 13(1), 31–39 (2003).
87. Young BA, Gruber TM, Gross CA. Views of transcription initiation. *Cell.* 109(4), 417–420 (2002).
88. Gomez JE, Chen JM, Bishai WR. Sigma factors of *Mycobacterium tuberculosis*. *Tuber Lung Dis.* 78, 175–83 (1997).
89. Lin W, Mandal S, Degen D, *et al.* Structural Basis of *Mycobacterium tuberculosis* Transcription and Transcription Inhibition. *Mol. Cell.* 66(2), 169–179 (2017).

CHAPTER 3

3 Introduction to computational chemistry and molecular modelling

3.1 Introduction

Computational chemistry is a sub-specialty of chemistry. It is also referred to as molecular modelling. It incorporates computational techniques to investigate and analyze biochemical or chemical problems from an atomistic and molecular viewpoint. Computational chemistry investigates the three-dimensional molecular structure, molecular dynamics and flexibility, physical properties and biological activities such as protein folding, stability and conformation of biological molecules. Computational research generates data that augments experimental studies using techniques that are less expensive and generates results within a shorter time frame. As a result, molecular modelling has been prominent in recent years in the discovery, design and development of new drug molecules. It increases the effectiveness of rational drug design process by feeding on the findings of experimental research to generate lead compounds and giving insights into their possible adverse effects. Of the three basic computational chemistry methods, molecular dynamics was largely employed in the research for this thesis. Molecular dynamics gave insights on the conformational insights of macromolecules interacting with small molecules bound to it. This chapter mainly describes the computational theories that support molecular mechanics, molecular dynamics and post analytic tools as applied in this present study.

3.2 Quantum Mechanics

Quantum mechanics is a branch of classical physics that defines molecules based on interactions between nuclei and electrons, and molecular geometry in terms of minimum energy arrangements of nuclei [1,2]. Using wave functions, quantum mechanics describes microscopic systems by completely characterizing all the physical properties of the system [2]. Nuclei and corresponding electrons of the systems are arranged in a three-dimensional space [2]. The electrons are then mapped using the continuous electronic density method and the energetics measured is solved by the Schrödinger equation [2].

3.2.1 The Schrödinger Wave Equation

The Schrödinger equation forms the bases of all approximations in quantum mechanics [3]. The equation is based on a model of an atom that was proposed by Erwin Schrödinger an Austrian physician in 1926, in which he used mathematical equations to describe the probability of locating an electron at an exact path [3]. In expanding on Neil Bohr's atom model, Schrödinger depicted the model as a nucleus that is surrounded by an electron cloud of high and low densities [2,4]. Schrödinger was able to postulate an energy relationship of the time independent wave equation by merging the classical differential equation which defines the profile of a simple harmonic standing wave and the De'Broglie's relation between matter and waves [4] . There is also a time dependent Schrödinger equation [1,5] which is the largely used one of the two. It defines the Hamiltonian operator as the sum of the kinetic energy and the potential energy. The general forms of the Schrödinger equation is as follows:

$$\mathbf{H}\Psi = \mathbf{E}\Psi \quad (\text{Eq. 3.2.1.1})$$

Where, H denotes the Hamiltonian operator, Ψ denotes the wave function (or eigenfunction) and \mathbf{E} , denoting the energy of the system also referred to as the operator energy eigen value [2,5]. This description is a probabilistic description of electron behavior. In order to replicate a relevant physical model of Schrödinger's equation, the wave function must be continuous, normalizable single valued and antisymmetric relative to electrons interchange [6]. The molecular Hamiltonian operator is derived from the sum of the atom's total potential energy (V) and the kinetic energy (T) represented as:

$$\mathbf{H} = \mathbf{V} + \mathbf{T} \quad (\text{Eq. 3.2.1.2})$$

When considering particles as point masses, while neglecting relativistic effects, the Hamiltonian will therefore constitute all the kinetic and potential energy operators for all the electrons and nuclei in a molecule. An advanced Hamiltonian is mathematically expressed as follows:

$$\mathbf{H} = \left[-\frac{\hbar^2}{8\pi^2} \sum_i \frac{1}{m_j} \left(\frac{\partial^2}{\partial x^2} + \frac{\partial^2}{\partial y^2} + \frac{\partial^2}{\partial z^2} \right) + \sum_i \sum_j \left\langle \frac{e_i e_j}{r_{ij}} \right\rangle \right] \quad (\text{Eq. 3.2.1.3})$$

Involving a multitude of mathematical equations, the Schrödinger equation is unable to be solved for a molecular system whose number of atoms may range in thousands [7–9]. A compensation for this challenge for molecular systems is the Born-Oppenheimer approximation

3.2.2 Born-Oppenheimer Approximation

The Born-Oppenheimer Approximation addresses the challenges and limitations of the Schrödinger equation as a result; it is one of the most essential approximations in molecular quantum mechanics [10]. The Born-Oppenheimer Approximation relies on the assumption that the motion of electrons and nuclei can be separated [11]. It was developed by Max Born and J. Robert Oppenheimer in 1927 after the publication of the Schrödinger equation, to illustrate how the nuclear motion in a molecule can be determined as a function of its electronic motion [11]. This approximation permits the Schrödinger's equation to be divided and expressed as an 'electronic' equation and a nuclear equation. Electrons have a lighter weight than nuclei; as a result, they have an increased velocity [10]. The difference in weight between the electrons and nuclei is accounted for by the Born-Oppenheimer approximation, and based on this difference, the electrons can therefore almost instantaneously respond to nuclei displacement [11]. Distribution of electrons within a molecular system is therefore defined by the location of the nuclei [12,13]. Hence as an alternative to solving the Schrödinger equation for every particle at the same time, the nuclear kinetic energy operator is ignored due to the fixed position of the nuclei while the equation is solved for electrons in the static electrical potential that arises from the nuclei in that arrangement [13–15].

The difference in velocities of the nuclei and electrons allow for the Born-Oppenheimer approximation to be applied, minimizing the complexity of the wave function of the Hamiltonian equation [15]. The simplified wave function of the Hamiltonian is mentioned as below:

$$H = -\frac{\hbar^2}{2m_e} \sum_i \nabla_i^2 - \frac{\hbar^2}{2} \sum_A \frac{1}{M_A} \nabla_A^2 - \sum_A \sum_i \frac{Z_A e^2}{r_{Ai}} + \sum_i \sum_{j>i} \frac{e^2}{r_{ij}} + \sum_A \sum_{B>A} \frac{Z_A Z_B e^2}{R_{AB}} \quad (\text{Eq. 3.2.2.1})$$

Where A and B denotes the nuclei, while i and j represent the electrons. M_A represents the nucleus A mass while m_e denotes an electron mass. R_{AB} represents a nuclei A and B inter-distance with r_{ij} being the distance between i and j electrons. Z_A is nucleus A charge while r_{Ai} represents nucleus A and electron i inter-distance.

Born-Oppenheimer approximation when applied minimizes the complexity of the Hamiltonian and the wave function due to differences between electron and nuclei velocities [14]. The instantaneous response of electrons to nuclear motions results in the wave simplified as follows:

$$\boldsymbol{\psi}(\mathbf{r}_{elec}) = \boldsymbol{\psi}(\mathbf{r}_{elec})(\mathbf{r}_{nucl}) \quad (\text{Eq. 3.2.2.2})$$

Which is subsequently changed to

$$\mathbf{H}_{EN}\boldsymbol{\psi}(\mathbf{r}_{el}) = \mathbf{E}_{EN}\boldsymbol{\psi}(\mathbf{r}_{el}) \quad (\text{Eq. 3.2.2.3})$$

Where \mathbf{H}_{EN} symbolizes a difference between terms based on their dependence on fixed nuclear positions (\mathbf{V}_{NN}) or their dependence on the non-fixed electron positions (\mathbf{H}_{el}). An energy term \mathbf{E}_{EN} is integrated which is derived from two sources; one being the fluctuating electron co-ordinates \mathbf{E} and fixed nuclear co-ordinates \mathbf{N} :

$$(\mathbf{H}_{el} + \mathbf{V}_{NN}) \boldsymbol{\psi}(\mathbf{r}_{el}) = \mathbf{E}_{EN}\boldsymbol{\psi}(\mathbf{r}_{el}) \quad (\text{Eq. 3.2.2.4})$$

It is important to note that Born-Oppenheimer approximation exhibits more accuracy when applied to electrons in ground states rather than those in excited states [2,10]. Upon solving the equation, it enables the construction of molecular potential energy curve and a potential energy surface of a polyatomic molecule [10]. It also allows for the identification and assessment of the equilibrated conformations for a given molecule with the lowest point on the surface [10,15].

3.2.3 Potential Energy Function

As a mathematical function, potential energy surface graphically portrays the energy of a molecule as a function of its geometry [16]. Thus it determines the vibrational motion of molecules relative to the position of the nuclei in a chemical reaction [16]. The concept of potential energy stems from the Born-Oppenheimer approximation in which variations in mass and magnitude of the velocity between electrons and nuclei is understood as the potential of atoms movement within a molecule which collide with each other, referred to as the adiabatic motion [15,16]. As displayed in the figure below, high potential energy regions display specifies a high-energy nuclear arrangements or molecular

conformations and whereas a low energy regions signifies low nuclear energy conformation and can be applied in computational chemistry for this purpose [2].

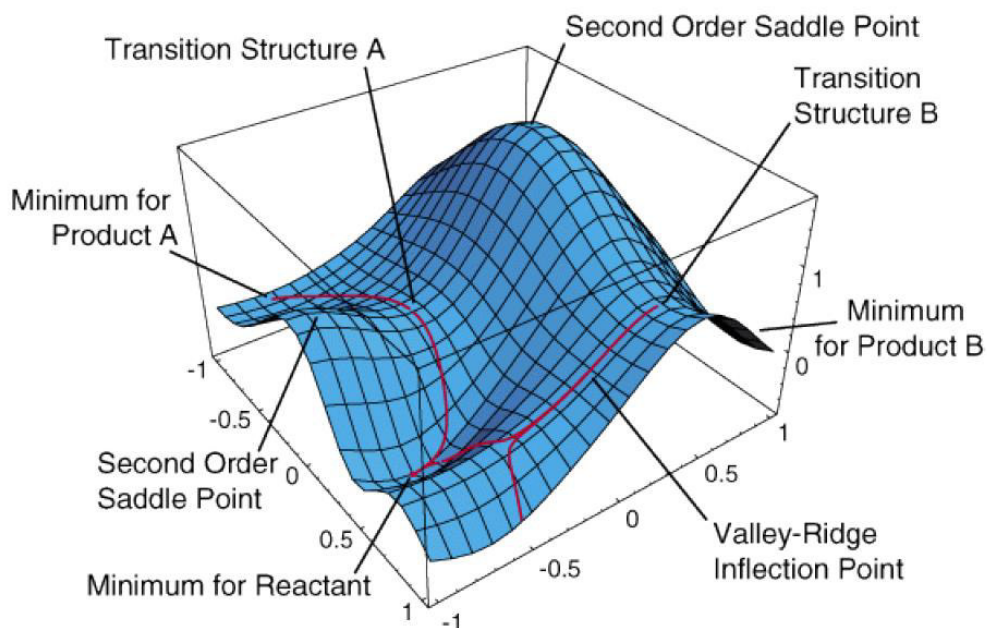


Figure 3.1: A graphical representation of a two-dimensional potential energy surface [17].

3.3 Molecular Mechanics

Molecular mechanics (MM) enables the molecular dynamics computations on large molecules by incorporating potential energy [18]. In modelling molecular systems, MM applies coulomb potential or harmonic oscillator [2,19]. It describes the molecular systems in bonded atoms, which have been distorted from some idealized geometry due to nonbonded van der Waals and Coulombic interactions [5,21]. MM incorporates a classical type models to predict the energy of a molecule as a function of its conformation [5]. By so doing, it enables the predictions of equilibrium geometries and transition states and also allows the prediction of relative energies between conformers or between different molecules [5]. As an alternative to quantum mechanics, MM are the methods of choice for protein simulations and adheres to the Newtonian laws of classical mechanisms and are essential in the study of conformational flexibility [19]. MM expresses the energy of a molecule as a function of its resistance toward bond stretching, atom crowding and bond bending and to use this energy equation

to find the bond angles, lengths and dihedrals corresponding to the minimum-energy geometry – or more precisely, to the various probable potential energy surface minima [21,22]. Nonetheless MM are appropriate for bond-breaking reactions just like most *ab initio* methods [23]. MM or the force-field method is mathematically described as follows;

$$E_{tot} = E_{str} + E_{bend} + E_{tors} + E_{vdw} + E_{elec} \quad (\text{Eq. 3.3.1})$$

Where,

E_{tot} = total energy,

E_{str} = bond-stretching energy,

E_{bend} = angle-bending energy

E_{tors} = torsional energy,

E_{vdw} = van der Waals energy

E_{elec} = electrostatic energy.

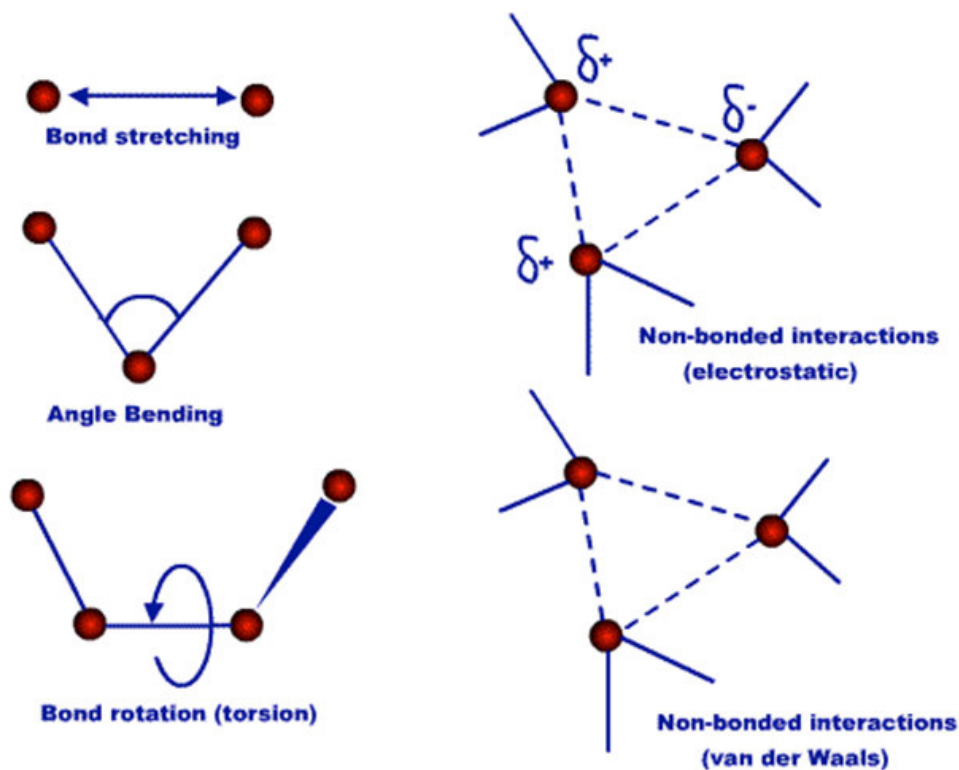


Figure 3.2: Diagrammatical depiction of bonded and non-bonded interactions acting in molecular motion [24].

3.4 Quantum Mechanics/Molecular Mechanics (QM/MM)

Most recently, the combination of both quantum mechanical and molecular mechanical methods [25,26] to form a hybrid of the two has rapidly gained prominence as a viable approach for the study of biomolecular mechanisms [26–28]. The underlining postulation that bonds are never created or broken renders MM inappropriate for studying the mechanisms of reaction for biomolecular systems [30]. QM methods on the other hand have huge computational cost, exhaustive, making calculations on the scale of entire solvated proteins currently obstinate [30,31]. QM/MM as a hybrid concept basically employs algorithms that blend the description accuracy of QM and the characteristic low computational cost of MM [32]. The technique of QM/MM encompasses two steps-wise domains, a QM and an MM phase [33]. In the QM phase, the reactive domain, which includes ligands and amino acids, are treated with QM techniques, which defines the electronic structures of molecules [32]. This MM phase defines interactions between atoms by incorporating a force field which acts as a potential energy function [31,34]. Amidst the notable advantages of hybrid QM/MM method over QM and MM, it may not be appropriate for every structure-based drug design study; hence further exploration of the technique may be required [32].

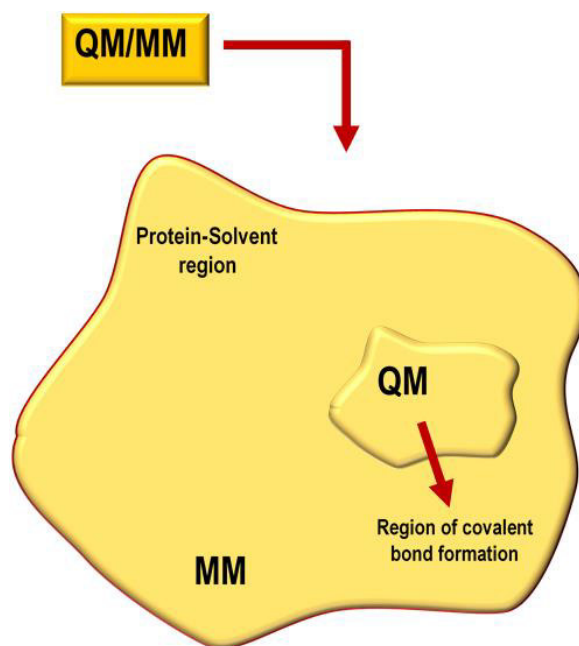


Figure 3.3: Characterization of the QM/MM components.

3.5 Force-Fields

Force fields for MD simulations should be compatible with biomolecules or at least proteins that are enclosed in a biologically relevant environment like an aqueous solution, must support drug-like molecules in solution phase and should be explicitly parameterized to reproduce intermolecular interaction [19]. As a mathematical function with set parameters, a force field can be used to describe the energy associated with the conformation of molecule [35]. The force field used to parameterize the *Mtb* RNAP protein in the studies reported in this thesis is the AMBER [36] force field while the GAFF were also used to interpret the ligands. Other commonly used force fields include CHARMM [37], GROMOS [38], OPLS-AA [39] and ENCAD [40,41]. Most force fields applied in MD simulation of proteins are harmonic motions in nature, along with a description of bond lengths and angles [35]. The main variations between the various force fields result come from the varied approaches to obtain the individual parameters, however, they largely yield similar findings which corroborate with experimental results [42].

3.6 Molecular Dynamics

Over the year's biological assays, crystallographic studies, and Nuclear Magnetic Resonance Spectroscopy have been employed to credibly demonstrate the crucial role of protein flexibility in ligand binding and to also give insights on biomolecular structures [43]. However, the notably huge expense, extensive computational labor and the static view portrayal of biomolecular systems prompted the search for alternative approaches such as computational techniques. Developed in the later part of the 1970s [44], Molecular Dynamics, has proven to be a viable technique [45,46] by reducing the computational complexity and cost associated with existing techniques through the incorporation of simple Newtonian equations based approximations in the prediction of atomic motions [45]. There are two main types of simulation techniques, namely, Monte Carlo and Classical MD simulation amidst other recently synthesized techniques [26]. The Monte Carlo method relies on probabilities by creating large numbers of configurations and transitioning from one state to the other in a specific statistical manner [47]. In an Classical MD simulation, trajectories of atoms and molecules are generated by mathematically solving the Newton's equation of motion for a system of interacting particles, in which forces between the particles and potential energy are defined by molecular mechanics force fields [48]. Trajectories specifies the particle position and velocity varies with time [49]. The preference of Classical MD to Monte Carlo is attributed to its ability to permit

time-dependent response and rheological properties amongst other dynamical properties [43]. In performing a Classical MD, the positions and velocities of particles, the force field and boundary conditions must be initially considered. The mathematical equation employed is described as follows;

$$\mathbf{F}_i = m_i \frac{d^2 \mathbf{r}_i(t)}{dt^2} \quad (\text{Eq. 3.6.1})$$

Where $\mathbf{r}_i(t)$ is the particle position vector is represented as $\mathbf{r}_i(t)$. The time-evolution is represented as t , while m denotes is the mass of the particle. The interacting force on the particle is represented as \mathbf{F}_i .

3.7 Molecular Dynamics Post analysis

A data set consisting of the coordinates and velocities of particles in a simulated system, referred to as MD trajectories [50] are generated after a given period of simulation. These trajectories can be analyzed using various post-dynamic computational tools. For the purpose of the studies reported in this thesis, post-dynamics analyses tools employed enabled the determination of; relative binding free energies, three-dimensional conformations and configurations, and to determine the state of thermodynamic equilibrium of the biomolecular system [51].

3.7.1 Systems' stability

3.7.1.1 Convergence

Convergence of a given system is attained when the system assumes a state of equilibrium [52,53]. This state of equilibrium is graphically depicted when the curve assumes a plateau shape [54]. As an empirical description of protein dynamics, convergence is based on fluctuation of bond angles and the vibrations of bond angles during protein unfolding [52]. Convergence vouch the accuracy and reproducibility of a given MD trajectory [52,55] and also gives insights on whether the simulated system achieves an energetically stable conformation.

3.7.1.2 Root Mean Square Deviation (RMSD)

After a molecular dynamic simulation, trajectories generated can be analyzed to unravel the structural equilibrium of a given system by calculating the RMSD [56]. RMSD is calculated as the spatial difference between two static structures of the same trajectory [49]. Mathematically, it is expressed as follows;

$$RMSD = \left(\frac{\sum_N (R_i - R_i^0)^2}{N} \right)^{\frac{1}{2}} \quad (\text{Eq. 3.7.1.2.1})$$

N represents the total number of atoms in the complex. R_i denotes the vector position of the $C\alpha$ atom in the reference conformation of particle i. This is calculated after aligning the structure to the initial conformation (O) using the least square fitting.

The number of conformations for a given simulated biomolecular system can be deduced from how long that system took to achieve equilibration, an information that can be obtained from RMSD calculations [54]. RMSD may also unveil biomolecules that exhibit ‘open’ and ‘close’ conformations [54].

3.7.1.3 Radius of Gyration (RoG)

Radius of Gyration as a post MD simulation analysis tool can be used to give insights into the compactness of the tertiary structure of a biomolecule [57,58]. The Radius of Gyration in a protein is calculated as the root mean square distance of the atoms from their common center of gravity [59]. RoG can unravel how folded or unfolded a biomolecule can be over a given simulation period [59]. The overall stability of a biomolecular structure over a given simulation period can also be deduced from the calculated RoG. Mathematically, RoG is calculated as follows;

$$r^2_{gyr} = \frac{(\sum_{i=1}^n W_i (r_i - r^-)^2)}{\sum_{i=1}^n W_i} \quad (\text{Eq. 3.7.1.3.1})$$

The r_i represents the position of the atom i^{th} atom while r^- is the center weight of atom i.

3.7.2 Conformational dynamics of System

3.7.2.1 Root mean square fluctuation

The fluctuation of the individual residues of a protein about an average position within a given

molecular simulation period is referred to the root mean square fluctuation (RMSF) [60]. RMSF unveils insights into the flexibility of various regions of the protein that parallels with the crystallographic β -factors [60]. RMSF is mathematically calculated as follows;

$$\mathbf{sRMSF}_i = \frac{(\mathbf{RMSF}_i - \overline{\mathbf{RMSF}})}{\sigma(\mathbf{RMSF})} \quad (\text{Eq. 3.7.2.1.1})$$

\mathbf{RMSF}_i represents the RMSF of the i^{th} residue, from which the average RMSF is subtracted. This is then divided by the RMSF's standard deviation to yield the resultant standardized RMSF.

3.7.2.2 Binding free Energy Calculations

The estimation of binding free energy calculations has become a very essential computational technique for understanding ligand-receptor interactions in drug design, determination of protein structures and protein-protein complex studies [61,62]. The most popular approaches employed in the estimation of the binding free energies of small ligands to biological macromolecules is the molecular mechanics energies combined with the Poisson–Boltzmann or generalized Born and surface area continuum solvation (MM/PBSA and MM/GBSA) methods [63–69]. Both techniques are employed after MD simulations of ligand-receptor complexes in which energies are averaged over from snapshots generated from MD trajectories to estimate the absolute total binding free energies [64]. They are typically based on molecular dynamics simulations of the receptor–ligand complex and are therefore transitional in both accuracy and computational effort between empirical scoring and strict alchemical perturbation methods [63]. MM/PBSA and MM/GBSA methods have been applied successfully to study a wide variety of problems [62,70,71]. For each snapshot, binding free energy is calculated for each molecular component (complex, receptor, and ligand), and the total ligand binding free energy is estimated as follows:

$$\Delta G_{\text{bind}} = G_{\text{complex}} - G_{\text{receptor}} - G_{\text{ligand}} \quad (1) \quad (\text{Eq. 3.7.2.2.1})$$

$$\Delta G_{\text{bind}} = E_{\text{gas}} + G_{\text{sol}} - T\Delta S \quad (2) \quad (\text{Eq. 3.7.2.2.2})$$

$$E_{\text{gas}} = E_{\text{int}} + E_{\text{vdw}} + E_{\text{ele}} \quad (3) \quad (\text{Eq. 3.7.2.2.3})$$

$$G_{\text{sol}} = G_{\text{GB/PB}} + G_{\text{SA}} \quad (4) \quad (\text{Eq. 3.7.2.2.4})$$

$$G_{\text{SA}} = \gamma \text{SASA} \quad (5) \quad (\text{Eq. 3.7.2.2.5})$$

E_{gas} shows the gas-phase energy; E_{int} is internal energy; while E_{ele} and E_{vdw} represents the electrostatic and Van der Waals interactions, respectively. The solvation free energy, denoted by G_{sol} represents the solvation free energy and can be decomposed into polar and nonpolar contribution states. The polar solvation contribution, $G_{\text{GB/PB}}$, is determined by solving the GB/PB equation, whereas, G_{SA} , the nonpolar solvation contribution is estimated from the solvent accessible surface area (SASA) determined using a water probe radius of 1.4 Å. T and S correspond to temperature and total solute entropy, respectively.

3.7.2.3 Residue Interaction Network

The exploration of the amino acids that make up a protein as well the amino acid-amino acid interactions that exist in the protein is an essential approach in unveiling very important molecular insight into the structural and functional dynamics of the protein [72]. Residue Interaction Network (RIN) as computational post-dynamics analysis tool makes it possible to visualize and comprehend the complex inter-residue interaction [70,71]. In the studies reported in this thesis, RIN was employed to unravel the impact of single active site mutation on the overall conformational and structural dynamics of *Mtb* when singly bound with Rifampin and upon co-binding with Rifampin and DAAP1. In the visual display of each RIN, amino acid were each represented by a node while inter-residue interactions were represented by edges [73]. Using plugins such as RINalyzer [73], Cytoscape [74] and NetworkAnalyser [75]. RIN was performed displaying all the various amino acid and their respective interactions. Visualization was done by integrating Cytoscape with UCSF chimera.

Reference

1. Rigby M. Physical chemistry, 3rd edition - ATKINS,PW,. *Nature*. 319, 820–820. (1986).
2. Jensen F. Introduction to Computational Chemistry. 3rd edition. John Wiley and Sons,England Available from:https://books.google.com/books/about/Introduction_to_Computational_Chemistry.html?id=RDIG48UcZfYC&pgis=1.
3. Schrödinger E. An undulatory theory of the mechanics of atoms and molecules. *Phys. Rev.* 28(6), 1049–1070 (1926).
4. Schleich WP, Greenberger DM, Kobe DH, Scully MO. Schrodinger equation revisited. *Proc. Natl. Acad. Sci.* 110(14), 5374–5379 (2013). Available from: <http://www.pnas.org/cgi/doi/10.1073/pnas.1302475110>.
5. Lewars EG. Computational Chemistry. Available from: <http://link.springer.com/10.1007/978-90-481-3862-3>.
6. Young DC. Chemistry Computational Chemistry A Practical Guide for Applying Techniques to Real-World Problems . Available from: <http://books.google.com/books?id=-pn8K53IUqgC&pgis=1>.
7. Nakatsuji H. Scaled Schrodinger equation and the exact wave function. *Phys. Rev. Lett.* 93(3), pp.30403–1. (2004).
8. Bahrami M et al. The Schrodinger-Newton equation and its foundations. *New J. Phys.* (16), pp.1–17 (2014).
9. Barde NP et al. Deriving time dependent Schrödinger equation from Wave-Mechanics, Schrödinger time independent equation, classical and Hamilton-Jacobi equations. *Leonardo Electron. J. Pract. Technol.* 14(26), pp.31–48 (2015).
10. Jecko T. On the mathematical treatment of the born-Oppenheimer approximation. *J. Math. Phys.* 55(5) (2014).
11. Born M, Oppenheimer R. Quantum theory of the molecules. *Ann. d. Phys.* , 457–484 (1927).
12. Liehr AD. On the use of the Born-Oppenheimer approximation in molecular problems. *Ann. Phys. (N. Y).* 1(3), pp.221–232 (1957). Available from: <http://www.sciencedirect.com/science/article/pii/000349165790009X>.
13. Ochkur VI. The Born-Oppenheimer method in the theory of atomic collisions. *Sov. Phys. JETP.* 18(2), p.503 (1965).
14. Huang XL, Yi XX. Born-Oppenheimer approximation in open systems. *Phys. Rev. A.* 80(3), 7 (2009). Available from: <http://arxiv.org/abs/0905.2741>.
15. Matsika S. The Born-Oppenheimer approximation. *J. Chem. Phys.* 133(22), 224103 (2010). Available from: <http://www.ncbi.nlm.nih.gov/pubmed/21241076>.
16. Truhlar DG. Potential Energy Surfaces. *Encycl. Phys. Sci. Technol.* 13, 9–17 (2001).
17. Available from: <http://www.chem.wayne.edu/~hbs/chm6440/PES>.

18. Maseras F, Morokuma K. IMOMM: A new integrated ab initio + molecular mechanics geometry optimization scheme of equilibrium structures and transition states. *J. Comput. Chem.* 16(9), pp.1170–1179 (1995). Available from: <http://dx.doi.org/10.1002/jcc.540160911>
19. Vanommeslaeghe K et al. Molecular mechanics. *Curr. Pharm. Des.* 20(20), pp.3281–92. (2014). Available from: <http://www.ncbi.nlm.nih.gov/pubmed/23947650>
20. Hehre WJ. A Guide to Molecular Mechanics and Quantum Chemical Calculations. .
21. Boeyens J. Molecular mechanics: theoretical basis, rules, scope and limits. *Coord. Chem. Rev.* 212(1), 3–10 (2001).
22. Zimmer M. Are classical molecular mechanics calculations still useful in bioinorganic simulations? *Coord. Chem. Rev.* 253(5–6), 817–826 (2009).
23. Senn HM, Thiel W. QM/MM methods for biomolecular systems. *Angew. Chem. Int.* (48), 1198–1229 (2009).
24. Molecular Mechanics. Indipedia India's Wikipedia OSDD. .
25. Levitt M. A simplified representation of protein conformations for rapid simulation of protein folding. *J. Mol. Biol.* 104(1), 59–107 (1976).
26. Adcock SA, McCammon JA. Molecular dynamics: Survey of methods for simulating the activity of proteins. *Chem. Rev.* 106(5), 1589–1615 (2006).
27. Shurki A, Warshel A. Structure/function correlations of proteins using MM, QM/MM, and related approaches: Methods, concepts, pitfalls, and current progress. *Adv. Protein Chem.* 66, 249–313 (2003).
28. Wang W, Donini O, Reyes C, Kollman P. BIOMOLECULAR SIMULATIONS: Recent Developments in Force Fields, Simulations of Enzyme Catalysis. *Annu. Rev. Biophys. Biomol. Struct.* (2001). Available from: <http://arjournals.annualreviews.org/doi/abs/10.1146/annurev.biophys.30.1.211>
29. Duarte F, Amrein BA, Blaha-Nelson D, Kamerlin SCL. Recent advances in QM/MM free energy calculations using reference potentials. *Biochim. Biophys. Acta.* 1850(5), 954–65 (2015).
30. Senn HM, Thiel W. QM/MM Methods for Biomolecular Systems. *Angew. Chemie Int. Ed.* 48(7), 1198–1229 (2009).
31. Sauer J, Sierka M. Combining quantum mechanics and interatomic potential functions in ab initio studies of extended systems. *J. Comput. Chem.* 21(16), 1470–1493 (2000).
32. Lu X, Fang D, Ito S, Okamoto Y, Ovchinnikov V, Cui Q. QM/MM free energy simulations: recent progress and challenges. *Mol. Simul.* 42(13), 1056–1078 (2016).
33. Bornemann F a., Nettelsheim P, Schütte C. Quantum-classical molecular dynamics as an approximation to full quantum dynamics. *J. Chem. Phys.* 105(3), 1074–1083 (1996). Available from: <http://scitation.aip.org.globalproxy.cvt.dk/content/aip/journal/jcp/105/3/10.1063/1.471952>

34. Honarparvar B, Govender T, Maguire GEM, Soliman MES, Kruger HG. Integrated approach to structure-based enzymatic drug design: Molecular modeling, spectroscopy, and experimental bioactivity. *Chem. Rev.* 114(1), 493–537 (2014).
35. González MA. Force fields and molecular dynamics simulations. *Collect. SFN.* 12, 169–200 (2011).
36. Case D a., T.E. Cheatham I, Darden T, *et al.* The Amber biomolecular simulation programs. *J. Comput. Chem.* 26(16), 1668–1688 (2005).
37. Brooks BR *et al.* CHARMM: A program for macromolecular energy, minimization, and dynamics calculations. *J. Comput. Chem.* 4(2), pp.187–217 (1983).
38. Christen M, Hünenberger PH, Bakowies D, *et al.* The GROMOS software for biomolecular simulation: GROMOS05. *J. Comput. Chem.* 26(16), 1719–1751 (2005).
39. Phillips JC, Braun R, Wang W, *et al.* Scalable molecular dynamics with NAMD. *J. Comput. Chem.* 26(16), 1781–1802 (2005).
40. Levitt M, Hirshberg M, Sharon R, Daggett V. Potential energy function and parameters for simulations of the molecular dynamics of proteins and nucleic acids in solution. *Comput. Phys. Commun.* 91(1–3), 215–231 (1995).
41. Monticelli L, National F. Force fields for classical molecular dynamics. *Methods Mol. Biol.* 924, pp.197–213 (2013). Available from: <http://link.springer.com/10.1007/978-1-62703-017-5>.
42. Durrant J, McCammon JA. Molecular dynamics simulations and drug discovery. *BMC Biol.* 9(71) (2011).
43. Nair PC, Miners JO. Molecular dynamics simulations: from structure function relationships to drug discovery. *insilico Pharmacol.* 2(4), 1–4 (2014).
44. McCammon JA, Gelin BR, Karplus M. Dynamics of folded proteins. *Nature.* 267(5612), 585–590 (1977). Available from: <http://www.nature.com/doi/10.1038/267585a0>.
45. Clementi E. Computational chemistry: Attempting to simulate large molecular systems. In: *Theory and Applications of Computational Chemistry.* , 89–114 (2005).
46. Weinhold F. Chemistry. A new twist on molecular shape. *Nature.* 411(6837), 539–41 (2001). Available from: <http://dx.doi.org/10.1038/35079225>.
47. Earl DJ, Deem MW. Monte Carlo simulations. *Methods Mol. Biol.* 443, 25–36 (2008). Available from: http://eutils.ncbi.nlm.nih.gov/entrez/eutils/elink.fcgi?dbfrom=pubmed&id=18446280&retmode=ref&cmd=prlinks%5Cnpapers3://publication/doi/10.1007/978-1-59745-177-2_2.
48. Cornell WD, Cieplak P, Bayly CI, *et al.* A second generation force field for the simulation of proteins, nucleic acids, and organic molecules. *J. Am. Chem. Soc.* 117(19), 5179–5197 (1995). Available from: <http://pubs.acs.org/doi/pdf/10.1021/ja00124a002%0Ahttp://pubs.acs.org/doi/abs/10.1021/ja00124a002>.
49. Parrill AL, Lipkowitz KB. Reviews in Computational Chemistry.
50. Cheatham TE, Kollman PA. Molecular dynamics simulation of nucleic acids. *Annu Rev Phys*

Chem. 51, 435–471 (2000).

51. Karplus M, McCammon JA. Molecular dynamics simulations of biomolecules. *Nat. Struct. Biol.* 9(9), 646–652 (2002). Available from: <http://www.nature.com/doi/10.1038/nsb0902-646>.

52. Galindo-Murillo R, Roe DR, Cheatham TE. Convergence and reproducibility in molecular dynamics simulations of the DNA duplex d(GCACGAACGAACGAACGC). *Biochim. Biophys. Acta - Gen. Subj.* 1850(5), 1041–1058 (2015).

53. Lyman E, Zuckerman DM. Ensemble-Based Convergence Analysis of Biomolecular Trajectories. *Biophys. J.* 91(1), 164–172 (2006). Available from: <http://linkinghub.elsevier.com/retrieve/pii/S0006349506717167>.

54. Knapp B, Frantal S, Cibena M, Schreiner W, Bauer P. Is an Intuitive Convergence Definition of Molecular Dynamics Simulations Solely Based on the Root Mean Square Deviation Possible? *J. Comput. Biol.* 18(8), 997–1005 (2011). Available from: <http://www.liebertonline.com/doi/abs/10.1089/cmb.2010.0237>.

55. Amadei A, Ceruso MA, Di Nola A. On the convergence of the conformational coordinates basis set obtained by the Essential Dynamics analysis of proteins' molecular dynamics simulations. *Proteins Struct. Funct. Genet.* 36(4), pp.419–424 (1999).

56. Kufareva I, Abagyan R. Methods of protein structure comparison. *Methods Mol. Biol.* 857, 231–57 (2012). Available from: <http://www.ncbi.nlm.nih.gov/pubmed/22323224><http://www.pubmedcentral.nih.gov/articlerender.fcgi?artid=PMC4321859><http://www.ncbi.nlm.nih.gov/pubmed/22323224><http://www.pubmedcentral.nih.gov/articlerender.fcgi?artid=PMC4321859>.

57. Huang Y, Paul DR. Effect of Molecular Weight and Temperature on Physical Aging of Thin Glassy Poly(2,6-dimethyl-1,4-phenylene oxide) Films. *J. Polym. Sci. Part B Polym. Phys.* 45(April), 1390–1398 (2007). Available from: <http://arxiv.org/abs/cond-mat/0406218>.

58. Pan L, Patterson JC. Molecular Dynamics Study of Zn(A β) and Zn(A β)₂. *PLoS One.* 8(9) (2013).

59. Lobanov MI, Bogatyreva NS, Galzitskaia O V. Radius of gyration is indicator of compactness of protein structure. *Mol. Biol. (Mosk).* 42(4), 701–706 (2008).

60. Bornot A, Etchebest C, De Brevern AG. Predicting protein flexibility through the prediction of local structures. *Proteins Struct. Funct. Bioinforma.* 79(3), 839–852 (2011).

61. Kalra P, Reddy TV, Jayaram B. Free Energy Component Analysis for Drug Design: A Case Study of HIV-1 Protease–Inhibitor Binding. *J. Med. Chem.* 44(25), 4325–4338 (2001). Available from: <http://www.scopus.com/inward/record.url?eid=2-s2.0-0035818886&partnerID=tZOtx3y1><http://pubs.acs.org/doi/abs/10.1021/jm010175z>.

62. Mhlongo NN, Soliman MES. Single H5N1 influenza A neuraminidase mutation develops resistance to oseltamivir due to distorted conformational and drug binding landscape: multiple molecular dynamics analyses. *RSC Adv.* 5(14), 10849–10861 (2015). Available from: <http://xlink.rsc.org/?DOI=C4RA13494J>.

63. Greenidge PA, Kramer C, Mozziconacci JC, Wolf RM. MM/GBSA binding energy prediction on the PDBbind data set: Successes, failures, and directions for further improvement. *J.*

Chem. Inf. Model. 53(1), 201–209 (2013).

64. Genheden S, Ryde U. The MM/PBSA and MM/GBSA methods to estimate ligand-binding affinities. *Expert Opin. Drug Discov.* 10(5), 449–461 (2015). Available from: <http://www.tandfonline.com/doi/full/10.1517/17460441.2015.1032936>.

65. Gohlke H, Kiel C, Case DA. Insights into Protein–Protein Binding by Binding Free Energy Calculation and Free Energy Decomposition for the Ras–Raf and Ras–RalGDS Complexes. *J. Mol. Biol.* 330(4), 891–913 (2003). Available from: <http://linkinghub.elsevier.com/retrieve/pii/S0022283603006107>.

66. Kormos BL, Benitex Y, Baranger AM, Beveridge DL. Affinity and Specificity of Protein U1A-RNA Complex Formation Based on an Additive Component Free Energy Model. *J. Mol. Biol.* 371(5), 1405–1419 (2007).

67. Hou T, Wang J, Li Y, *et al.* Assessing the performance of the MM/PBSA and MM/GBSA methods: I. The accuracy of binding free energy calculations based on molecular dynamics simulations. *J. Chem. Inf. Comput. Sci.* 51(1), 69–82 (2011). Available from: <http://www.pubmedcentral.nih.gov/articlerender.fcgi?artid=3029230&tool=pmcentrez&rendertype=abstract>.

68. Liu H, Yao X, Wang C, Han J. In silico identification of the potential drug resistance sites over 2009 influenza A (H1N1) virus neuraminidase. *Mol Pharm.* 7(3), 894–904 (2010). Available from: <http://www.ncbi.nlm.nih.gov/pubmed/20420444>.

69. Xue W, Pan D, Yang Y, Liu H, Yao X. Molecular modeling study on the resistance mechanism of HCV NS3/4A serine protease mutants R155K, A156V and D168A to TMC435. *Antiviral Res.* 93(1), 126–137 (2012).

70. Moonsamy S, Bhakat S, Walker RC, Soliman MES. Single Active Site Mutation Causes Serious Resistance of HIV Reverse Transcriptase to Lamivudine: Insight from Multiple Molecular Dynamics Simulations. *Cell Biochem. Biophys.* 74(1), 35–48 (2016).

71. Ndagi U, Mhlongo NN, Soliman ME. The impact of Thr91 mutation on c-Src resistance to UM-164: molecular dynamics study revealed a new opportunity for drug design. *Mol. BioSyst.* 13(6), 1157–1171 (2017). Available from: <http://xlink.rsc.org/?DOI=C6MB00848H>.

72. Amitai G, Shemesh A, Sitbon E, *et al.* Network analysis of protein structures identifies functional residues. *J. Mol. Biol.* 344(4), 1135–1146 (2004).

73. Doncheva NT, Klein K, Domingues FS, Albrecht M. Analyzing and visualizing residue networks of protein structures. *Trends Biochem. Sci.* 36(4), 179–182 (2011). Available from: <http://dx.doi.org/10.1016/j.tibs.2011.01.002>.

74. Shannon P, Markiel A, Owen Ozier, *et al.* Cytoscape: a software environment for integrated models of biomolecular interaction networks. *Genome Res.* (13), 2498–2504 (2003).

75. Assenov Y, Ramírez F, Schelhorn SESE, Lengauer T, Albrecht M. Computing topological parameters of biological networks. *Bioinformatics.* 24(2), 282–284 (2008).

CHAPTER 4

Submitted Article

Co-inhibition as a Strategic Therapeutic Approach to Overcome Rifampin Resistance in TB Therapy: Atomistic Insights

Clement Agoni^a, Pritika Ramharack^a, Mahmoud E. S. Soliman^{a,b,c*}

^a Molecular Bio-computation and Drug Design Research Laboratory, School of Health Sciences,
University of KwaZulu-Natal, Westville Campus, Durban 4001, South Africa.

*Corresponding Author: Mahmoud E.S. Soliman

Health Sciences, University of KwaZulu-Natal, Westville Campus, Durban 4001, South Africa.

^b Department of Pharmaceutical Organic Chemistry, Faculty of Pharmacy, Zagazig
University, Zagazig, Egypt.

^c College of Pharmacy and Pharmaceutical Sciences, Florida Agricultural and Mechanical
University, FAMU, Tallahassee, Florida 32307, USA.

Email: soliman@ukzn.ac.za

Telephone: +27 (0) 31 260 8048, Fax: +27 (0) 31 260 7872

Abstract

Background: Amidst the current global challenge of anti-microbial resistance, RNA polymerase remains a paramount therapeutic target for Tuberculosis. Dual binding of Rifampin and a novel compound, DAAPI, demonstrated the suppression of Rifampin resistance. However, a paucity of data elucidating the structural mechanism of action of this synergistic interaction prevails.

Methodology/Results: Molecular dynamic simulations unraveled the synergistic inhibitory characteristics of DAAPI and Rifampin. Co-binding induced a stable protein, increased the degree of compactness of binding site residues around Rifampin and subsequently an improved binding affinity towards Rifampin.

Conclusions: Findings established a structural mechanism by which DAAPI stabilizes *Mycobacterium tuberculosis* RNA polymerase, thus suppressing Rifampin resistance. This study will assist toward the design of novel inhibitors to combat resistance associated with tuberculosis.

Keywords: Tuberculosis therapy, Rifampin-resistance, *Mycobacterium tuberculosis*, thermodynamics binding energy, RNA polymerase

1. Introduction

Tuberculosis (TB), caused by *Mycobacterium Tuberculosis* (*Mtb*), is the leading cause of morbidity from an infectious disease worldwide [1]. Despite the persistent research being conducted on a global scale towards designing effective anti-resistant small drug molecules, *Mtb*'s defense mechanism is equally evolving resulting in drug resistance. Resistance can occur due to a number of reasons, including possible genetic mutations upon bacterial replication [2]. The bacteria's survival strategies against current therapeutic regimens has given rise to fatal strains that have now become resistant to most available therapies.

In many countries such as South Africa, *Mtb* may join forces with immuno-compromising HIV/AIDS, thus creating an incurable and lethal co-infection [3]. It is therefore imperative to map out new strategies in the design of TB inhibitors that will be effective in overcoming resistance and be able to bind with a high affinity to an enzymatic target, thus structurally inhibiting *Mtb* indefinitely.

Of the various *Mtb* therapeutic targets, the DNA-dependent RNA polymerase (RNAP) plays one of the most crucial roles in bacterial RNA synthesis [4–7]. Structurally, *Mtb* RNAP has five subunits which make up its core. These subunits are required for the elongation step of transcription [8]. Also, *Mtb* RNAP has a sixth σ -subunit (σ factor) that plays a crucial role in promoter recognition and transcription initiation [8]. Amongst the prominent front-line anti-TB drugs is Rifampin [9–11]. By binding to its active site on the RNAP, Rifampin functions through a steric occlusion mechanism, inhibiting transcription and preventing the extension of 2-3 nucleotide RNA products [10–12]. In spite of RIF's initial therapeutic efficacy against TB, the drug has now become ineffective to some *Mtb* strains due to the introduction of

evasive alterations on key target enzymes during the replication and transmission of *Mtb*. In 2016, the World Health Organization (WHO) reported an annual occurrence of as many as 600,000 new cases of Rifampin resistance with 2015 recording an estimated 480,000 Rifampin resistance TB cases. It is evident that Rifampin-resistance intensifies the array of challenges already associated with TB infection [1,13,14], thus supporting the crucial need to explore alternative strategies that will combat resistance and pave the road toward discovering a cure for TB. Synergistic inhibition/dual inhibition has been previously proven over time to be an effective approach when facing the challenge of drug resistance [15–17], and hence can be explored.

The first crystal structure of *Mtb* RNAP was recently released in complex with RIF and a novel class of experimentally validated *Mtb* RNAP inhibitors called $N\alpha$ -aroyl-N-aryl-phenylalaninamides (AAPs). These novel inhibitors uniquely bind to a separate hydrophobic pocket on *Mtb* RNAP, a site totally different from the binding site of Rifampin. Experimental findings demonstrated a synergistic effect when a prototype of these novel inhibitors, DAAPI and Rifampin are co-bound at their respective pockets, suppressing Rifampin resistance and inhibiting bacterial growth [18].

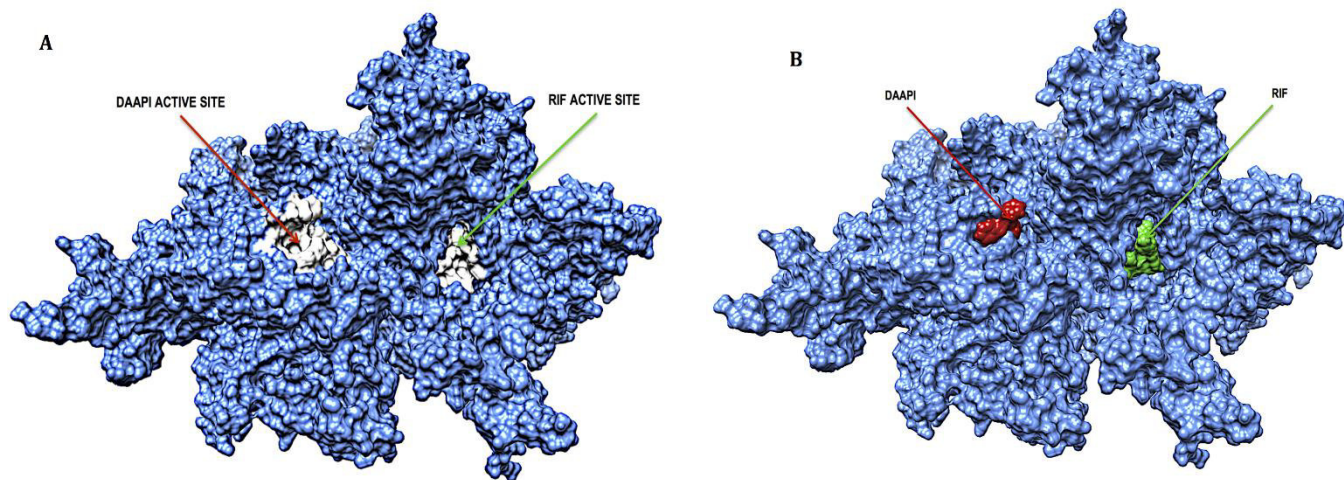


Figure 4.1: X-ray crystal structure of *Mtb* RNAP showing binding active sites (A) and bound (B) of RIF and DAAPI

In this study we have divulged, for the first time, a structural mechanism of inhibition of *Mtb* RNAP using a synergistic approach. By employing a wide range of extensive molecular and bioinformatics tools, we define and compare *Mtb* RNAP's structural and dynamic characteristics when bound as a dual inhibitor system. Furthermore, the comprehensive description of the conformational adaptations of RNAP's structural machinery offers vital insights into preventing RIF resistance, as well as provides a binding landscape to assist in the design of novel inhibitors with improved therapeutic properties on the *Mtb* RNAP.

2. Computational Methods

2.1 Systems' Preparation

In performing the MD simulation, X-ray crystal structures of *Mtb* RNAP were derived from the Protein Data Bank (PDB) with their respective PDB codes as follows; free RNAP (PDB: 5UHA), RNAP in complex with Rifampin (PDB: 5UHB), RNAP in complex with D-AAP1 (PDB: 5UHE) and RNAP in complex with both Rifampin and D-AAP1 (PDB: 5UHG) [18]. The *Mtb* RNAP and 3-D structures of Rifampin and D-AAP1 were prepared using the UCSF Chimera software package [19]. Lin *et al* (2017) reported conclusive experimental evidence

that co-administration of Rifampin and D-AAPI bound at independent hydrophobic pockets, result in additive antibacterial activity and also suppresses the emergence of RIF resistance. A 50ns molecular dynamics (MD) simulation was performed on four prepared systems (APO, RIF, DAAPI and RIFDAAPI). Per our knowledge, this study is the longest MD simulation involving *Mtb* RNAP.

2.2 Molecular Dynamic (MD) Simulations

The AMBER14 package [20,21] was used to perform a 50ns MD simulation for all systems. In handling *Mtb* RNAP, the FF14SB AMBER force field was used. The restrained electrostatic potential in the ANTECHAMBER was used to compute partial atomic charges for Rifampin and DAAPI [22]. Na⁺ and Cl⁻ which served as counter ions were added to neutralize our enzyme using the LEAP module of AMBER14. The Leap module was also used to add hydrogens atoms to *Mtb* RNAP. Each systems was enclosed within an 8 Å box of TIP3P water molecules ensuring that all portions of the enzymes or enzyme complexes were covered by the water molecules throughout the simulation period. All systems were minimized in two separate minimization stages. The first minimization incorporated a restraint potential of 100 kcal/mol Å² and was performed over the steepest descent minimization of 1000 cycles. The second minimization was also performed over the steepest descent minimization of 1000 cycles but without a restraint potential. All systems were then heated from 0K TO 300K for 50ps in the canonical ensemble (NVT) in which all solutes atoms were restrained at a force constants of 10 kcal/mol Å². All systems were subsequently equilibrated at 300K for 500ps in the isothermal, isobaric ensemble (NPT) at constant pressure of 1 bar in which all constraints were removed. This pressure was maintained using

the Berendsen barostat. To restrain all atoms that were covalently bonded to a hydrogen, SHAKE algorithm was incorporated. Without restraints, a 50ns MD simulation was conducted for all systems using the NPT ensemble.

2.3 Post-Dynamic Analysis

The trajectories generated after MD simulations were each saved every 1ps and were subsequently analyzed using the CPPTRAJ module of the AMBER14 package.

2.3.1 Binding free energy calculations

The Molecular Mechanics/Generalized-Born Surface Area (MM/GBSA) [23] technique was used to calculate the binding free energy of Rifampin and DAAPI in all systems. A total of 5000 snapshots were generated from the 50ns trajectory. Using the approach below, the binding free (ΔG) were estimated.

$$\Delta G_{\text{bind}} = G_{\text{complex}} - G_{\text{receptor}} - G_{\text{ligand}} \quad (1)$$

$$\Delta G_{\text{bind}} = E_{\text{gas}} + G_{\text{sol}} - T\Delta S \quad (2)$$

$$E_{\text{gas}} = E_{\text{int}} + E_{\text{vdw}} + E_{\text{ele}} \quad (3)$$

$$G_{\text{sol}} = G_{\text{GB}} + G_{\text{SA}} \quad (4)$$

$$G_{\text{SA}} = \gamma \text{SASA} \quad (5)$$

Where ΔG_{bind} is a summation of gas phase, E_{gas} and the solvation energy, G_{sol} less the entropy ($T\Delta S$) term. The, E_{gas} is obtained by a summation of the internal energy E_{int} , electrostatic energy E_{ele} and the van der Waals energy, E_{vdw} generated from systems. The total solvation energy is calculated by a summation of the total energy contributions of polar states (G_{GB}) and non-polar states (G_{SA}). G_{SA} is calculated using the solvent accessible surface

area (SASA), generated by 1.4 Å radius water probe. By solving the G_{GB} equation, the energy contributions of polar states can be determined. S represented the total entropy of the solute while T represented temperature. Final energy per-residue decomposition was also calculated using the MMGBSA method [24].

3. Results and Discussion

3.1 Systems' stability

Systems' stability was evaluated by calculating the root mean square deviation (RMSD) for all four systems. The C- α atoms of all systems, with the exception of the RIF system, reached convergence and hence achieved stability after approximately 20ns (Figure S1). The flexibility of amino acid residues for all systems; APO, DA-API, RIF and RIFDA-API, were evaluated and compared by calculating the root mean square fluctuation (RMSF) of the *Mtb* RNAP backbone [25]. The "1750-2000" region of the RIF system showed greater flexibility due to the obvious fluctuation of unbound residues at this region, as it encloses the DA-API active site. Increased fluctuation was observed in the region that encompassed the active site of Rifampin (residues "100-700"). However, in the co-bound system, there was a decrease in residue fluctuation in this same region.

It can be deduced from the systems' stability analyses that there is an improvement in structural stability of *Mtb* RNAP protein structure from when it is unbound, to when bound with Rifampin alone and then finally achieving highest stability upon co-binding as depicted in figure 4.2.

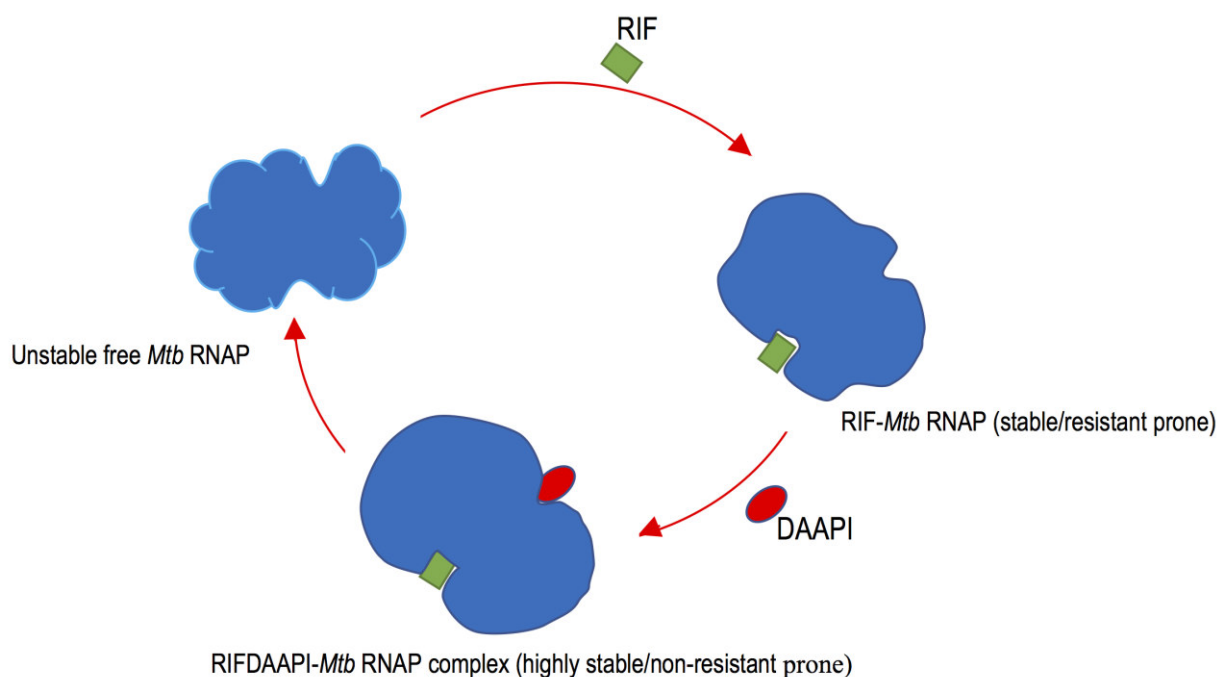


Figure 4.2: Schematic depiction of *Mtb* RNAP complex stability increase upon binding of Rifampin and DAAPI.

3.2 Thermodynamic binding landscape in RIF and DAAPI co-inhibition

To gain an understanding into the energy dynamics of Rifampin binding to *Mtb* RNAP alone, and upon co-binding with DAAPI, the relative binding free energies were calculated using MM/GBSA method [23]. The binding free energy of the Rifampin when bound alone was calculated to be -49 kcal/mol while binding free energy for DAAPI when bound alone was -21.61 kcal/mole as shown in Fig 4.3 and Table 4.1. Binding free energies for Rifampin and DAAPI when co-bound on *Mtb* RNAP were also calculated as follows; Rifampin (-51.41 kcal/mol) and DAAPI (-16.01 kcal/mol). Interestingly, as shown in figure 4.3, there is an binding free energy of Rifampin when co-bound with DAAPI. This is could be an indication that inhibitory potency of DAAPI increased the binding affinity of Rifampin to *Mtb* RNAP

and hence could possibly be the basis for the predicted suppression of Rifampin resistance in the presence of DAAPI[18]. This is further corroborated by the increase in van der Waals interactions as shown in figure 4.3 and Table 4.1.

Table 4.1: Binding free energy of DAAPI and RIF bound alone and when co-bound to *Mtb* RNAP

		ENERGY COMPONENT (KCAL/MOL)				
INDIVIDUALLY		ΔE_{vdw}	ΔE_{ele}	ΔG_{gas}	ΔG_{solv}	ΔG_{bind}
	DAAPI	-23.31 ± 0.30	-33.35 ± 0.65	-56.66±0.67	35.04±0.48	-21.61±0.34
	RIF	-59.35 ± 0.37	-38.31±0.63	-97.67±0.65	47.72±0.44	-49.94±0.41
CO-BOUND						
	DAAPI	-25.79 ± 0.28	-11.45 ± 0.31	-37.25±0.44	21.24±0.29	-16.01±0.29
	RIF	-63.58 ± 0.39	-22.59±0.54	-86.18±0.69	34.76±0.42	-51.41±0.55

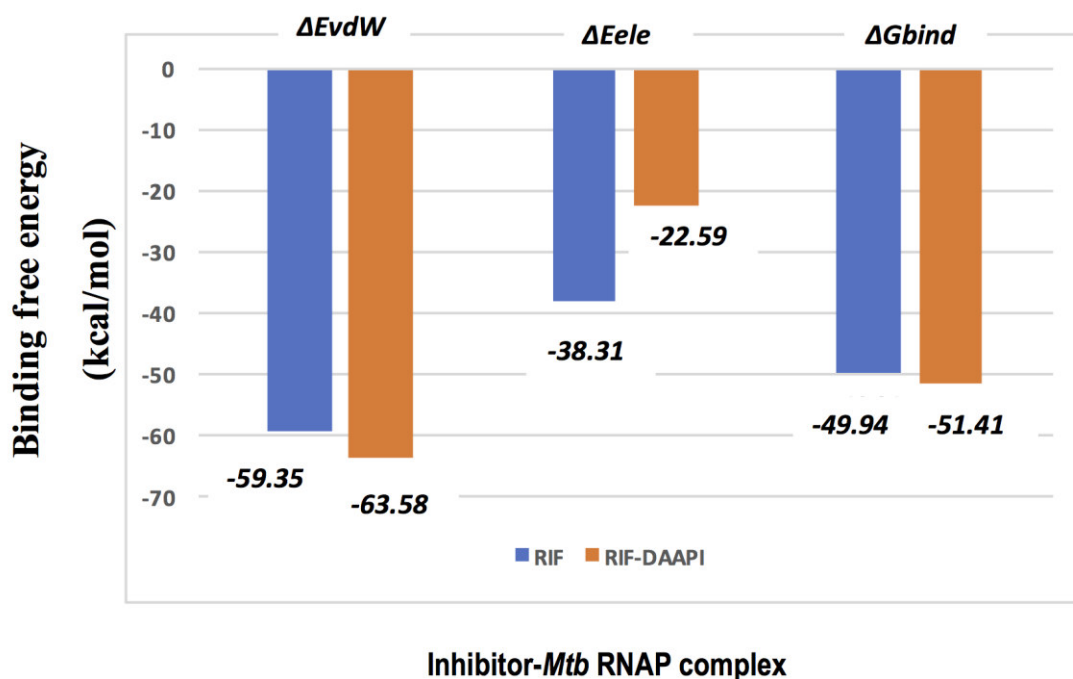


Figure 4.3: Binding free energy of Rifampin (RIF) in the absence and presence of DAAPI

Although thermodynamics revealed that co-binding of Rifampin and DAAPI improved binding affinity of Rifampin, it would be misleading to rely on these findings alone [26]. As result, we employed the Radius of gyration to give further molecular insights on the flexibility and compactness of residues involved in the binding of Rifampin.

3.3 Compactness of Rifampin active site residues in the presence and absence of DAAPI

We calculated the Radius of Gyration (RoG) of the active site residues of Rifampin to explore the impact of the co-binding on them. Radius of gyration demonstrates the compactness of protein structures, unveiling insights into complex changes in the molecular structure[27]. With RoG we unraveled the flexibility or compactness of the selected active site residues throughout the simulation. When Rifampin was bound alone, active site residues showed a distinguishably higher RoG over the 50ns simulation, with an average RoG of 11.61 Å. This portrayed a less compact structure when compared with the dual system.

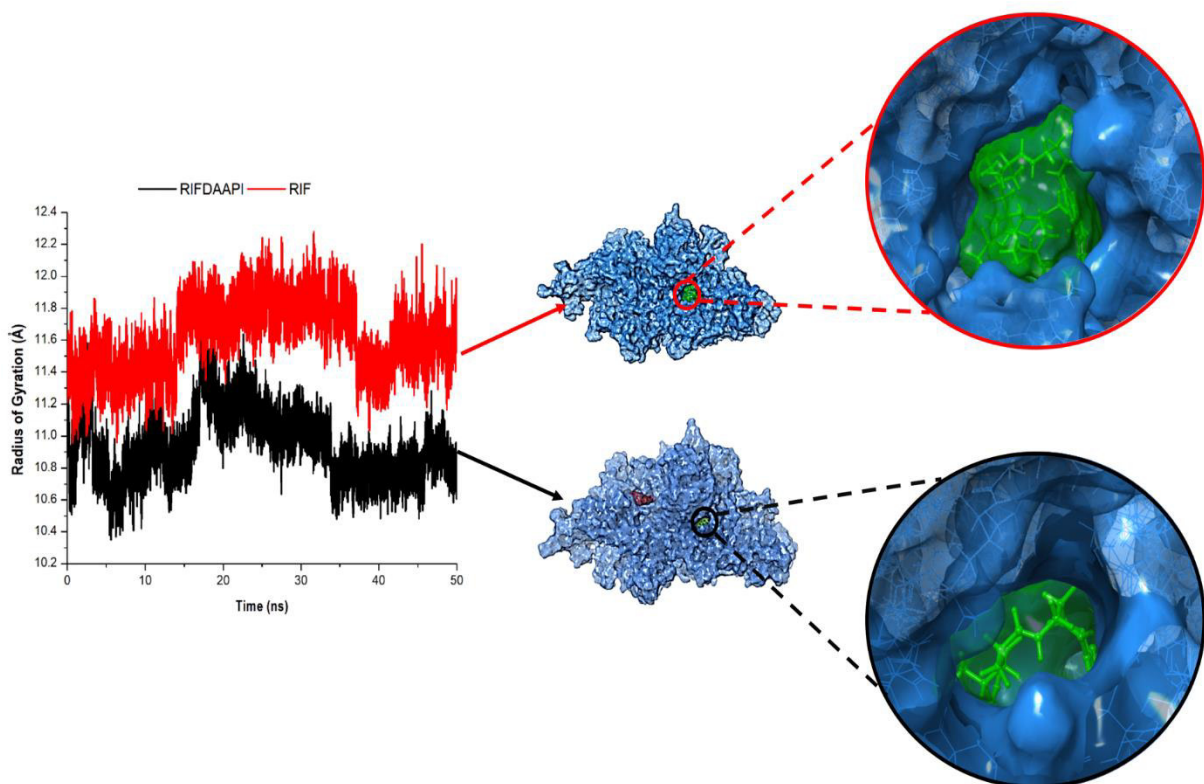


Figure 4.4: Comparative compactness of Rifampin binding site residues of *Mtb* RNAP in the presence and absence of DAAPI.

However, a demonstrably lower RoG was observed in the co-bound system (10.93Å). This decrease in RoG indicates an increase in compactness of the active site residues (Figure 4.5). It can therefore be deduced that the presence of DAAPI impacted a level of rigidity on Rifampin active site residues, translating into an increased stability in the binding of Rifampin. This was validated by the increased binding affinity of Rifampin in the co-bound system as elucidated above. It also confers with the experimentally demonstrated synergistic effects generated upon co-binding of Rifampin and DAAPI [18].

3.4 Energy analysis of RIF and DAAPI binding sites' residues

To portray the collective drug-binding landscape at atomistic level, the binding energy contribution from each active site residues of DAAPI and RIF was calculated, thus the per-residue binding footprints using the MM/GBSA method. Table S1 and S2 shows the decomposed energies contributed by each active site residue for RIF and DAAPI respectively. However figure 4.5 shows highest energy contributing active sites residues and a representation of the interaction of these ligands with their respective binding site residues. As evident from Figure 4.5(A), residues ARG 427(-3.133 kcal/mol), SER 429(-1.604 kcal/mol) and PHE 412(-4.1.30 kcal/mol) were found to contribute the most towards the binding of RIF, while ARG 1958(-4.578) and ILE 1975 (-1.121 kcal/mol) with optimal residue energy contributions $\Delta G_{\text{bind}} > -1\text{kcal/mol}$. These collectively contributed to the total binding free energies of Rifampin and DAAPI calculated in the thermodynamics.

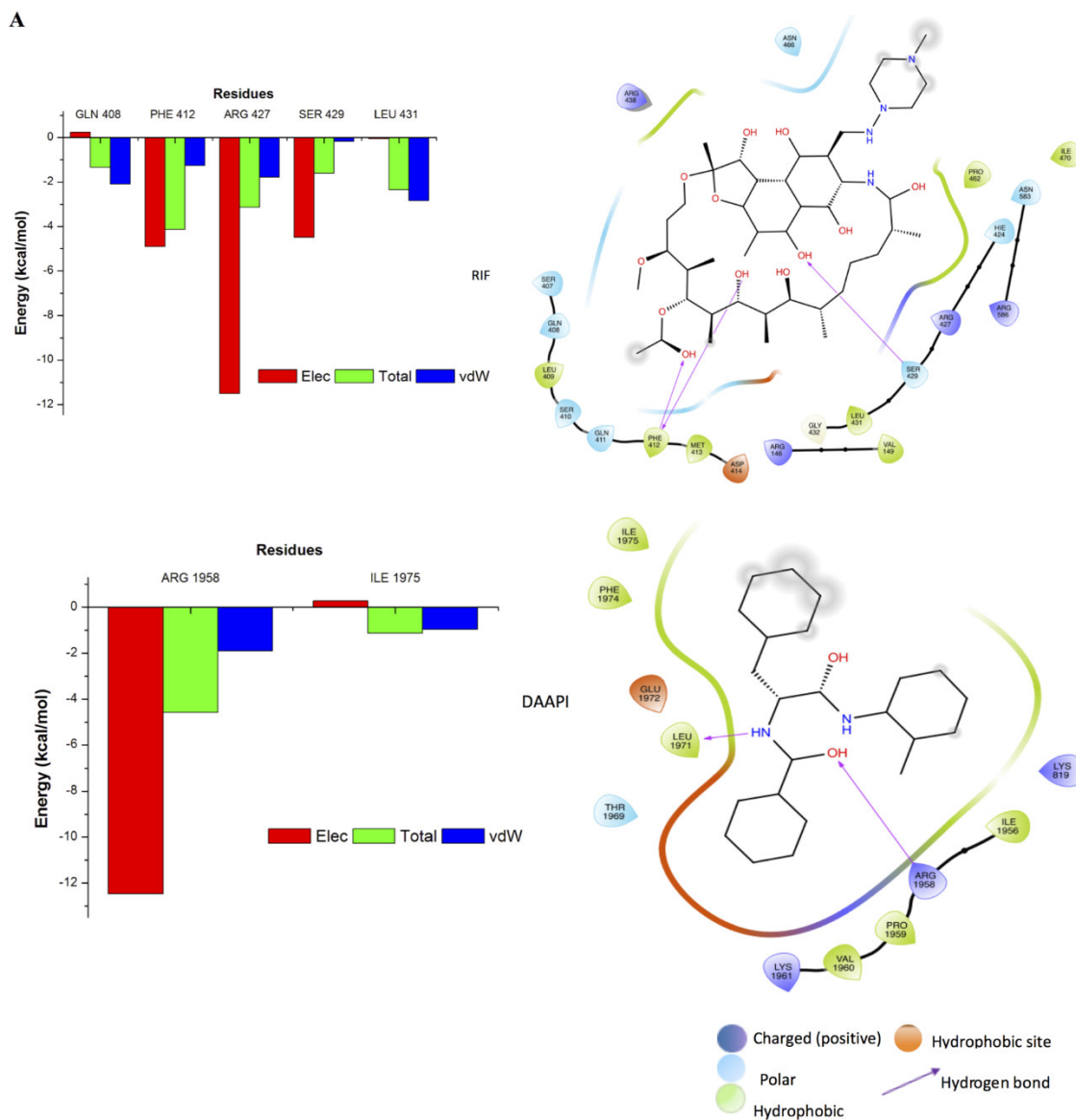


Figure 4.5. Total residue binding free energies, van der Waals (vdW), electrostatic (Elec) energy components for residues with binding energies > -1 kcal/mol and corresponding ligand interactions for Rifampin (RIF) (A) DAAPI (B)

4. Conclusions

Computational analytical tools were used to understand the co-inhibitory mechanism of RIF and a novel inhibitor, DAAPI, toward the suppression of RIF resistance. DAAPI, a recently synthesized inhibitor has been experimental proven to subdue the emergence of RIF resistance, while still incorporating an additive antibacterial activity. To this end, comparative MD simulations and analyses were performed in order to explore the binding landscape and structural features associated with synergistic dual inhibition. Results demonstrated that the co-bound *Mtb* RNAP system induced a more stable, compact protein structure, when compared to systems in which RIF and DAAPI are bound alone. Thermodynamic calculations indicated that DAAPI exerts some level of stability and stronger RIF-*Mtb* RNAP interactions, complemented by compactness of RIF binding site residues when co-bound with DAAPI and an increased van der Waals interactions. As a result, the calculated binding free energy of RIF in the presence of DAAPI was higher compared to when bound alone as elucidated in the thermodynamics. This mechanism could explain the suppression of RIF resistance as previously reported. Per-residue energy decomposition analysis revealed that, amino acid residues: SER 429, PHE 412 and LEU 431 are key residues that largely contribute to the binding of RIF, while ARG 1958 and ILE 1975 were vital to the binding of DAAPI. This knowledge will contribute to a greater comprehension of binding landscapes of these inhibitors at a molecular level. Based on this study, RIF and DAAPI demonstrate a synergistic mechanism of inhibition.

Reference

1. World Health Organization (WHO). WHO | Global tuberculosis report 2017. Available from: http://www.who.int/tb/publications/global_report/en/.
2. Sandgren, A. Strong, M. Muthukrishnan, P. Weiner, BK. Church, GM. Murray, MB. Tuberculosis drug resistance mutation database. *PLoS Med.* 6(2), 0132–0136 (2009).
3. Pietersen, E. Ignatius, E. Streicher, EM. Long-term outcomes of patients with extensively drug-resistant tuberculosis in South Africa: A cohort study. *Lancet.* 383(9924), 1230–1239 (2014).
4. Chopra, I. Hesse, L. O'Neil, AJ. Exploiting current understanding of antibiotic action for discovery of new drugs. *J Appl Microbiol.* 92(Suppl:4S-15S) (2002).
5. Chopra, I. Bacterial RNA polymerase: a promising target for the discovery of new antimicrobial agents. *Curr Opin Investig Drugs.* 8(600), 7 (2007).
6. Darst, SA. New inhibitors targeting bacterial RNA polymerase. *Trends Biochem Sci.* 29(159e60) (2004). Available from: <http://dx.doi.org/10.1016/j.tibs.2004.02.005>.
7. Villain-Guillot, P. Bastide, L. Gualtieri, MLJ. Progress in targeting bacterial transcription. *Drug Discov Today.* 12(200e8) (2007). Available from: <http://dx.doi.org/10.1016/j.drudis.2007.01.005>.
8. Bortoluzzi, A. Muskett, FW. Waters, LC. Mycobacterium tuberculosis RNA Polymerase-binding Protein A (RbpA) and Its Interactions with Sigma Factors. 288(20), 14438–14450 (2013).

9. Artsimovitch, I. Vassilyeva, MN. Svetlov, D. Allosteric Modulation of the RNA Polymerase Catalytic Reaction Is an Essential Component of Transcription Control by Rifamycins. *122*, 351–363 (2005).
10. Campbell, EA. Korzheva, N. Mustaev A, Murakami, K. Nair, S. Goldfarb, A. *et al.* Structural Mechanism for Rifampicin Inhibition of Bacterial RNA Polymerase. *Cell*. 104, 901–912 (2001).
11. Feklistov, V. Mekler, Q. Jiang, L. Westblade, H. Irschik, R. Jansen, A. *et al.* Rifamycins do not function by allosteric modulation of binding of Mg²⁺ to the RNA polymerase active center. *Proc. Natl. Acad. Sci. USA*. 105(14820) (2008).
12. Mustaev, A. Zaychikov, E. Severinov, K. Kashlev, M. Polyakov, A. Nikiforov, V. *et al.* Topology of the RNA polymerase active center probed by chimeric rifampicin-nucleotide compounds. *Proc Natl Acad Sci USA*. 91(12036) (1994).
13. Aristoff, P. Garcia, G. Kirchoff, PS. Hollis Showalter, HD. Rifamycins--obstacles and opportunities. *Tuberculosis*. , 90, 94 (2010).
14. Rothstein, DM. Rifamycins, alone and in combination. *Cold Spring Harb. Perspect. Med.* 6(7) (2016).
15. Fitzgerald, J. Schoeberl, B. Nielsen, UB. Sorger, P. Systems biology and combination therapy in the quest for clinical efficacy. *Nat Chem Biol*. 2(9) (2006).
16. Komarova, N. Boland, C. Cancer: calculated treatment. *Nature*. 499(7458), 291±2 (2013).

17. Gayvert KM, Aly O, Platt J, Bosenberg MW, Stern DF, Elemento O. A Computational Approach for Identifying Synergistic Drug Combinations. *PLoS Comput Biol.* 13(1), e1005308 (2017). Available from: <https://www.ncbi.nlm.nih.gov/pubmed/28085880>.
18. Lin W, Mandal S, Degen D, Liu, Y, Ebright, Y W, Li, S *et al.* Structural basis of Mycobacterium tuberculosis transcription and transcription inhibition. *Mol. Cell.* 66, 169–179 (2017).
19. Pettersen, EF, Goddard, TD, Huang, CC, Couch, GS, Greenblatt, DM, Meng, E C. *et al.* UCSF Chimera - A visualization system for exploratory research and analysis. *J. Comput. Chem.* 25(13), 1605–1612 (2004).
20. Salomon-Ferrer, R, Gotz, AW, Poole, D, Le Grand, S, Walker, RC. Routine microsecond molecular dynamics simulations with AMBER on GPUs. 2. Explicit solvent particle mesh ewald. *J. Chem. Theory Comput.* 9(9), 3878–3888 (2013).
21. Case Da TE, Cheatham, I, Darden, T. The Amber biomolecular simulation programs. *J. Comput. Chem.* 26(16), 1668–1688 (2005). Available from: <http://onlinelibrary.wiley.com/doi/10.1002/jcc.20290/pdf>.
22. Wang, J, Wolf, RM, Caldwell, JW, Kollman, PA, Case, DA. Development and testing of a general Amber force field. *J. Comput. Chem.* 25(9), 1157–1174 (2004).
23. Genheden, S, Ryde U. The MM/PBSA and MM/GBSA methods to estimate ligand-binding affinities. *Expert Opin. Drug Discov.* 10, 449–461 (2015).
24. Miller, BR, McGee, TD, Swails, JM, Homeyer, N, Gohlke, H, Roitberg, AE.

MMPBSA.py: An efficient program for end-state free energy calculations. *J. Chem. Theory Comput.* 8(9), 3314–3321 (2012).

25. Wassenaar, TA. molecular dynamics hands-on session II. (2014). Available from: <http://www.nmr.chem.uu.nl/~tsjerk/course/md-tutorial/analysis.%0Ahtml>.
26. Singh, N. Warshel, A. Absolute Binding Free Energy Calculations: On the Accuracy of Computational Scoring of Protein-ligand Interactions. *Proteins.* 78(7), 1705–1723 (2010). Available from: <http://www.ncbi.nlm.nih.gov/pmc/articles/PMC2868600/>.
27. Lobanov, MI. Bogatyreva, NS. Galzitskaia, OV. Radius of gyration is indicator of compactness of protein structure. *Mol. Biol. (Mosk).* 42(4), 701–706 (2008).

CHAPTER 5

Submitted Article

Synergistic Interplay of The Co-administration of Rifampin And Newly Developed Anti-TB Drug: Could It Be a Promising New Line of TB Therapy?

Clement Agoni^a, Pritika Ramharack^a, Mahmoud E. S. Soliman^{a*}

^a Molecular Bio-computation and Drug Design Research Laboratory, School of Health Sciences, University of KwaZulu-Natal, Westville Campus, Durban 4001, South Africa.

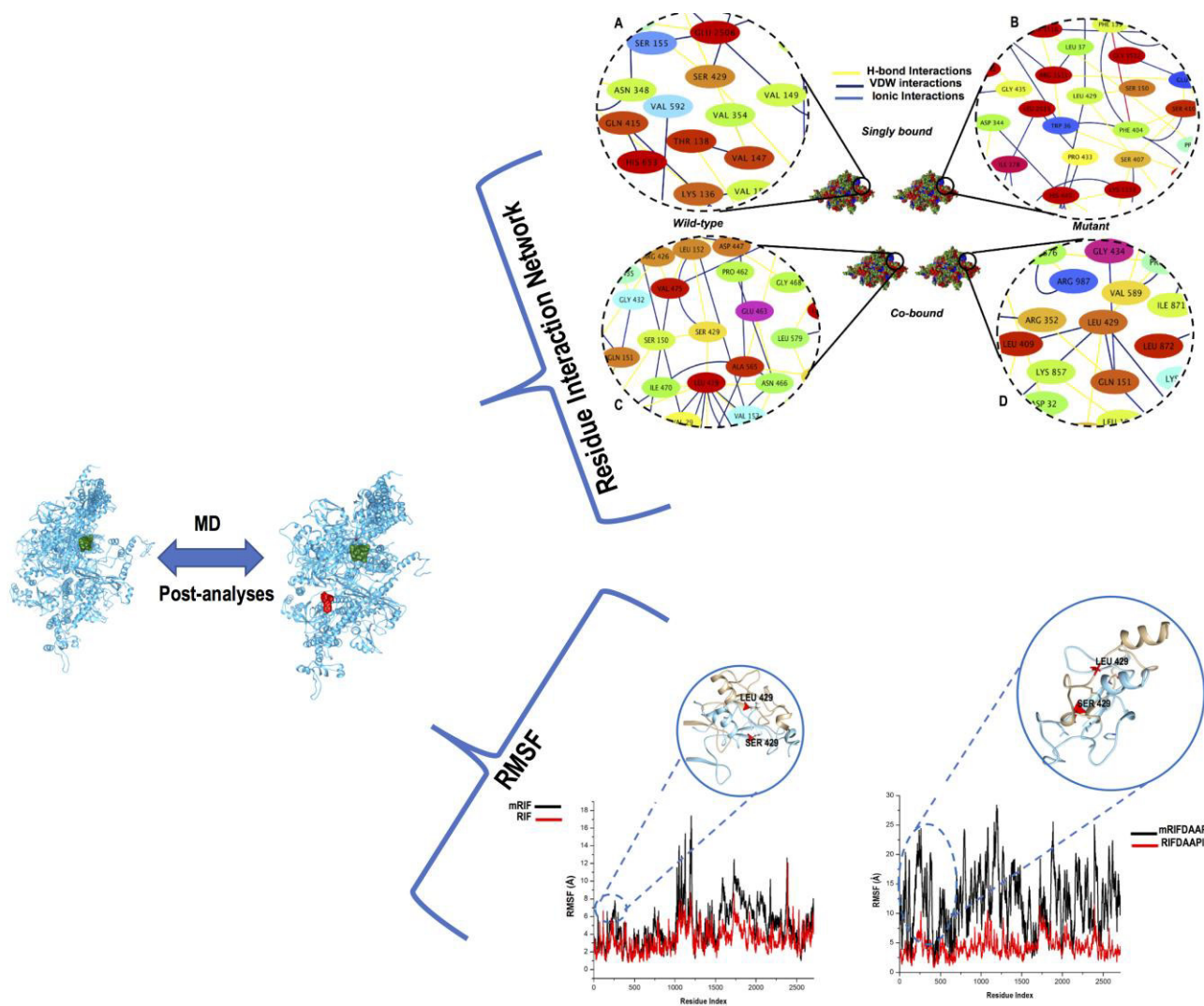
*Corresponding Author: Mahmoud E.S. Soliman

School of Health Sciences, University of KwaZulu-Natal, Westville Campus, Durban 4001, South Africa.

Email: soliman@ukzn.ac.za

Telephone: +27 (0) 31 260 8048, Fax: +27 (0) 31 260 7872

GRAPHICAL ABSTRACT



Abstract

Rifampin resistance has been a large contributor to the global epidemic of antimicrobial resistance, thus dampening the existing efforts being made to control the crisis of Tuberculosis. Previous studies that attempted to provide insights into the structural mechanism of Rifampin resistance did not utilize the X-ray crystal structure of *Mycobacterium tuberculosis* RNA polymerase due to its unavailability. In this study, we provide an atomistic mechanism behind Rifampin resistance when the recently resolved crystal structure of *Mycobacterium tuberculosis* RNA polymerase is subjected to a single active site mutation. We also identify and rationalize the structural interplay of this mutation upon co-binding of Rifampin with a novel inhibitor, DAAPI. The mutation distorted the overall conformational landscape of *Mycobacterium tuberculosis* RNA polymerase, resulting in a reduction of binding affinity of Rifampin and an overall shift in the residue interaction network of *Mycobacterium tuberculosis* RNA polymerase and upon single binding. Interestingly, co-binding with DAAPI, though impacted by the mutation exhibited improved Rifampin binding interactions amidst a distorted residue interaction network. Findings offer vital conformational dynamics and structural mechanisms of mutant enzyme-single ligand and mutant enzyme- dual ligand interactions which could potentially shift the current therapeutic protocol of TB infections, thus aiding in the design of novel *Mycobacterium tuberculosis* RNA polymerase inhibitors with improved therapeutic features against the mutant protein.

Keyword: *Mycobacterium Tuberculosis* RNA polymerase, Co-inhibition, Rifampin resistance

1. Introduction

The rapid evolution of infectious pathogenic agents leading to the emergence of resistant variants is currently a dilemma for the scientific community. This burden has not been any different regarding Tuberculosis (TB). The emergence of resistant *Mycobacterium Tuberculosis (Mtb)* strains is currently a global crisis and has subsequently complicated the existing efforts being made to control the global Tuberculosis epidemic [1,2]. As a result, TB currently ranks above HIV as the leading cause of morbidity from an infectious disease [2].

The resistance to Rifampin, a major first-line anti-TB drug [3–5], accounts for a significant proportion of the total global statistics on *Mtb* drug resistance. In a 2016 report by the WHO, an estimated number of 480,000 TB cases in 2015 were either infected with Rifampin resistant strains or patients developed resistance in the course of antibiotic treatment [2,6]. Rifampin functions by binding to the β subunit of the DNA dependent enzyme, RNA polymerase (RNAP) to prevent the extension of RNA beyond 2-3 nucleotides through steric occlusion mechanism [7–9], hence inhibiting transcription. Due the critical role played by Rifampin in the treatment of TB, resistance to Rifampin is a potential threat to current TB control measures. Synergistic inhibition from combination of Rifampin and other drugs have been reported to be an effective approach in targeting of drug resistance [10–12], nonetheless, it could be explored further.

Rifampin resistance is largely attributed to a spontaneous single amino acid mutation occurring at the Rifampin-Resistant Determining Region, a region with three distinct loci near the center of the β -subunit of RNAP [6,13]. Clinical isolation and identification of most rifampin resistant strains have reportedly shown amino acid substitutions at positions

occurring in the Rifampin-cluster I of the *rpoB* gene [6]. However amongst these residue positions, mutations S531L and H526Y accounts for about 41% and 36% respectively of Rifampin resistance [7,14–17].

To give the first direct structural and molecular insights responsible for Rifampin resistance, Molodtsov *et al* in 2016 [6] synthesized crystal structures of *E. coli* RNAP together with some clinically isolated mutants and concluded that each mutant elicited different structural and/or surface electrostatic potential changes which make the RIF binding interface less favorable for binding RIF [6]. Also, based on a 10ns simulation, Nusrath *et al* [18] reported RIF resistance due to changes in binding interactions with RIF as a result of mutation of some active site residues. However, Nusrath *et al* used a homology modelled *Mtb* RNAP with RNAP of *Thermus thermophiles* as a template.

In light of the short falls of these previous studies, notably (i) lack of crystal structure of *Mtb* RNAP and (ii) short molecular dynamic simulations, our study aims to overcome these shortfalls by incorporating more reliable, valid and reproducible techniques. We therefore report the first account of the molecular interaction between Rifampin and a mutant RNAP generated from a recently crystallized *Mtb* RNAP, in a much longer molecular dynamic simulation. Using sophisticated molecular techniques and bioinformatics tools, we also attempt to give a molecular interpretation of the possible influence of a mutation on the active site of Rifampin on the synergistic effect yielded when rifampin is co-administered with a novel RNAP-targeted inhibitor, DAAPI [19]. Conclusions from this study will offer vital conformational dynamics and structural mechanisms of the mutant- single ligand and mutant-

dual ligand interactions that will aid in the design of novel *Mtb* RNAP inhibitors with improved therapeutic features against the mutant target proteins.

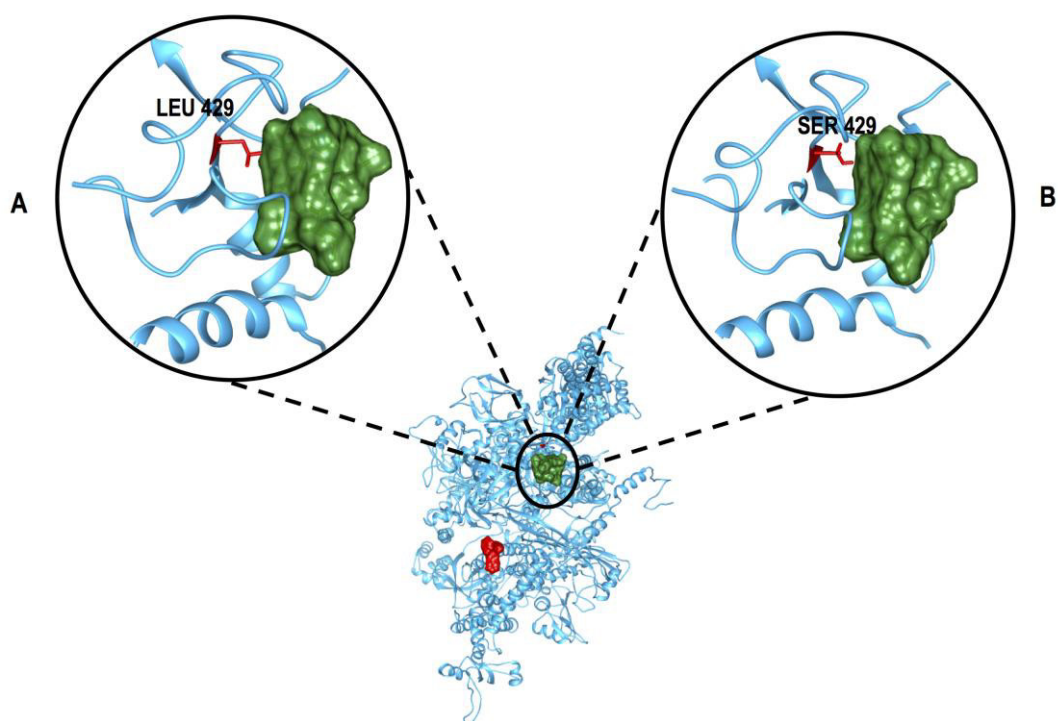


Figure 5.1. 3-D structure of *Mtb* RNAP depicting RIF's active site mutation (SER429→LEU429).

2. Computational Methods

2.1 Preparation of Systems

The X-ray crystal structures of *Mtb* RNAP were extracted from the Protein Data Bank (PDB) with the following PDB codes; Wild type *Mtb* RNAP (PDB: 5UHA), Wild type *Mtb* RNAP in complex with Rifampin (PDB: 5UHB) and Wild type *Mtb* RNAP in complex with both Rifampin and DAAPI (PDB: 5UHG) [19] . The proteins were then prepared following standard procedure using the UCSF Chimera software package [20]. A point mutation was introduced at position 429 located on the Rifampin binding site, where Serine (SER 429) was replaced with Leucine (LEU 429) (from S to L) to obtain the mutant structures of *Mtb* RNAP using Chimera [20]a. The 3-D structures of the RIF and DAAPI were derived from their complexes with RNAP and prepared on Chimera software as well. We then performed a 50ns molecular dynamics simulation of our prepared systems, the longest simulation involving an *Mtb* RNAP to our best of knowledge. The systems included; RIF (wild type *Mtb* in complex with RIF), mRIF (mutated *Mtb* RNAP in complex with Rifampin), mRIFDAAPI (mutated *Mtb* RNAP in complex with Rifampin and DAAPI) and RIFDAAPI (wild *Mtb* RNAP complex with Rifampin and DAAPI).

2.2 Molecular Dynamic (MD) Simulations

MD simulations were performed on all systems over a 50ns period to establish the effect of mutation S431L on the binding of Rifampin in the presence or absence of a separately co-bound inhibitor, DAAPI. The MD simulation was carried out using the graphics processing unit of the PMEMD engine incorporated in the AMBER14 suite [21,22] following established in-house protocols reported in many of our previous studies[23–28] . Due to

missing residues (E1-M206), all residues after M206 were renumbered as per the LEAP module. This resulted in the adjustment of the residue of interest from S431L to S429L.

2.3 Post-Molecular Dynamic Simulation Analysis

Coordinates generated for each system after simulation were each saved at an interval of 1ps. Generated MD trajectories were then analyzed. RMSD, RMSF, thermodynamic calculations RIN, Hydrogen bonds and occupancy analysis as post-MD simulations analysis techniques were carried out using the CPPTRAJ and PTRAJ modules incorporated in the AMBER 14 suite.

2.3.1 Binding affinity analyses

The estimation of binding free energy in this study was performed using the Molecular Mechanics/Generalized Born Surface Area (MM/GBSA) method [29]. A method employed in many of our previous reports [24,25,27,30,31]. 5000 snapshots were taken from the 50ns trajectory of each simulated system to average the binding free energies .

2.3.2 Residue Interaction Network exploration

A representative snapshot at the end of the 50ns MD simulation trajectory of each simulated system was utilized to generate the residue interaction network (RIN). Cytoscape [32] and the RINalyzer plugin [33] were employed to visualize generated RIN. In a RIN, protein residues denoted by nodes and while their corresponding non-covalent interactions are represented by edges. Edges are denotes an interaction types such as hydrogen bonds amongst others. The NetworkAnalyzer [34] plugin of Cytoscape was used to analyze the node degree and node connectivity. The RINalyzer plugin was then used to analyze the

closeness centrality and shortest path betweenness of complex topological parameters in network.

3. Results and Discussion

3.1 Conformational stability of wild and mutant singly bound/co-bound *Mtb* RNAP

The stability of the 3D backbones atoms of the *Mtb* RNAP were unraveled by assessing the root mean square deviation (RMSD), with respect to the starting structures during the period of simulation. The RMSD of the simulated systems graphically monitored their convergence (Figure S1). It was observed that all mutant systems (mRIF, mRIFDAAPI) appeared to have reached convergence at an elevated energy compared to the wild systems (RIF, RIFDAAPI) (Figure S1). This could possibly indicate that the single active site mutation affected the overall conformational stability of *Mtb* RNAP by increasing the number of conformations of the protein.

3.2 Exploration of Residue Interaction Network in singly/co-bound mutant and wild-type *Mtb* RNAP

Exploring and analyzing the residue interaction network in wild or mutant *Mtb* RNAP when bound to Rifampin, DAAPI or both unveiled further insights into the structural, functional and conformational dynamics of role of individual residues [35–37]. Previous studies from our group has successfully applied RIN to characterize the implication of residue mutation to drug resistance [24,25]. Using the representative protein structures from our 50ns MD simulation, we investigated the interplay of single active mutation, S429L, with the neighboring network of residues that interacted with our residues of interest.

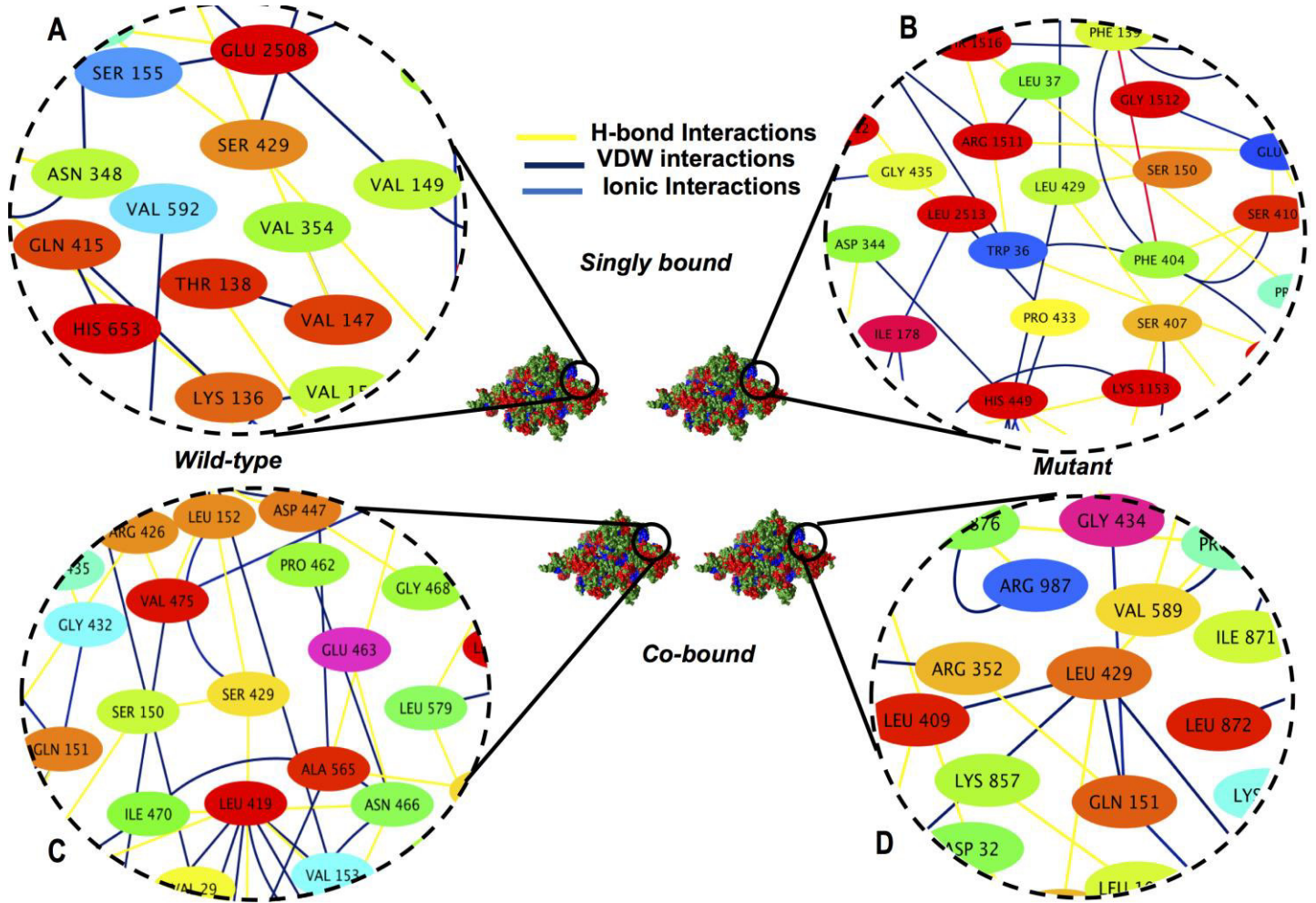


Figure 5.3: Residue Interaction Network around mutation site (S429L) of *Mtb* RNAP upon single binding with Rifampin alone (A and B) and co-binding with Rifampin and DAAPI (C and D).

Upon a close exploration of RIN in the singly bound systems (Figure 5.3A and 5.3B), it was obvious that the mutation altered the overall network of residues in the mutated system (mRIF) compared to the wild (RIF). Residues that interacted with Ser 429 in the singly bound wild-type wild were different from those interacting with Leu 429 upon the mutation. In the wild, Ser 429 interacted with Val 354, Ser 155 and Glu 2508 (Figure 5.3A). However, upon

the mutation to Leu, Leu 429 interacted with Ser 407, Ser 150 and Pro 433 (Figure **5.3B**). It can also be observed that Ser 429 forms more H-bond interactions with neighboring residues as compared to Leu 429 in the mutated system corroborating with the decreased binding affinity elucidated in thermodynamics analysis (Table 5.1).

In the co-bound systems (Figure **5.3C and 5.3D**), it could be observed that regardless of the residue network distortion caused by the mutation, there was a visible increase in the number of interactions that Leu 429 was engaged in when compared with Ser 431. Notable amongst such interactions were van der Waals interaction. Mutation in the co-bound generally improved the stability of Rifampin-*Mtb* RNAP interactions besides changing the landscape of *Mtb* RNAP and the atomic interactions between the Rifampin-*Mtb* RNAP and the key residues. These could have played critical roles in strengthening the binding of Rifampin in the presence of DAAPI. This confers with higher binding affinity of Rifampin upon co-binding than when singly bound as described in the thermodynamics analysis, amidst the single active site mutation.

3.3 Binding Energy profile of Rifampin to singly/co-bound Mtb RNAP upon single active site mutation.

To further understand the implication of the single active mutation on the binding of Rifampin to *Mtb* RNAP alone or when co-bound with DAAPI, we estimated the binding free energy of Rifampin in all the simulated complexes over the 50ns simulation period using the MM/GBSA [29] technique (Table 5.1).

Table 5.1: MM/GBSA-based binding free energy profile of Rifampin in all simulated systems

System	Energy components (kcal/mol)				
	ΔE_{vdw}	ΔE_{ele}	ΔG_{gas}	ΔG_{sol}	ΔG_{bind}
RIF	-59.35 ± 0.37	-38.31 ± 0.63	-97.67 ± 0.65	47.72 ± 0.44	-49.94 ± 0.41
mRIF	-61.06 ± 0.41	-22.07 ± 0.88	-83.13 ± 1.06	39.53 ± 0.72	-43.59 ± 0.58
mRIFDAAPI	-57.88 ± 0.49	-40.91 ± 1.00	-98.79 ± 1.07	51.46 ± 0.80	-47.34 ± 0.52
RIFDAAPI	-63.58 ± 0.39	-22.59 ± 0.54	-86.18 ± 0.69	34.76 ± 0.42	-51.41 ± 0.55

The calculated binding free energy (ΔG_{bind}) of Rifampin in all simulated systems were as follows; RIF and RIFDAAPI (singly and co-bound wild systems), 49.94 ± 0.41 kcal/mol and -51.41 kcal/mol respectively, the singly and co-bound mutated systems (mRIF and mRIFDAAPI) were -43.59 ± 0.58 kcal/mol and -47.34 ± 0.52 kcal/mol respectively.

There was an overall reduction in the binding affinity in the mutant systems due to the mutation, which impaired the binding of Rifampin, thus reducing its effectiveness against the mutant RNAP. This corroborates with the experimental evidence, which indicates that mutation of any residue at the Rifampin resistance-determining region impairs the binding of Rifampin [38,39]. The decrease in binding affinity of Rifampin when singly bound to mutant *Mtb* RNAP(mRIF) system could be attributed to the notable decrease in the electrostatic interactions, while the binding energy of the co-bound mutant system (mRIFDAAPI) system could be due to the significant decrease in the van der Waals interaction (Table 5.1). Interestingly, however, when comparing the binding free energy of

Rifampin upon co-binding and single binding in the mutant systems', it can be observed that the co-bound mutant system had a higher binding free energy (-47.34 kcal/mol) than the singly bound mutant system (-43.59 kcal/mol). This suggests that regardless of the mutation in the binding site of Rifampin on *Mtb* RNAP, co-binding with DAAPI could have exerted some synergistic property which induced a stronger binding of Rifampin as experimentally predicted by Lin *et al* [19].

Hydrogen bonds (H-bonds) Patterns

The stability and structural integrity of *Mtb* RNAP-ligand interaction is majorly dependent on H-bond interactions [40,41]. H-bond formation between residues is vital in monitoring of the conformation of *Mtb* RNAP. In singly bound systems, the wild *Mtb* RNAP system (RIF) showed the highest average of 1289.97 H-bond interactions when compared with the singly bound mutated system (mRIF) which showed an average of 1283.23 H-bond interactions (Figure 5.4A) over the 50ns simulation period. However, it was interesting to note that upon co-binding with DAAPI, the mutant system (mRIFDAAPI) had a higher average number of H-bond interactions (1313.19) than the co-bound wild system (RIFDAAPI), which showed an average number of 1293.72 H-bond interactions (Figure 5.4B).

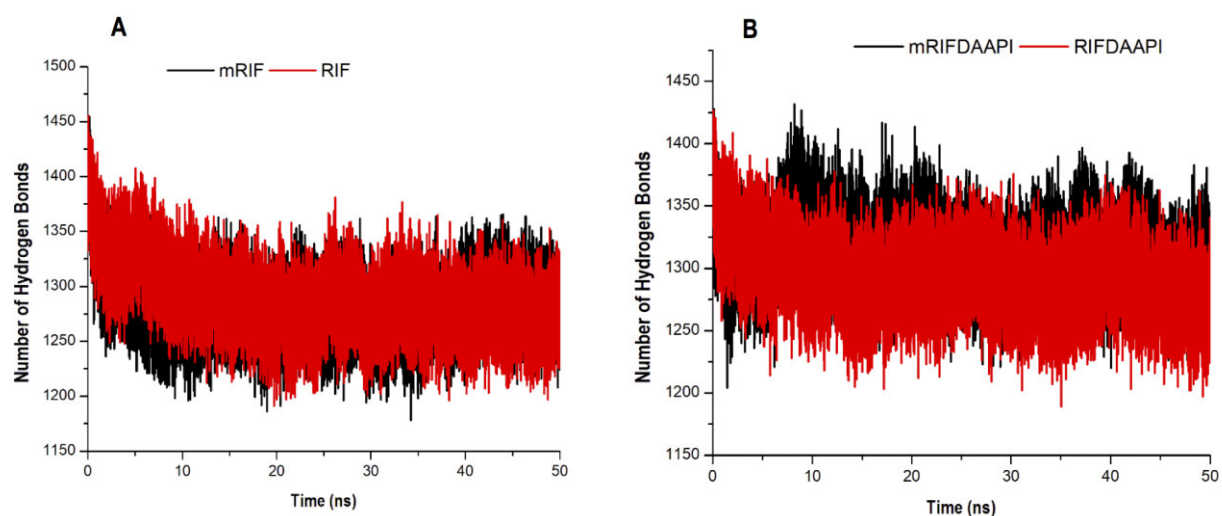


Figure 5.4: Number of inter-molecular hydrogen bond (H-bond) interactions observed during the molecular dynamic simulation in singly bound (**A**) and co-bound (**B**) systems in both mutated and the wild systems.

The decrease in H-bond formation when Rifampin was singly bound to the mutated *Mtb* RNAP could be attributed to the destabilization of H-bond interactions triggered by the single active site mutation, S429L. The mutated residue, Serine, is a hydrophilic polar residue that participated in hydrogen bonding with LEU152 (Table S1). Mutation of Serine to a hydrophobic residue, Leucine, possibly induced localized conformational changes in *Mtb* RNAP resulting in a to the loss of established H-bonds. The decrease in the number of H-bond interaction led to structural distortions and conformational changes, which ultimately affected the binding of Rifampin [42], hence the decreased binding free energy of Rifampin in the mutant system as shown in the calculated thermodynamics (Table 5.1). The relatively higher average H-bonds interactions in the co-bound mutated *Mtb* RNAP when compared to the singly bound mutant *Mtb* RNAP suggest that the co-bound mutant gained extra stability

amidst the mutation and could be attributed to the presence of DAAPI, which possibly influenced the increase in formation of H-bond interactions amongst residues. This corroborates with the increased residue-residue interactions in the RIN analyses of the co-bound mutant enzyme coupled with a subtle increase in binding free energy of Rifampin from -43.59 kcal/mol when singly bound to -47.34 kcal/mol upon co-binding with DAAPI amidst the mutation. This also confers with the experimental prediction of the suppression of the emergence of Rifampin in the presence of DAAPI [19].

3.2 Flexibility and Compactness of Residues of singly bound/co-bound mutant and wild *Mtb* RNAP over 50ns

The conformational properties of a *Mtb* RNAP, as a protein is largely influenced by the individual amino acids that form the building block of the protein [43,44]. Interactions of active site residues with either Rifampin, DAAPI or both may to trigger conformational modifications in the structure of *Mtb* RNAP which could distort its function [44]. Understanding the fluctuations of the individual residues of a *Mtb* RNAP upon the binding of Rifampin, DAAPI or both with or without mutation gives insight into the overall flexibility of the various regions of *Mtb* RNAP that corresponds to its crystallographic β factors [45]. The Root Mean Square Fluctuation (RMSF) enabled the exploration of structural dynamics upon ligand binding in the various systems and was calculated from the MD trajectories generated after the MD simulation (Figure 5).

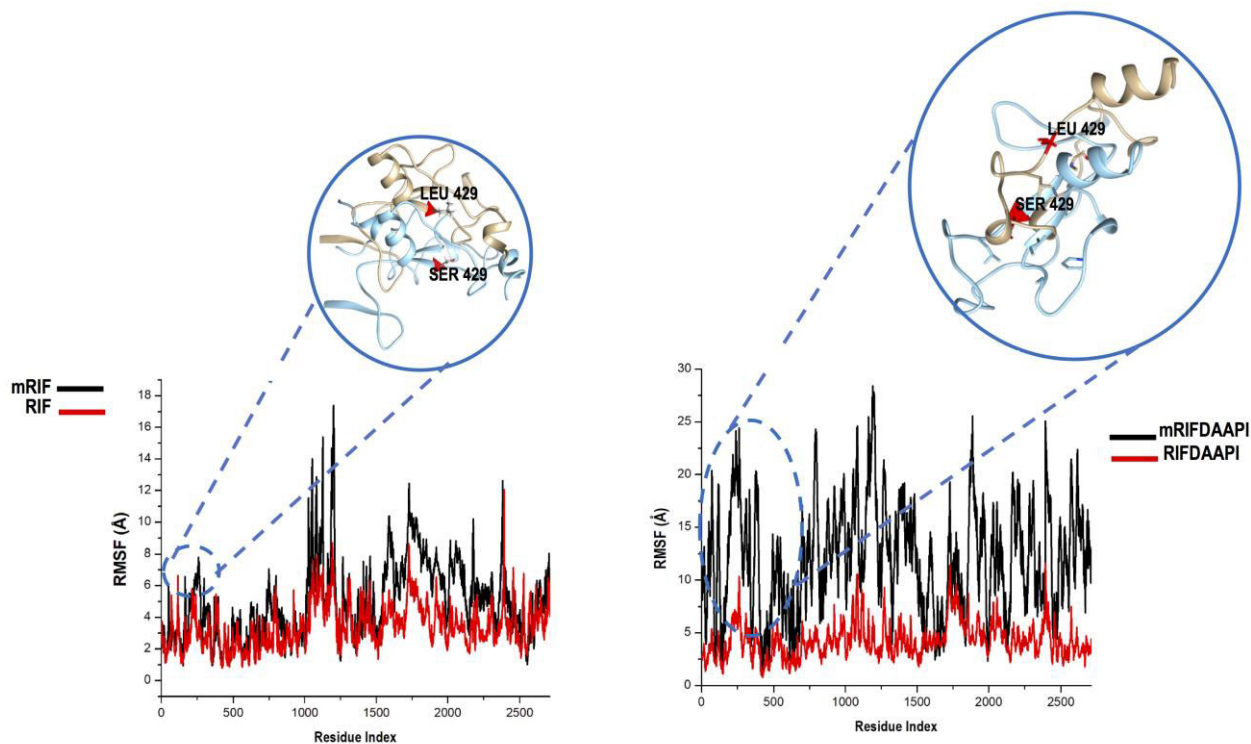


Figure 5.5: The Root Mean Square Fluctuations (RMSF) of mutant S429L (black) with respect to wild type *Mtb* RNAP (red) for 50 ns trajectory using C α atoms upon single binding and co-binding. The region marked with blue circle encompasses the residue of interest involved and shows increase fluctuation in S429L for both singly bound and co-bound systems.

Overall, the mutated *Mtb* RNAP systems (mRIF, mRIFDAAPI) showed marked flexibility of residues in protein structures, thus depicting visible residue fluctuations (Figure 5.5) when compared with the wild systems (RIF, RIFDAAPI). This clearly indicates that the single active site mutation destabilized the entire protein structure of *Mtb* RNAP in both singly bound and co-bound states. There was also a notable increase in fluctuation of residues

around the region of mutation compared to relatively more compact residues around the same region in the wild systems upon single binding and co-binding. This visible increase in flexibility of active site residues upon mutation consequently affects the binding affinity of Rifampin.

4. Conclusion

In this study, we utilized computational techniques to explore the ramifications of a single active site mutation on the binding of Rifampin to the recently resolved crystal structure of *Mtb* RNAP. We provide multidimensional insights on the impact of this mutation in a co-bound system with the novel inhibitor, DAAPI. Molecular dynamics simulations, thermodynamics calculations, hydrogen bond interactions and RIN analyses were employed to achieve our objectives. Results showed that, single active site mutation decreased the binding affinity of Rifampin, decreased the H-bond interactions and induced structural rearrangement around the mutant site in *Mtb* RNAP when Rifampin is bound alone. However, amidst the structural rearrangement around the mutation site, there was an improved interaction amongst neighboring residues coupled with an increased H-bond and van der Waal interaction upon co-binding with Rifampin and DAAPI. Also, Rifampin bound stronger to *Mtb* RNAP in combination with DAAPI than when bound alone amidst the single active site mutation. Results are consistent with the earlier reports of the drastic effect of active site mutation on the binding of Rifampin to *Mtb* RNAP, while conferring with the experimental prediction of the suppression of Rifampin resistance upon co-binding of Rifampin with DAAPI. Findings also provide critical molecular insights for future design of novel *Mtb* RNAP inhibitors to eradicate drug resistance in TB.

5. Acknowledgements

The authors acknowledge the School of Health Science, University of KwaZulu-Natal, Westville campus for financial assistance, and The Centre of High Performance Computing (CHPC, www.chpc.ac.za), Cape Town, RSA, for computational resources.

6. Conflicts of Interest

Authors declare no financial and intellectual conflict of interests.

Reference

1. Keshavjee, S. Farmer, PE. Tuberculosis, drug resistance, and the history of modern medicine. *N. Engl. J. Med.* 367(10), 931–6 (2012). Available from: <http://www.nejm.org/doi/full/10.1056/NEJMra1205429>.
2. World Health Organization (WHO). WHO | Global tuberculosis report 2017. Available from: http://www.who.int/tb/publications/global_report/en/.
3. Aristoff, P. Garcia, G. Kirchoff, PS. Hollis Showalter, HD. Rifamycins--obstacles and opportunities. *Tuberculosis.* , 90, 94 (2010).
4. Rothstein, DM. Rifamycins, alone and in combination. *Cold Spring Harb. Perspect. Med.* 6(7) (2016).
5. Sensi, P. History of the development of rifampin. *Rev. Infect. Dis.* 5, S402–S406 (1983).
6. Molodtsov, V. Scharf, NT. Stefan, MA. Garcia, GA. Murakami, KS. Structural basis for rifamycin resistance of bacterial RNA polymerase by the three most clinically important RpoB mutations found in *Mycobacterium tuberculosis*. *Mol. Microbiol.*

103(6), 1034–1045 (2017). Available from:

<http://doi.wiley.com/10.1111/mmi.13606>.

7. Campbell, EA. Korzheva, N. Mustaev A, Murakami, K. Nair, S. Goldfarb, A. *et al.* Structural Mechanism for Rifampicin Inhibition of Bacterial RNA Polymerase. *Cell*. 104, 901–912 (2001).
8. Feklistov, V. Mekler, Q. Jiang, L. Westblade, H. Irschik, R. Jansen, A. *et al.* Rifamycins do not function by allosteric modulation of binding of Mg²⁺ to the RNA polymerase active center. *Proc. Natl. Acad. Sci. USA*. 105(14820) (2008).. Available from: <http://dx.doi.org/10.1073/pnas.0802822105>.
9. Mustaev, A. Zaychikov, E. Severinov, K.. Topology of the RNA polymerase active center probed by chimeric rifampicin-nucleotide compounds. *Proc Natl Acad Sci USA*. 91(12036) (1994).
10. Drusano, GL. Sgambati, N. Eichas, A. Brown, DL. Kulawy, R. Louie, A. The combination of rifampin plus moxifloxacin is synergistic for suppression of resistance but antagonistic for cell kill of *Mycobacterium tuberculosis* as determined in a hollow-fiber infection model. *MBio*. 1(3) (2010).
11. Drusano, GL. Neely, M. Guilder MV. Analysis of Combination Drug Therapy to Develop Regimens with Shortened Duration of Treatment for Tuberculosis. *Cell*. 9(7) (2014).
12. Kaushik, A. Makkar, N. Pandey, P. Parrish, N. Singh, U. Lamichhane, G. Carbapenems and Rifampin exhibit synergy against *Mycobacterium tuberculosis* and *Mycobacterium abscessus*. *Antimicrob. Agents Chemother*. 59(10), 6561–6567 (2015).

13. Sandgren, A. Strong, M. Muthukrishnan, P. Weiner, BK. Church, GM. Murray, MB. Tuberculosis drug resistance mutation database. *PLoS Med.* 6(2), 0132–0136 (2009).
14. Cummings, MP. Segal, MR. Few amino acid positions in rpoB are associated with most of the rifampin resistance in Mycobacterium tuberculosis. *BMC Bioinformatics.* 5, 137 (2004). Available from: <http://www.scopus.com/inward/record.url?eid=2-s2.0-13244262710&partnerID=tZOtx3y1>.
15. Goldstein, BP. Resistance to rifampicin: a review. *J. Antibiot. (Tokyo).* 67(9), 625–630 (2014). Available from: <http://www.nature.com/doi/10.1038/ja.2014.107>.
16. Artsimovitch, I. Vassylyeva, MN. Svetlov, D.. Allosteric Modulation of the RNA Polymerase Catalytic Reaction Is an Essential Component of Transcription Control by Rifamycins. 122, 351–363 (2005).
17. Gill, SK. Garcia, GA. Rifamycin inhibition of WT and Rif-resistant Mycobacterium tuberculosis and Escherichia coli RNA polymerases in vitro. *Tuberculosis.* 91(5), 361–369 (2011).
18. Nusrath, UA. Hassan, S. Indira KV. Revathy, R. Hanna, LE. Insights into RpoB clinical mutants in mediating rifampicin resistance in Mycobacterium tuberculosis. *J. Mol. Graph. Model.* 67, 20–32 (2016).
19. Lin W, Mandal S, Degen D. Liu, Y. Ebright, Y W. Li, S *et al.* Structural basis of Mycobacterium tuberculosis transcription and transcription inhibition. *Mol. Cell.* 66, 169–179 (2017).
20. Pettersen, EF. Goddard, TD. Huang, CC. Couch, GS. Greenblatt, DM. Meng, E C. *et al.* UCSF Chimera - A visualization system for exploratory research and analysis. *J. Comput. Chem.* 25(13), 1605–1612 (2004).

21. Salomon-Ferrer, R. Gotz, AW. Poole, D. Le Grand, S. Walker, RC. Routine microsecond molecular dynamics simulations with AMBER on GPUs. 2. Explicit solvent particle mesh ewald. *J. Chem. Theory Comput.* 9(9), 3878–3888 (2013).
22. Case Da TE. Cheatham, I. Darden, T. The Amber biomolecular simulation programs. *J. Comput. Chem.* 26(16),1668–1688(2005). Available from:
<http://onlinelibrary.wiley.com/doi/10.1002/jcc.20290/pdf>.
23. Bahareh, H. Govender, T. Maguire, GEM. Soliman, MES. Kruger, HG. Integrated approach to structure-based enzymatic drug design: molecular modeling, spectroscopy, and experimental bioactivity. *Chem. Rev.* (2013).
24. Moonsamy, S. Bhakat, S. Walker, RC. Soliman, MES. Single Active Site Mutation Causes Serious Resistance of HIV Reverse Transcriptase to Lamivudine: Insight from Multiple Molecular Dynamics Simulations. *Cell Biochem. Biophys.* 74(1), 35–48 (2016).
25. Ndagi, U. Mhlongo, NN. Soliman, MES. The impact of Thr91 mutation on c-Src resistance to UM-164: molecular dynamics study revealed a new opportunity for drug design. *Mol. BioSyst.* 13(6), 1157–1171 (2017). Available from:
<http://xlink.rsc.org/?DOI=C6MB00848H>.
26. Bhakat, S. Martin, AJM. Soliman MES. An integrated molecular dynamics, principal component analysis and residue interaction network approach reveals the impact of M184V mutation on HIV reverse transcriptase resistance to lamivudine. *Mol. Biosyst.* 10(8), 2215–28 (2014). Available from:
<http://www.ncbi.nlm.nih.gov/pubmed/24931725>.
27. Oguntade, S. Ramharack, P. Soliman, MES. Characterizing the ligand-binding

landscape of Zika NS3 helicase-promising lead compounds as potential inhibitors.

Future Virol. 12(6), 261–273 (2017). Available from:

<http://www.futuremedicine.com/doi/10.2217/fv1-2017-0014>.

28. Ramharack, P. Soliman, MES. Zika virus NS5 protein potential inhibitors: an enhanced in silico approach in drug discovery. *J Biomol Struct Dyn.* , 1–16 (2017).
29. Genheden, S. Ryde, U. The MM/PBSA and MM/GBSA methods to estimate ligand-binding affinities. *Expert Opin. Drug Discov.* 10, 449–461 (2015).
30. Mhlongo, NN. Soliman, MES. Single H5N1 influenza A neuraminidase mutation develops resistance to oseltamivir due to distorted conformational and drug binding landscape: multiple molecular dynamics analyses. *RSC Adv.* 5(14), 10849–10861 (2015). Available from: <http://xlink.rsc.org/?DOI=C4RA13494J>.
31. Kumalo, HM. Soliman, MES. Per-Residue Energy Footprints-Based Pharmacophore Modeling as an Enhanced In Silico Approach in Drug Discovery: A Case Study on the Identification of Novel β -Secretase1 (BACE1) Inhibitors as Anti-Alzheimer Agents. *Cell. Mol. Bioeng.* 9(1), 175–189 (2016).
32. Shannon, P. Markiel, A. Owen, O.. Cytoscape: a software environment for integrated models of biomolecular interaction networks. *Genome Res.* (13), 2498–2504 (2003).
33. Doncheva, NT. Klein, K. Domingues, FS. Albrecht, M. Analyzing and visualizing residue networks of protein structures. *Trends Biochem. Sci.* 36(4), 179–182 (2011). Available from: <http://dx.doi.org/10.1016/j.tibs.2011.01.002>.
34. Assenov, Y. Ramírez F, Schelhorn SESE, Lengauer T, Albrecht M. Computing topological parameters of biological networks. *Bioinformatics.* 24(2), 282–284 (2008).

35. Amitai, G. Shemesh, A. Sitbon, E. Shklar, M. Netanel, D. Venger, I. *et al.* Network analysis of protein structures identifies functional residues. *J. Mol. Biol.* 344(4), 1135–1146 (2004).
36. Vishveshwara, S. Ghosh, A. Hansia, P. Intra and inter-molecular communications through protein structure network. *Curr. Protein Pept. Sci.* 10(2), 146–60 (2009). Available from: <http://www.ncbi.nlm.nih.gov/pubmed/19355982>.
37. del Sol, A. Fujihashi, H. Amoros, D. Nussinov, R. Residues crucial for maintaining short paths in network communication mediate signaling in proteins. *Mol. Syst. Biol.* 2 (2006). Available from: <http://msb.embopress.org/cgi/doi/10.1038/msb4100063>.
38. Ramaswamy, SMJ. Molecular genetic basis of antimicrobial agent resistance in *Mycobacterium tuberculosis*: 1998 update. *Tuber. lung Dis.* 79, 3–29 (1998).
39. Jin, DJ. Gross, CA. Mapping and sequencing of mutations in the *Escherichia coli* *rpoB* gene that lead to rifampicin resistance. *J. Mol. Biol.* 202(1), 45–58 (1988).
40. Patil, R. Das, S, Stanley, A. Yadav, L. Sudhakar, A. Varma, AK. Optimized hydrophobic interactions and hydrogen bonding at the target-ligand interface leads the pathways of drug designing. *PLoS One.* 5, e12029 (2010).
41. De Azevedo Jr WF. MolDock applied to structure-based virtual screening. *Curr. Drug Targets.* 11(3), 327–34 (2010).
42. Chen, D. Oezguen, N. Urvil, P. Ferguson, C. Dann, SM. Savidge, TC. Regulation of protein-ligand binding affinity by hydrogen bond pairing. *Sci. Adv.* 2(3), e1501240 (2016). Available from: <http://www.ncbi.nlm.nih.gov/pubmed/27051863>
<http://www.pubmedcentral.nih.gov/articlerender.fcgi?artid=PMC4820369>.

43. Spassov, VZ. Yan, L. Flook, PK. The dominant role of side-chain backbone interactions in structural realization of amino acid code . ChiRotor : A side-chain prediction algorithm based on side-chain backbone interactions. , 494–506 (2007).
44. Lewis, J. Raff, M. Roberts, K. Book Reviews.(2003).
45. Wassenaar T. A molecular dynamics hands-on session II. Available from:
www.nmr.chem.uu.nl/~tsjerk/course/md-tutorial/analysis.

CHAPTER 6

Conclusion and Future Perspectives

6.1 Conclusions

The emergence of Rifampin resistance has contributed immensely to global TB epidemic with an increase in new reported cases in the last few years. As a result, finding viable approaches of combating Rifampin resistance has become extremely paramount. Over these last few years anti-Rifampin resistance approaches have been proposed, nonetheless, researchers are still working tirelessly in the design therapeutic approaches and potential small drug molecules that can be co-administered with Rifampin to curb the menace of Rifampin resistance.

The major aims of this thesis were to unravel molecular insights into the suppression of the emergence of resistance to Rifampin by a novel $N\alpha$ -aroyl-N-aryl-phenylalaninamides (AAPI) prototype inhibitor co-bound to *Mtb* RNAP; and to also provide a molecular understanding of the interplay of a single active site mutation on the emergence Rifampin resistance amidst single binding of Rifampin or upon co-binding with both Rifampin and the novel inhibitor prototype, DAAPI. Results from this work confirmed the following conclusions:

1. Co-binding with both Rifampin and DAAPI induced a more stable and compact *Mtb* RNAP than when *Mtb* RNAP was singly bound to either Rifampin or the novel inhibitor, DAAPI.
2. Thermodynamic calculations indicated that DAAPI exerts some level of stability and stronger Rifampin-*Mtb* RNAP interactions, which was complemented by a notable compactness of Rifampin binding site residues and increased van der Waals interactions upon co-binding.
3. The calculated binding free energy of Rifampin in the presence of DAAPI was higher compared to when bound alone as elucidated in the thermodynamics possibly explaining reason for the suppression of RIF resistance as previously experimentally predicted.
4. Per-residue energy decomposition analysis revealed that, amino acid residues: SER 429, PHE 412 and LEU 431 are key residues that largely contribute to the binding of RIF, while ARG 1958 and ILE 1975 were vital to the binding of DAAPI. This knowledge will contribute to a greater comprehension of binding landscapes of these inhibitors at a molecular level. Based on this study, Rifampin and DAAPI demonstrate a synergistic mechanism of inhibition

5. Single active site mutation decreased the binding affinity of Rifampin, decreased the H-bond interactions and induced structural rearrangement around the mutant site in *Mtb* RNAP when Rifampin is bound alone.
6. Amidst the structural rearrangement around the mutation site, there was an improved interaction amongst neighboring residues coupled with an increased H-bond and van der Waal interaction upon co-binding with Rifampin and DAAPI.
7. Rifampin bound stronger to *Mtb* RNAP in combination with DAAPI than when bound alone amidst the single active site mutation. Results are consistent with the earlier reports of the drastic effect of active site mutation on the binding of Rifampin to *Mtb* RNAP, while also conferring with the experimental prediction of the suppression of Rifampin resistance upon co-binding of Rifampin with DAAPI.

Overall, this study has provided essential conformational and structural molecular insights into the design and development of new TB therapeutic approaches as well novel anti-TB inhibitors through molecular modeling and CADD

6.2 Future Scope and beyond

Using computational tools, the studies reported in this thesis complemented and justified previously reported experimental findings, providing reliable molecular insights which can be employed in future studies. Computational perspective unraveled in these studies opened up some future scopes, which can serve as the bases for future research.

1. Findings from this thesis supports that co-binding of Rifampin and the novel inhibitor, DAAPI on *Mtb* RNAP suppresses the emergence of Rifampin resistance as previously predicted experimentally. Further research could still, however, be carried out to provide potential pharmacophoric features in the design and development of new small molecules inhibitors that can singly target *Mtb* RNAP to suppress anti-TB resistance. Single acting drugs will reduce the risk of toxicity and will be relatively less expensive than the co-administration of two separate drugs.
2. To further examine the validity of the simulation and parameters proposed for describing the systems studied, the simulation could be performed in triplicate of longer periods of molecular dynamic simulations for each system. The triplicate of the run can be use evaluate

parameters proposed and to further understand the impact of co-binding Rifampin and DAAPI on the emergence of Rifampin resistance as well the revealing the impact of single active site mutation.

APPENDIX

APPENDIX A

Supplementary Documents for submitted paper: **Clement Agoni**, Ramharack P . and Soliman M E (2017) Co-inhibition as a Strategic Therapeutic Approach to Overcome Rifampin Resistance in TB Therapy: Atomistic Insights, *Future Medicinal Chemistry*, Manuscript ID: FMC-2017-00197

APPENDIX B

Supplementary Documents for submitted paper: **Clement Agoni**, Ramharack P. and Soliman M E (2017) Synergistic Interplay of The Co-administration of Rifampin And Newly Developed Anti-TB Drug: Could It Be a Promising New Line of TB Therapy?, *Receptor and Signal Transduction*, Manuscript ID: LRSTS-2017-0113

**Co-inhibition as a Strategic Therapeutic Approach to Overcome
Rifampin Resistance in TB therapy: Atomistic insights**

Supplementary Material:

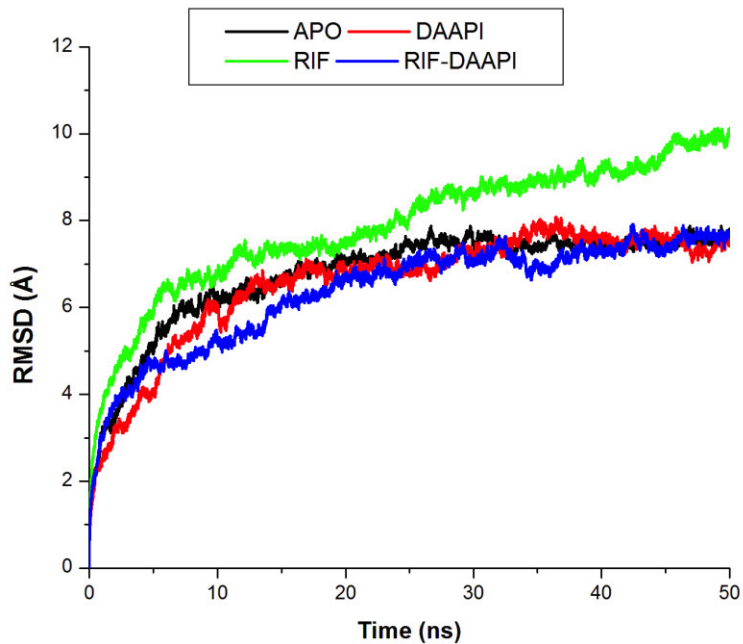


Figure S1. The C α root mean square deviations (RMSD) of the backbone atoms relative to the starting minimized structure over 50ns simulation for APO, RIF, DAAPI and RIF-DAAPI.

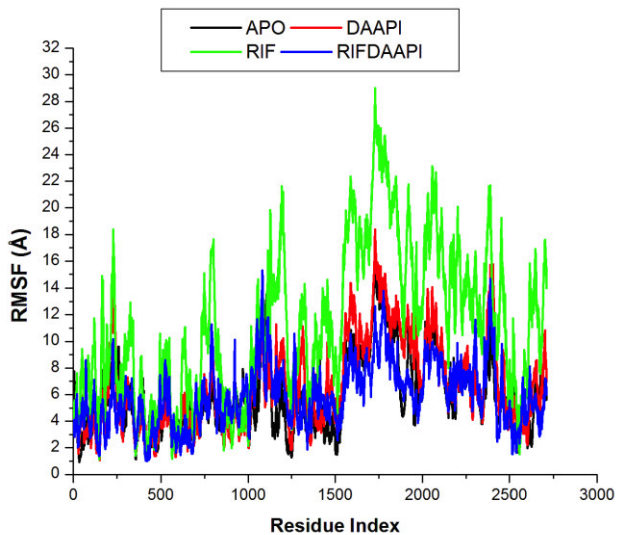


Figure S2. RMSF of C- α atoms for APO, DAAPI, RIF and RIFDAAPI over 50ns of simulation.

Table S1: Decomposition of the relative binding free energies on per residue basis for the Rifampin-*Mtb* RNAP complex.

Residue	ΔE_{vdw}	ΔE_{elec}	$\Delta G_{nonpolar}$	ΔG_{polar}	$\Delta G_{binding}$
ARG 146	-0.218 ± 0.048	-1.220 ± 0.415	-0.007 ± 0.009	1.596 ± 0.408	0.150 ± 0.114
THR 406	-0.089 ± 0.038	-0.126 ± 0.087	-0.006 ± 0.016	0.277 ± 0.104	0.056 ± 0.037
SER 407	-0.280 ± 0.073	-0.132 ± 0.174	-0.027 ± 0.012	0.413 ± 0.251	-0.025 ± 0.091
GLN 408	-2.102 ± 0.434	0.241 ± 0.690	-0.320 ± 0.040	0.839 ± 0.599	-1.341 ± 0.503
LEU 409	-0.272 ± 0.054	0.254 ± 0.050	0.000 ± 0.000	-0.329 ± 0.075	-0.347 ± 0.075
SER 410	-0.584 ± 0.145	0.370 ± 0.191	-0.038 ± 0.015	-0.073 ± 0.213	-0.325 ± 0.102
PHE 412	-1.260 ± 0.675	-4.909 ± 0.701	-0.335 ± 0.023	2.373 ± 0.331	-4.130 ± 0.586
MET 413	-0.730 ± 0.106	-0.431 ± 0.102	-0.003 ± 0.003	0.836 ± 0.193	-0.328 ± 0.189
ASP 414	-1.950 ± 0.242	1.868 ± 0.713	-0.142 ± 0.020	-0.516 ± 0.855	-0.740 ± 0.606
GLN 415	-0.097 ± 0.012	0.048 ± 0.034	0.000 ± 0.000	0.026 ± 0.052	-0.024 ± 0.035
HIE 424	-1.034 ± 0.235	1.196 ± 0.397	-0.048 ± 0.011	-0.652 ± 0.285	-0.538 ± 0.338
ARG 427	-1.789 ± 0.588	-11.515 ± 1.521	-0.225 ± 0.026	10.396 ± 1.070	-3.133 ± 0.806
SER 429	-0.179 ± 0.520	-4.498 ± 0.677	-0.033 ± 0.014	3.107 ± 0.194	-1.604 ± 0.321
LEU 431	-2.847 ± 0.474	-0.054 ± 0.219	-0.285 ± 0.047	0.839 ± 0.217	-2.348 ± 0.516
GLY 432	-0.958 ± 0.318	0.106 ± 0.153	-0.101 ± 0.030	0.385 ± 0.227	-0.568 ± 0.352
ARG 438	-0.445 ± 0.347	0.936 ± 0.629	-0.086 ± 0.090	-0.207 ± 0.859	0.199 ± 0.315

THR 461	-0.050 ± 0.012	-0.163 ± 0.081	0.000 ± 0.000	0.340 ± 0.087	0.128 ± 0.037
PRO 462	-0.500 ± 0.215	0.255 ± 0.118	-0.082 ± 0.026	0.012 ± 0.160	-0.315 ± 0.278
GLU 463	-0.260 ± 0.161	-1.559 ± 0.586	-0.025 ± 0.029	1.920 ± 0.856	0.076 ± 0.281
GLY 464	-0.033 ± 0.017	0.082 ± 0.044	-0.000 ± 0.000	-0.026 ± 0.036	0.023 ± 0.027
PRO 465	-0.106 ± 0.094	0.133 ± 0.068	-0.003 ± 0.012	-0.052 ± 0.080	-0.028 ± 0.067
ASN 466	-0.947 ± 0.751	0.151 ± 0.976	-0.161 ± 0.136	0.712 ± 1.193	-0.245 ± 0.444
ARG 586	-0.827 ± 0.258	0.286 ± 0.494	-0.124 ± 0.044	1.065 ± 0.407	0.400 ± 0.249
GLN 587	-0.132 ± 0.058	0.086 ± 0.120	-0.018 ± 0.028	0.147 ± 0.107	0.083 ± 0.054
HIP 653	-0.881 ± 0.271	0.264 ± 0.559	-0.177 ± 0.029	1.258 ± 0.573	0.464 ± 0.435

Table S2: Decomposition of the relative binding free energies on per-residue basis for the DA-API-*Mtb* RNAP complex.

Residues	ΔE_{vdw}	ΔE_{elec}	$\Delta G_{\text{nonpolar}}$	ΔG_{polar}	$\Delta G_{\text{binding}}$
LYS 819	-0.296 ± 0.499	-6.244 ± 3.980	-0.173 ± 0.134	6.697 ± 3.795	-0.015 ± 0.683
ARG1958	-1.909 ± 0.784	-12.471 ± 1.359	-0.473 ± 0.067	10.276 ± 1.179	-4.578 ± 1.007
PRO1959	-0.231 ± 0.136	-0.096 ± 0.161	-0.033 ± 0.025	0.351 ± 0.264	-0.009 ± 0.077
VAL1960	-0.292 ± 0.216	0.176 ± 0.077	-0.032 ± 0.031	-0.112 ± 0.042	-0.259 ± 0.213
LYS1961	-0.032 ± 0.023	0.574 ± 0.292	-0.000 ± 0.002	-0.476 ± 0.259	0.066 ± 0.032
SER1962	-0.015 ± 0.011	0.113 ± 0.044	-0.000 ± 0.000	-0.104 ± 0.040	-0.006 ± 0.011
THR1969	-0.038 ± 0.022	-0.093 ± 0.099	-0.000 ± 0.001	0.113 ± 0.103	-0.018 ± 0.021
LEU1971	-0.823 ± 0.513	-0.222 ± 0.425	-0.225 ± 0.149	0.500 ± 0.624	-0.770 ± 0.479
GLU1972	-0.376 ± 0.293	-2.091 ± 0.527	-0.058 ± 0.049	2.306 ± 0.666	-0.219 ± 0.207
PHE1974	-0.221 ± 0.255	0.155 ± 0.069	-0.047 ± 0.076	-0.079 ± 0.116	-0.193 ± 0.250
ILE1975	-0.959 ± 0.447	0.276 ± 0.120	-0.226 ± 0.094	-0.212 ± 0.105	-1.121 ± 0.499
HIS1978	-0.182 ± 0.189	0.107 ± 0.074	-0.034 ± 0.047	0.108 ± 0.228	-0.001 ± 0.067

**Synergistic Interplay of the Co-administration of Rifampin and Newly
Developed Anti-TB Drug: Could It Be a Promising New Line of TB Therapy?**

Supplementary Material:

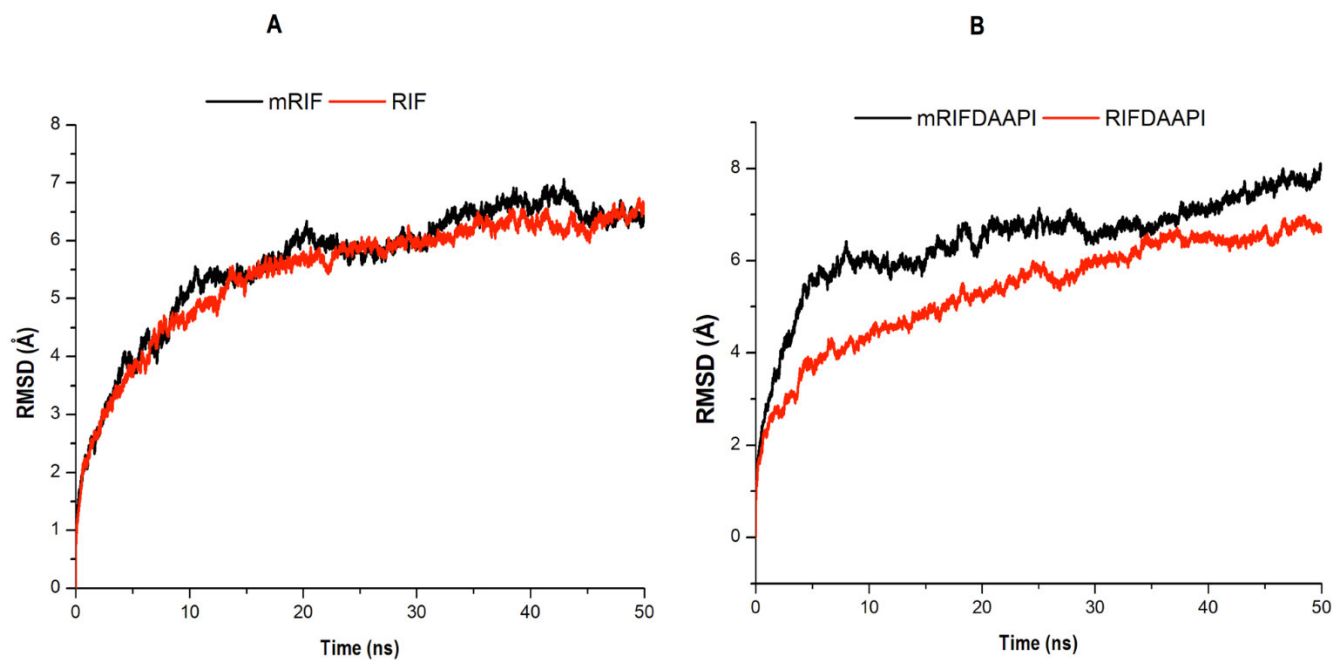


Figure S1: Comparative root mean square deviation of mutated and unmutated systems upon single binding of Rifampin (A) and upon co-binding with DAAPI (B).

Table S1: Hydrogen bond occupancy of interacting active site residues of Rifampin in the wild singly bound RIF system

H-bond Acceptor	H-bond Donor	Frames	Occupancy (%)	Average distance (Å)	Average angle (degree)
GLU_460@O	THR_564H	51218	98	2.691	164.4725
ASP_414@O	SER_420@H	49795	95	2.6798	164.1854
VAL_149@O	ARG_352@H	43667	84	2.8222	156.2499
SER_429@O	LEU_152@H	39931	77	2.8528	162.2017
ARG_146@O	PHE_139@H	37463	72	2.8735	163.767
GLN_408@O	GLN_411@H	36926	71	2.8592	164.305
GLN_415@O	SER_651@H	36616	70	2.7474	154.7249
ARG_586@O	ASN_416@H	28731	55	2.8594	156.9693
LEU_431@O	GLN_151@H	27193	52	2.8683	158.6173
MET_413@O	ASN_652@H	22997	44	2.8831	161.8032
LEU_409@O	GLN_411@H	21170	41	2.8741	146.3306
SER_410@O	ARG_146@H	18535	36	2.8195	157.1721
THR_461@O	ASN_583@H	18225	35	2.8662	160.3019
MET_413@O	GLN_415@H	16657	32	2.8534	145.4704
ASN_466@O	LEU_469@H	15364	29	2.8936	149.7248
GLU_463@O	GLU_463@H	13599	26	2.8103	150.6947
ARG_427@O	SER_150@H	11365	22	2.7575	155.2029
HIP_653@O	HIP_724@H	11161	21	2.7923	150.2511
SER_407@O	LEU_409@H	7930	15	2.925	156.2667
ARG_438@O	TYR_2443H	1888	4	2.7435	161.8803
PRO_462@O	GLY_464@H	1436	3	2.8886	145.2237
GLY_464@O	ASN_466@H	724	1	2.8639	148.5496
HIE_424@O	ARG_427@H	679	1	2.9171	148.1715

Table S2: Hydrogen bond occupancy of interacting active site residues of Rifampin in the mutated singly bound mRIF systems

H-bond Acceptor	H-bond Donor	Frames	Occupancy (%)	Average distance (Å)	Average angle (degree)
ASP_414@O	SER_420@H	51498	96	2.6634	164.3344
SER_410@O	ARG_146@H	40928	77	2.8249	153.7175
SER_407@O	SER_410@H	38174	72	2.6779	162.8938
GLN_411@O	VAL_149@H	35000	66	2.8558	164.3801
MET_413@O	GLN_415@H	34835	65	2.8326	147.6212
GLU_460@O	SER_472@H	27373	51	2.7076	160.6573
GLN_408@O	GLN_411@H	27085	51	2.8511	160.663
GLN_411@O	VAL_147@H	26990	51	2.879	156.6565
GLY_432@O	GLY_435@H	23506	44	2.8739	149.299
GLU_463@O	GLU_463@H	23375	44	2.8186	152.4317
LEU_409@O	GLN_411@H	20707	39	2.8585	144.7838
THR_461@O	ASN_583@H	17024	32	2.865	156.8918
ARG_146@O	PHE_139@H	15682	29	2.8859	149.9139
GLN_415@O	LYS_136@H	13208	25	2.8348	156.9629
LEU_431@O	GLN_151@H	11045	21	2.8482	158.4389
LEU_429@O	GLN_151@H	9978	19	2.8482	161.5036
HIE_424@O	ARG_427@H	9665	18	2.9137	155.7397
ARG_427@O	SER_150@H	9122	17	2.8902	148.9958
ASN_466@O	LEU_469@H	3095	6	2.9024	147.4206
PRO_465@O	ARG_446@H	2384	4	2.8093	156.9627
GLY_464@O	ASN_466@H	1925	4	2.801	144.8855
ARG_438@O	GLN_1050@H	1319	2	2.8586	153.5162
GLN_587@O	LYS_865@H	555	1	2.8253	158.0322

Table S3: Hydrogen bond occupancy of interacting active site residues of Rifampin in the mutated co-bound mRIFDAAPI system

H-bond acceptor	H-bond donor	Frames	Occupancy (%)	Average distance (Å)	Average angle (degree)
ASP_414@O	ARG_586@H	42953	80	2.8136	160.106
GLY_432@O	GLY_435@H	31455	57	2.8685	148.5645
LEU_429@O	LEU_152@H	28082	52	2.8784	160.2063
ASN_466@O	ILE_470@H	23971	45	2.883	156.5121
LEU_431@O	GLN_151@H	17412	32	2.8605	156.2142
MET_413@O	ASN_652@H	16329	31	2.8725	161.0883
GLN_415@O	THR_655@H	16023	30	2.7309	160.6464
GLU_463@O	GLU_463@H	13978	26	2.8196	151.1642
PRO_465@O	ILE_467@H	11920	22	2.8904	145.2289
LEU_409@O	VAL_149@H	8876	17	2.8977	157.4278
SER_410@O	ARG_146@H	8603	16	2.8299	154.4312
SER_407@O	SER_410@H	8582	16	2.9033	151.681
PHE_412@O	HIE_424@H	4541	8	2.835	147.5039
ARG_427@O	SER_150@HG	4258	8	2.7567	154.5606
GLN_408@O	GLN_408@H	4212	8	2.8466	147.9696
PRO_462@O	GLY_464@H	3165	6	2.8546	145.9462
THR_461@O	ASN_583@H	1816	3	2.8704	156.5311
GLN_587@O	ASN_416@H	1393	3	2.9009	143.1098
HIE_424@O	ARG_427@H	1118	2	2.9292	158.4036
ARG_438@O	ALA_441@H	1055	2	2.9276	156.69
ASN_466@O	ARG_438@H	805	2	2.8421	155.8878

Table S4: Hydrogen bond occupancy of interacting active site residues of Rifampin in the wild co-bound RIFDAAPI system

H-bond Acceptor	H-bond donor	Frames	Occupancy (%)	Average distance (Å)	Average angle (degree)
SER_429@O	LEU_152@H	45061	89	2.8221	161.642
LEU_431@O	GLN_151@H	42712	85	2.8328	162.4605
GLN_411@O	VAL_147@H	39170	78	2.8585	164.6051
GLY_435@O	ARG_2515@H	34708	69	2.8434	156.9005
LEU_428@O	GLY_471@H	31810	63	2.8679	157.117
ARG_426@O	LEU_473@H	30994	61	2.875	164.3169
GLU_460@O	SER_561@H	30825	61	2.6395	164.5575
ASP_414@O	SER_420@H	28594	57	2.6835	163.0455
GLY_432@O	GLY_435@H	26042	52	2.868	146.9922
VAL_149@O	GLN_151@H	18941	38	2.8254	147.734
ARG_586@O	ASN_416@H	17845	38	2.8582	152.341
GLU_463@O	ASN_466@H	16677	33	2.8441	159.5455
MET_413@O	GLN_415@H	16036	32	2.8193	146.7779
HIE_424@N	ASP_414@H	15776	31	2.9252	157.215
ASN_466@O	LEU_469@H	15191	30	2.8967	151.335
LEU_409@O	VAL_149@H	14222	28	2.8999	161.9313
SER_407@O	SER_410@H	12432	25	2.9129	161.3599
THR_461@O	ASN_583@H	8550	17	2.8557	161.4456
HIP_653@O	HIP_724@H	8496	17	2.7966	148.1274
ARG_427@O	SER_150@H	7492	15	2.7185	155.8104
GLY_464@O	ILE_467@H	6425	13	2.9088	161.8643
SER_410@O	ARG_146@H	5887	12	2.8938	149.5393

